

THE UNIVERSITY OF CHICAGO

A LIMIT ON THE BRANCHING RATIO OF THE FLAVOR-CHANGING TOP  
QUARK DECAY  $T \rightarrow ZC$

A DISSERTATION SUBMITTED TO  
THE FACULTY OF THE DIVISION OF THE PHYSICAL SCIENCES  
IN CANDIDACY FOR THE DEGREE OF  
DOCTOR OF PHILOSOPHY

DEPARTMENT OF PHYSICS

BY  
ALEXANDER A. PARAMONOV

CHICAGO, ILLINOIS

JUNE 2009



## ABSTRACT

We have used the Collider Detector at Fermilab (CDF-II) to set upper limits on the branching ratio of the flavor-changing neutral-current (FCNC) top quark decay  $t \rightarrow Zc$  using a technique employing ratios of  $W$  and  $Z$  production, measured in  $1.52 \text{ fb}^{-1}$  of  $p\bar{p}$  data. The analysis uses a comparison of two decay chains,  $p\bar{p} \rightarrow t\bar{t} \rightarrow WbWb \rightarrow \ell\nu bj\bar{j}b$  and  $p\bar{p} \rightarrow t\bar{t} \rightarrow ZcWb \rightarrow \ell^+\ell^-cj\bar{j}b$ , to cancel systematic uncertainties in acceptance, efficiency, and luminosity. We validate the MC modeling of acceptance and efficiency for lepton identification over the multi-year dataset also using a ratio of  $W$  and  $Z$  production, in this case the observed ratio of inclusive production of  $W$  to  $Z$ -bosons, a technique that will be essential for precision comparisons with the standard model at the LHC. We introduce several methods of determining backgrounds to the  $W$  and  $Z$  samples. To improve the discrimination against SM backgrounds to top quark decays, we calculate the top mass for each event with two leptons and four jets assuming it is a  $t\bar{t}$  event with one of the top quarks decaying to  $Zc$ . The upper limit on the  $\text{Br}(t \rightarrow Zc)$  is estimated from a likelihood constructed with the  $\ell^+\ell^-cj\bar{j}b$  top mass distribution and the number of  $\ell\nu bj\bar{j}b$  events. Limits are set as a function of the helicity of the  $Z$ -boson produced in the FCNC decay. For 100%-longitudinally-polarized  $Z$ -bosons we find a limit of 8.3% (95% C.L.).

## ACKNOWLEDGMENTS

First of all, I would like to thank Henry J. Frisch. I am glad that I had an opportunity to work with this man and to learn from him. I apologize for doing some analysis in my own way; I felt that I can perform those analysis more rigorously. Often I was wrong but I learned a lesson. I am also grateful for Henry's support in relationships with CDF colleagues. A number of issues were resolved solely due to Henry's wisdom. Lastly, I would like to say that I owe Henry a lot and I promise to buy him a lunch when I get a good job.

Second of all, I must thank my mother Irina and my sister Julia. I am grateful to both of them for giving me moral inspiration during these five years and for reminding me that I am a part of the family. I am guilty for not listening to their advices when it was clear that I am wrong.

I also wish to thank my friends and colleagues. The list of names is long so I apologize in advance if I miss somebody. I am grateful to Beate Heinemann, Kevin Lannon, and Jason Nielsen for their patience and enormous help as CDF internal reviewers of our paper. I thank Koji Nakamura and Eugene JJ Schmidt for training me as a CDF Ace. Being a CDF Ace was a lot of fun. Once I had to push the big red crash button when there was an emergency. I am in debt to Harold Sanders and Mircea Bogdan for introducing me to the basics of electronics when we were working on the TDC board for CDF. Steve Levy, Dan Krop, Carla Grosso-Pilcher, Un-Ki Yang, Andrey Loginov, and Eric Brubaker have always been good colleagues and they advised me on a number physics-related issues. Thank you all for your help.

This study would not be possible without the help of numerous theorists and CDF conveners; I am in debt to all of you. Johan Alwall, Michelangelo Mangano, Fabio Maltoni, Michele Papucci, Rikkert Fredrix, and Zack Sullivan clarified different theoretical aspects of the analysis for us. Michel Herquet helped us with implementing new physical processes into Monte Carlo simulations. Ben Brau, Chris Hays, Jane Nachtman, and Alexei Safonov have been guiding us through non-linear multi-iterative quests of CDF paper approval.

I am blessed to find so many good friends at the University of Chicago, I highly treasure all the time spent together. I thank Collin Wolfe, Jahred Adelman, Wojciech Fedorko, Shawn Kwang, Eric Feng, Anton Kapliy, Scott Wilbur, and Tudor Costin for being around, supporting me, and going out for a drink.

My special thanks are addressed to Mary Heintz and Nobuko McNeill. Mary's prompt and tireless system maintenance has been invaluable. Mrs. McNeill supported me in my crusade against bureaucracy in Russia and at the University of Chicago.

Finally, I would love to thank all my teachers at the university: Young-Kee Kim, Melvyn Shochet, Yau Wah, Dean Eastman, Emil Martinec, Carlos Wagner, Joseph Lykken, Guy Savard, Sean Carroll, and Eric Isaacs. It was my pleasure to learn from you.

## TABLE OF CONTENTS

ABSTRACT . . . . .	iii
ACKNOWLEDGMENTS . . . . .	iv
LIST OF FIGURES . . . . .	ix
LIST OF TABLES . . . . .	xiii
Chapter	
1 INTRODUCTION . . . . .	1
2 APPARATUS: THE CDF II DETECTOR . . . . .	6
3 INTRODUCTION TO THE ANALYSIS STRATEGY . . . . .	9
4 EVENT SELECTION . . . . .	11
4.1 Lepton Identification . . . . .	11
4.1.1 Electron Selection . . . . .	12
4.1.2 Muon Selection . . . . .	13
4.1.3 Corrections due to modeling of electrons and muons in the MC events . . . . .	13
4.2 Jet Identification . . . . .	14
4.3 Photon Identification . . . . .	14
4.4 Missing $E_T$ Reconstruction . . . . .	15
4.5 Additional Kinematic Variables Used In the Analysis . . . . .	15
5 PRODUCTION OF $Z$ BOSONS WITH JETS . . . . .	17
6 PRODUCTION OF $W$ BOSONS WITH JETS . . . . .	27
7 STANDARD MODEL CONTRIBUTIONS TO EVENTS WITH A $W$ OR A $Z$ BOSON AND JETS . . . . .	35
7.1 Monte Carlo Simulations of the Standard Model Processes . . . . .	35
7.2 Electroweak Backgrounds . . . . .	36
7.3 Fake $Z$ Background from Hadron Jets Misidentified as Leptons . . . . .	36
7.4 Fake $W$ backgrounds from Hadron jets . . . . .	37
7.5 Cosmic Ray Backgrounds . . . . .	38

8	USING R AS A PRECISE CHECK OF THE MONTE CARLO SIMULATIONS . . . . .	43
9	TAGGING OF HEAVY FLAVOR JETS . . . . .	45
10	OVERVIEW OF THE FCNC ANALYSIS . . . . .	47
11	MEASURING TOP QUARK PAIR PRODUCTION IN EVENTS WITH A W BOSON AND FOUR JETS . . . . .	49
	11.1 Estimating the Relative Contributions from $t\bar{t}$ ; the $W$ +HF Processes $W + b\bar{b}$ , $W + c\bar{c}$ , and $W + c$ ; and non- $W$ Background . . . . .	49
	11.2 Fake $W$ backgrounds in the $t\bar{t}$ Sample . . . . .	51
12	THE CONTRIBUTION FROM FCNC DECAYS OF TOP QUARK PAIRS TO EVENTS WITH $W/Z$ BOSONS AND JETS . . . . .	57
	12.1 Acceptances for $t\bar{t}$ decays . . . . .	57
	12.2 Properties of the FCNC $t \rightarrow Zc$ coupling . . . . .	58
13	MEASURING THE CONTRIBUTIONS FROM FCNC AND SM PROCESSES IN EVENTS WITH A $Z$ -BOSON AND FOUR JETS . . . . .	61
	13.1 Fitting the Top Mass . . . . .	63
14	SYSTEMATIC UNCERTAINTIES . . . . .	68
	14.1 Systematic Uncertainties on the Acceptances . . . . .	68
	14.2 Systematic Uncertainties of the Backgrounds . . . . .	73
15	STATISTICAL EVALUATION OF THE LIMITS ON $BR(T \rightarrow ZC)$ . . . . .	77
	15.1 Numerical Computation of the Likelihood Distribution Function . . . . .	80
	15.2 Computation of the Posterior $P(Br(t \rightarrow Zc) DATA)$ . . . . .	80
	15.3 Computation of the Upper Limits on $Br(t \rightarrow Zc)$ . . . . .	82
16	CONCLUSIONS AND RESULTS . . . . .	84
Appendix		
A	DETAILS OF LEPTON SELECTION CRITERIA . . . . .	85
B	CORRECTIONS TO IDENTIFICATION EFFICIENCIES, ACCEPTANCES, AND TRIGGER EFFICIENCIES FOR ELECTRONS AND MUONS . . . . .	87
C	PHOTON IDENTIFICATION CRITERIA . . . . .	88
D	LIST OF SIMULATED DATASETS . . . . .	89

E SUMMARY TABLE OF ACCEPTANCES AND EFFICIENCIES . . . . . 91

F LIST OF EVENTS WITH A Z-BOSON AND FOUR JETS . . . . . 92

REFERENCES . . . . . 99

## LIST OF FIGURES

1.1	A Feynman diagram for one of the processes contributing to $t\bar{t} \rightarrow WbWb \rightarrow \ell\nu bj\bar{j}b$ decay chain. The $t\bar{t}$ pair is produced in a collision of $p$ and $\bar{p}$ . . . . .	3
1.2	A Feynman diagram for one of the processes contributing to $t\bar{t} \rightarrow ZcWb \rightarrow \ell\ell c j\bar{j}b$ decay chain. The $t\bar{t}$ pair is produced in a collision of $p$ and $\bar{p}$ . . . . .	4
2.1	An elevation view of one half of the CDF Run II detector. The detector is approximately symmetric around the collision point. . . . .	8
5.1	Distributions in the invariant mass, $M_{inv}(\ell^+\ell^-)$ , for $Z \rightarrow e^+e^-$ events (upper figure) and $Z \rightarrow \mu^+\mu^-$ events (lower figure). Points represent observed data. The distributions expected from the Standard Model are shown as the stacked histograms. . . . .	18
5.2	Distributions in transverse momentum, $p_T$ , for $Z \rightarrow e^+e^-$ events (upper figure) and $Z \rightarrow \mu^+\mu^-$ events (lower figure). The distributions expected from the Standard Model are shown as stacked histograms. Points represent observed data. We have selected events with $66 < M_{inv}(\ell^+\ell^-) < 116$ GeV for these histograms. . . . .	20
5.3	Distributions in total transverse energy, $H_T$ , for $Z \rightarrow e^+e^-$ events (upper figure) and $Z \rightarrow \mu^+\mu^-$ events (lower figure). The distributions expected from the Standard Model are shown as stacked histograms. Points represent observed data. We have selected events with $66 < M_{inv}(\ell^+\ell^-) < 116$ GeV for these histograms. . . . .	21
5.4	Distributions in missing transverse momentum, $\cancel{E}_T$ , for $Z \rightarrow e^+e^-$ events (upper figure) and $Z \rightarrow \mu^+\mu^-$ events (lower figure). The distributions expected from the Standard Model are shown as stacked histograms. Points represent observed data. We have selected events with $66 < M_{inv}(\ell^+\ell^-) < 116$ GeV for these histograms. . . . .	22
5.5	Distributions in number of jets for $Z \rightarrow e^+e^-$ events (upper figure) and $Z \rightarrow \mu^+\mu^-$ events (lower figure). The distributions expected from the Standard Model are shown as stacked histograms. Points represent observed data. We have selected events with $66 < M_{inv}(\ell^+\ell^-) < 116$ GeV for these histograms. . . . .	23

5.6	Distributions in rapidity of $Z$ -bosons for $Z \rightarrow e^+e^-$ events (upper figure) and $Z \rightarrow \mu^+\mu^-$ events (lower figure). The distributions expected from the Standard Model are shown as stacked histograms. Points represent observed data. We have selected events with $66 < M_{inv}(\ell^+\ell^-) < 116$ GeV for these histograms. . . . .	24
5.7	Distributions in pseudo rapidity, $\eta$ , of the leptons (electrons or muons) observed in $Z \rightarrow e^+e^-$ events (upper figure) and $Z \rightarrow \mu^+\mu^-$ events (lower figure). The distributions observed from data are presented with points. The expected distributions are shown as stacked histograms. . . . .	25
5.8	Distributions in transverse momentum, $p_T$ , of the leptons observed in $Z \rightarrow e^+e^-$ events (upper figure) and $Z \rightarrow \mu^+\mu^-$ events (lower figure). Points represent observed data. Stacked histograms correspond to Standard Model predictions. . . . .	26
6.1	Distributions in transverse mass, $M_{trans}(\ell\nu)$ , for $W \rightarrow e\nu$ events (upper figure) and $W \rightarrow \mu\nu$ events (lower figure). Observed data are presented with points. Predictions of the Standard Model are shown with stacked histograms. . . . .	28
6.2	Distributions in total transverse energy, $H_T$ , for $W \rightarrow e\nu$ events (upper figure) and $W \rightarrow \mu\nu$ events (lower figure), where $M_{trans}(\ell\nu) > 20$ GeV. The discrepancy at large $H_T$ in the <code>wewk8m</code> ( $W \rightarrow \mu\nu$ ) muon sample does not appear in the analogous plot for $Z \rightarrow \mu^+\mu^-$ , and so has no effect on this analysis. Observed data are shown with points. The expected distributions are presented with stacked histograms. . . . .	29
6.3	Distributions in missing transverse energy, $\cancel{E}_T$ , for $W \rightarrow e\nu$ events (upper figure) and $W \rightarrow \mu\nu$ events (lower figure), where $M_{trans}(\ell\nu) > 20$ GeV. Observed data are shown with points. The expected distributions are presented with stacked histograms. . . . .	30
6.4	Distributions in number of jets, $N_{jets}$ , for $W \rightarrow e\nu$ events (upper figure) and $W \rightarrow \mu\nu$ events (lower figure), where $M_{trans}(\ell\nu) > 20$ GeV. Observed data are shown with points. The expected distributions are presented with stacked histograms. . . . .	31
6.5	Distributions in transverse momentum, $p_T$ , of the charged lepton in $W \rightarrow e\nu$ events (upper figure) and $W \rightarrow \mu\nu$ events (lower figure), where $M_{trans}(\ell\nu) > 20$ GeV. Observed data are shown with points. The expected distributions are presented with stacked histograms. . . . .	32

6.6	A further check of the lepton and $\cancel{E}_T$ modeling of the simulations: Distributions in pseudo rapidity, $\eta$ , of the leptons in $W \rightarrow e\nu$ events (upper figure) and $W \rightarrow \mu\nu$ events (lower figure). Positive-charge leptons are shown by squares (data) and the green line (SM simulations); negative-charge by triangles (data) and the red line (SM simulations). . . . .	33
7.1	Distributions in missing transverse energy, $\cancel{E}_T$ , for $W \rightarrow e\nu$ events with 1, 2, 3, and 4 or more jets, where $M_{trans}(\ell\nu)$ is more than 20 GeV and $\cancel{E}_T$ is not required to be greater than 25 GeV. The observed distributions are compared to those from SM expectations and non- $W$ events (labeled “anti-selected-electron” in text) in order to estimate the QCD background. . . . .	39
7.2	Distributions in missing transverse energy, $\cancel{E}_T$ , for $W \rightarrow \mu\nu$ events with 1, 2, 3, and 4 or more jets, where $M_{trans}(\ell\nu)$ is more than 20 GeV and $\cancel{E}_T$ is not required to be greater than 25 GeV. The observed distributions are compared to those from SM expectations and non- $W$ events (labeled “anti-selected-electron in text) in order to estimate the QCD background. . . . .	40
7.3	The distribution $ \vec{P}(\mu^+\mu^-) $ of muon pairs from $Z$ -boson candidates (solid), expected events from MC simulations (stacked histogram), and from a cosmic ray sample (dashed). Cosmic ray muons produce a very narrow peak at $ \vec{P}(\mu^+\mu^-)  = 0$ GeV, while real $Z \rightarrow \mu^+\mu^-$ decays occupy only a small area in the 3-dimensional phase space near $ \vec{P}(\mu^+\mu^-)  = 0$ . The most probable number of cosmic ray events in the search sample is zero. . . . .	42
11.1	Distributions in missing transverse energy, $\cancel{E}_T$ , for $W \rightarrow e\nu$ events with 1, 2, 3, and 4 or more jets, where $M_{trans}(\ell\cancel{E}_T)$ is more than 20 GeV, $\cancel{E}_T$ is not required to be greater than 25 GeV, and at least one jet is b-tagged. The observed distributions are compared to those from SM expectations and non- $W$ events (labeled “anti-electron” in text) in order to estimate the QCD background. We let the overall normalization float. . . . .	52
11.2	Distributions in missing transverse energy, $\cancel{E}_T$ , for $W \rightarrow \mu\nu$ events with 1, 2, 3, and 4 or more jets, where $M_{trans}(\ell\cancel{E}_T)$ is more than 20 GeV, $\cancel{E}_T$ is not required to be greater than 25 GeV, and at least one jet is b-tagged. The observed distributions are compared to those from SM expectations and non- $W$ events (labeled “anti-electron” in text) in order to estimate the QCD background. We let the overall normalization float. . . . .	53

11.3	The measured distributions (points) in the number of jets in $W \rightarrow e\nu$ events (upper figure) and $W \rightarrow \mu\nu$ events (lower figure) with at least one b-tagged jet and $M_{trans} > 20$ GeV, compared to SM expectations (stacked histogram). . . . .	54
11.4	The measured distribution (points) in total transverse momentum, $H_T$ , in events with a b-tagged jet and $M_{trans}(\ell E_T > 20$ GeV, compared to SM expectations (stacked histogram), for the $W \rightarrow e\nu$ events (upper figure) and the $W \rightarrow \mu\nu$ events (lower figure). . . . .	55
13.1	The measured distribution (points) in the number of jets in events with a $Z$ and a b-tag, compared to SM expectations (stacked histogram), for the electron channel (upper figure) and the muon channel (lower figure). We normalize to the average of the $Z \rightarrow e^+e^-$ and $Z \rightarrow \mu^+\mu^-$ 2-jet bins. The 1-jet bin is not used in this measurement.	62
13.2	The measured distribution (points) in the fitted top mass in events with a $Z$ and four jets with at least one b-tagged jet, compared to the SM expectations (stacked histogram), for $Z \rightarrow e^+e^-$ events (upper figure) and $Z \rightarrow \mu^+\mu^-$ events (lower figure). . . . .	66
13.3	The measured distribution (points) in the fitted top $\chi^2$ in events with a $Z$ and four jets with at least one B-tagged jet, compared to the SM expectations (stacked histogram), for the electron channel (upper figure) and for the muon channel (lower figure). . . . .	67
14.1	The measured distribution (points) in the number of jets in events with an inclusive decay of $Z \rightarrow \mu^+\mu^-$ , compared to SM expectations (stacked histogram). The “Z+Jets” processes (Drell-Yan, Z+b, and Z+c) are modeled with ALPGEN. . . . .	74
14.2	The ratio between the measured distribution (DATA) and the SM expectations (MC) in the number of jets in events with an inclusive decay of $Z \rightarrow \mu^+\mu^-$ . The “Z+jets” processes (Drell-Yan, Z+b, and Z+c) contribution to the SM expectations are modeled with ALPGEN.	75
15.1	The likelihood distribution $L(B_Z, N_{t\bar{t}})$ calculated as a function of $N_{t\bar{t}}$ and $Br(t \rightarrow Zc)$ . The distribution shown is for FCNC decays of $t \rightarrow Zc$ with 100% longitudinally polarized $Z$ -bosons. . . . .	81
15.2	The distribution for $P(B_Z DATA)$ , calculated for 100% longitudinally polarized $Z$ -bosons. . . . .	83

## LIST OF TABLES

5.1	Summary of the acceptance-times-efficiency for inclusive $Z$ production measured from the Monte Carlo samples. . . . .	17
5.2	Comparison of the numbers of observed $Z$ +jets events versus expectations. . . . .	19
6.1	Summary of the acceptance-times-efficiency for inclusive $W$ production measured from the Monte Carlo samples. . . . .	34
6.2	Summary of the numbers of inclusive $W$ events observed in the data compared to Standard Model simulations. The Background fractions correspond to events where there are no real $W$ -bosons. . . . .	34
7.1	Fractions of non- $W$ events in events with one tight lepton and no other leptons, and with $\cancel{E}_T > 25$ GeV and $M_{trans}(\ell + \cancel{E}_T) > 20$ GeV. . . . .	38
11.1	Fractions of the non- $W$ QCD events in events with a tight lepton ( $e$ or $\mu$ ), $\cancel{E}_T > 25$ GeV, $M_{trans}(\ell \cancel{E}_T) > 20$ GeV, and at least one B-tagged jet. (The fit for $W \rightarrow \mu\nu + 4$ jets returned 0 events due to the low statistics of the sample. In any case this number should be comparable with the one for inclusive $W$ 's so we take 2.6% for the tagged sample.) . . . . .	51
11.2	The acceptance times efficiency for inclusive $t\bar{t} \rightarrow WbWb$ production measured from the Monte Carlo samples. . . . .	56
11.3	Summary of the numbers of “ $W + 4$ jets” events. At least one jet in each event is required to be B-tagged. . . . .	56
13.1	The acceptance times efficiency for the dilepton signature from inclusive FCNC decay of $t\bar{t} \rightarrow ZcZc \rightarrow l^+l^- + ccjj$ for different values of the longitudinal fraction of $Z$ bosons, for electron pairs and muon pairs separately. The SM branching ratios for the $Z \rightarrow \ell^+\ell^-$ decays are included. Note that this channel depends on the square of the FCNC branching ratio for the $Z$ , and so its contribution is suppressed relative to that from the case where only one $Z$ decays by FCNC (see Table 13.2). . . . .	63

13.2	Summary of the acceptance times efficiency for the dilepton signature from inclusive FCNC decays of $t\bar{t} \rightarrow ZcWb \rightarrow \ell^+\ell^- + cj\bar{j}b$ , for different values of the longitudinal fraction of $Z$ bosons, for electron pairs and muon pairs separately. Note that the FCNC branching ratio enters only to the first power, and so this would be the dominant contribution to the FCNC signal. . . . .	63
13.3	Summary of the acceptance times efficiency for the contribution to the single lepton + $\cancel{E}_T$ signature from the inclusive FCNC decays of $t\bar{t} \rightarrow WbZc \rightarrow \ell\cancel{E}_T + cj\bar{j}b$ (i.e. the decay of a $Z$ boson is mis-identified as the decay of a $W$ boson) and $t\bar{t} \rightarrow WbZc \rightarrow \ell\nu + bj\bar{j}c$ . Standard model branching ratios are included. The acceptance $A_{WZ \rightarrow \ell\cancel{E}_T}$ is the sum of acceptances for the both decay modes which contribute to the signature of $\ell + \cancel{E}_T + 4jets$ . . . . .	64
13.4	The acceptance times efficiency for the contribution to the single lepton + $\cancel{E}_T$ signature from the inclusive FCNC decay of $t\bar{t} \rightarrow ZcZc \rightarrow \ell + \cancel{E}_T + cj\bar{j}c$ , where the di-leptonic decay of at least one $Z$ boson has been mis-identified as the decay of a $W$ boson. Standard model branching ratios are included. Note that this channel depends on the square of the FCNC branching ratio for the $Z$ , and so its contribution is suppressed relative to that from the case where only one $Z$ decays by FCNC (see Table 13.3). . . . .	65
14.1	Summary table of the relative systematic uncertainties on the acceptances. Correlations are taken into account in the calculation of the limit. The abbreviation $\sigma_\ell$ stands for the systematic uncertainty due to lepton identification and triggering. The lepton-related systematic uncertainties should be added separately depending to the final state used. . . . .	69
14.2	The relative systematic uncertainties on the backgrounds for 4-jet semi-leptonic and dilepton final states of $t\bar{t}$ pairs. The contributions from Monte Carlo and Mistags are (conservatively) taken to be correlated in the computation of the limit. The normalization uncertainties are contributed from the finite statistics of the 2-jet bin in $W+HF$ and $Z+HF$ samples. . . . .	73
16.1	The upper limits on the FCNC branching ratio $\text{Br}(t \rightarrow Zc)$ in % as a function of the longitudinal fraction of the $Z$ -bosons in the FCNC coupling ( $t \rightarrow Zc$ ) at 95% CL. The limits labeled “Gaussian prior” use as input the theoretical cross-section of $\sigma(p\bar{p} \rightarrow t\bar{t})$ ; the limits labeled “Flat prior” are theory-independent. . . . .	84

A.1	Summary of the muon identification cuts. "DOF" stands for degrees of freedom (i.e. the number of COT hits - 5). . . . .	85
A.2	Summary of the central (CEM) electron identification cuts. . . . .	86
A.3	Summary of the plug (PEM) electron identification cuts. . . . .	86
B.1	Summary of the lepton scale factors. The Monte Carlo efficiencies are <i>multiplied</i> by these to match those in the data. . . . .	87
B.2	Summary of the lepton trigger efficiencies. The Monte Carlo events are re-weighted to correct for the trigger inefficiencies. . . . .	87
C.1	Summary of cuts for selection of Central Photons. . . . .	88
D.1	The Monte Carlo-simulated samples used for the SM backgrounds in the analysis. Variable $K$ is a scale factor; it is a ratio between LO and NLO cross-sections. . . . .	89
E.1	Summary of the numbers of interest for electron and muon datasets. The table includes acceptances, efficiencies, numbers of background events, and numbers of observed events. . . . .	91
F.1	Summary of event number 184466/383360. The event contains a $Z$ boson and four jets. . . . .	92
F.2	Summary of event number 183097/3797423. The event contains a $Z$ boson and four jets. . . . .	92
F.3	Summary of event number 203509/331412. The event contains a $Z$ boson and four jets. . . . .	93
F.4	Summary of event number 221532/2166426. The event contains a $Z$ boson and four jets. . . . .	93
F.5	Summary of event number 222322/2329377. The event contains a $Z$ boson and four jets. . . . .	94
F.6	Summary of event number 222801/1282328. The event contains a $Z$ boson and four jets. . . . .	94
F.7	Summary of event number 196368/115764. The event contains a $Z$ boson and four jets. . . . .	95
F.8	Summary of event number 192987/336742. The event contains a $Z$ boson and four jets. . . . .	95
F.9	Summary of event number 203190/7183703. The event contains a $Z$ boson and four jets. . . . .	96
F.10	Summary of event number 178684/2540865. The event contains a $Z$ boson and four jets. . . . .	96
F.11	Summary of event number 151974/194905. The event contains a $Z$ boson and four jets. . . . .	97

F.12	Summary of event number 164352/57731. The event contains a $Z$ boson and four jets. . . . .	97
F.13	Summary of event number 166779/3467414. The event contains a $Z$ boson and four jets. . . . .	98
F.14	Summary of event number 222271/20319806. The event contains a $Z$ boson and four jets. . . . .	98

# CHAPTER 1

## INTRODUCTION

Physics is the way we understand basic processes of nature quantitatively. A set of ideas describing some set of the processes is called a “physical model”. A physical model is developed by expanding its coverage to describe new phenomena that contradict the previous model. Our study is an attempt to find a specific contradiction between the observed data and predictions of the Standard Model (SM). Unfortunately, we were not able to find any statistically significant discrepancies so we ended setting a limit on the measured quantity.

New phenomena in particle physics are more and more challenging to discover. Often a discovery requires finding a small anomaly in a large amount of experimental data. The anomaly should not be caused by detector effects or poor SM predictions so that it demands precise modeling of the SM processes. Some SM processes are not easy to describe accurately using existing Monte Carlo simulations. In the end a number of systematic uncertainties must be thoroughly understood to make an analysis robust.

In our analysis we look for Beyond the Standard Model (BSM) events where we do not expect any significant backgrounds from SM processes. Therefore, any signal is an indication that we see a new physical phenomenon.

The existing SM simulations are required to be tuned using the observed data. The observed data are divided into signal and control regions. The control regions

are used to adjust the SM expectations, which are then propagated into the signal regions. This approach makes the analysis robust against theory-driven uncertainties.

The Standard Model allows the top quark to decay only to an on-shell  $W$ -boson and another quark at tree level. The quark can have bottom, strange, or down flavor. Decays with the bottom quark have the highest branching ratio. The present measured top quark's mass is value of the  $170.9 \pm 1.8$  GeV. The top quark is heavier than sum of the mass of the  $W$ -boson and the other quark so that the produced  $W$ -bosons are on-shell.

The SM does not allow any Flavor Changing Neutral Current (FCNC)  $t \rightarrow Zc$  decays to happen at tree level. The SM decays  $t \rightarrow Zc$  are suppressed since the SM Lagrangian does not contain any flavor-changing neutral terms such as  $d \rightarrow s$  as an algebraic consequence of its SU(2) structure [1]. The decay proceeds only through radiative corrections, with a predicted branching ratio  $\text{Br}(t \rightarrow Zc)$  of about  $10^{-14}$  [2]. The decays are associated with the neutral current since the charge of the produced quark is the same as that of the top quark. The ‘‘Flavor Changing’’ indicates that the produced quark has a different flavor from that of top (i.e. the flavor must be ‘‘charm’’ or ‘‘up’’ in the case of the FCNC decays of the top quarks).

Some extensions of the SM predict measurable rates of the  $t \rightarrow Zc$  decays [1, 3, 4] and the Tevatron affords us the unique opportunity to search for the FCNC decays as it is the only place where the top quarks can be produced directly until the LHC turns on. Observation of *any* signal will be a sign of new physics.

The production of top quark pairs,  $t\bar{t}$ , is the preferred channel at the Tevatron to observe the FCNC transition  $t \rightarrow c$ , as single top production would have a smaller cross-section and much larger QCD backgrounds in the  $Zc$  final state. We have used the CDF-II detector [5] to search for the case in which one of the top quarks decays to

$Zc$  and the other one decays to  $Wb$ . In order to get a sample of high purity, we select the leptonic decays of the  $Z$ -boson,  $Z \rightarrow e^+e^-$  and  $Z \rightarrow \mu^+\mu^-$ . In this scenario, the FCNC signature is a pair of oppositely-charged leptons forming a  $Z$ -boson, and four jets (the  $Z$ -boson decays leptonically and the  $W$ -boson decays hadronically), with the event being kinematically consistent with the FCNC  $t\bar{t}$  decay hypothesis. In addition, we require at least one displaced secondary vertex as a sign of heavy-flavor quark (b or c-quark) to further suppress hadronic backgrounds.

To minimize the systematic uncertainties on the particle identification and trigger efficiencies, geometric acceptances, and luminosity, we use a technique based on the simultaneous comparison of two decay chains using events in two final states:

1.  $p\bar{p} \rightarrow t\bar{t} \rightarrow WbWb \rightarrow \ell\nu bj\bar{j}b$  (see Figure 1.1),
2.  $p\bar{p} \rightarrow t\bar{t} \rightarrow ZcWb \rightarrow \ell^+\ell^- cj\bar{j}b$  (see Figure 1.2).

Many of the systematic uncertainties contributing to both decay chains are correlated and tend to cancel, improving the precision and robustness of the result.

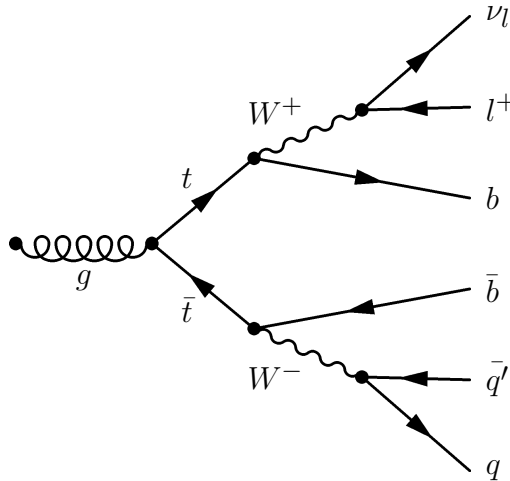


Figure 1.1: A Feynman diagram for one of the processes contributing to  $t\bar{t} \rightarrow WbWb \rightarrow \ell\nu bj\bar{j}b$  decay chain. The  $t\bar{t}$  pair is produced in a collision of  $p$  and  $\bar{p}$ .

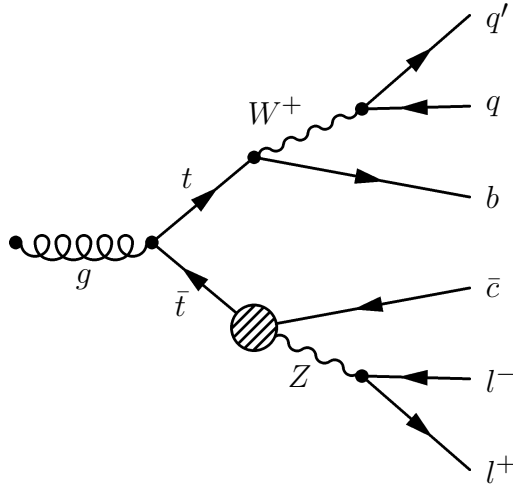


Figure 1.2: A Feynman diagram for one of the processes contributing to  $t\bar{t} \rightarrow ZcWb \rightarrow llcjjb$  decay chain. The  $t\bar{t}$  pair is produced in a collision of  $p$  and  $\bar{p}$ .

The final states  $l\nu bj\bar{j}b$  and  $l^+l^-cj\bar{j}b$  contain products of the leptonic decays of  $W \rightarrow l\nu$  and  $Z \rightarrow ll$ . Therefore, a comparison of inclusive  $W \rightarrow l\nu$  and  $Z \rightarrow ll$  production, for which there exists a precise NNLO prediction [6], allows us to validate the lepton identification and trigger efficiencies in the Monte Carlo predictions of signal and SM backgrounds to a few percent. We use a measurement of the value of the ratio  $R$ , defined as:

$$R = \frac{\sigma(W^\pm) \cdot BR(W \rightarrow e\nu)}{\sigma(Z) \cdot BR(Z \rightarrow e^+e^-)} \quad (1.1)$$

for this check.

The present study employs leptonic decays of  $W$ 's and  $Z$ 's using data collected at CDF Run II at the Tevatron up to 31st of January of 2007. The data correspond to an integrated luminosity of  $1.52 \text{ fb}^{-1}$ . All events are triggered with high- $p_T$  electrons and muons.

The current limit on the branching ratio for  $t \rightarrow Zc$  cited by the PDG [7] is from CDF using data from Run I of the Tevatron; the limit is 33% at 95% C.L. [8]. The limit from indirect precision measurements at LEP is lower, 13.7% at 95% C.L. [9].

There is a recently published CDF limit using a different technique, of 3.7% at 95% C.L., more restrictive than the result presented here [10].

## CHAPTER 2

### APPARATUS: THE CDF II DETECTOR

The CDF II detector is a cylindrically-symmetric spectrometer designed to study  $p\bar{p}$  collisions at the Fermilab Tevatron. The collisions occur at  $\sqrt{s} = 1.96$  TeV every 396 ns. The detector has already been described in detail in the literature [5]. An elevation view of the CDF II detector is presented in Figure 2.1. Here we briefly describe the detector subsystems relevant for the analysis.

Tracking systems are used to measure the momenta of charged particles and to trigger on and identify leptons with large transverse momentum [11]. A multi-layer system of silicon strip detectors [12], which identifies tracks in both the  $r - \phi$  and  $r - z$  views [13], and the central outer tracker (COT) [14] are contained in a superconducting solenoid that generates a magnetic field of 1.4 T. The COT is a 3.1 m long open-cell drift chamber that makes up to 96 measurements along the track of each charged particle in the region  $|\eta| < 1$ . Sense wires are arranged in 8 alternating axial and  $\pm 2^\circ$  stereo super-layers with 12 wires each. For high momentum tracks, the COT  $p_T$  resolution is  $\sigma_{p_T}/p_T^2 \simeq 0.0017 \text{ GeV}^{-1}$ .

Segmented calorimeters with towers arranged in a projective geometry, each tower consisting of an electromagnetic and a hadronic compartment [15, 16], cover the central region,  $|\eta| < 1$  (CEM/CHA), and the ‘end plug’ region,  $1 < |\eta| < 3.6$  (PEM/PHA). In both the central and end plug regions, systems with finer spatial resolution are used to make profile measurements of electromagnetic showers at shower maximum [17] for electron identification (the CES and PES systems,

respectively). Electrons are reconstructed in the CEM with an  $E_T$  resolution of  $\sigma(E_T)/E_T \simeq 13.5\%/\sqrt{E_T/\text{GeV}} \oplus 2\%$  [15] and in the PEM with an  $E_T$  resolution of  $\sigma(E_T)/E_T \simeq 16.0\%/\sqrt{E_T/\text{GeV}} \oplus 1\%$  [18]. Jets are identified using a cone in  $\eta - \phi$  space [13] of radius 0.4 as a group of electromagnetic and hadronic calorimeter towers; the jet energy resolution is approximately  $\sigma \simeq 0.1 \cdot E_T(\text{GeV}) + 1.0 \text{ GeV}$  [19].

Muons are identified using the central CMU, CMP, and CMX [20, 21] muon systems, which cover the kinematic region  $|\eta| < 1$ . The CMU system uses four layers of planar drift chambers to detect muons with  $p_T > 1.4 \text{ GeV}$  in the central region of  $|\eta| < 0.6$ . The CMP system consists of an additional four layers of planar drift chambers located behind 0.6 m of steel outside the magnetic return yoke, and detects muons with  $p_T > 2.0 \text{ GeV}$ . The CMX detects muons in the region  $0.6 < |\eta| < 1.0$  with four to eight layers of drift chambers, depending on the polar angle.

The beam luminosity is measured using two sets of gas Cherenkov counters, located in the region  $3.7 < |\eta| < 4.7$ . The total uncertainty on the luminosity is estimated to be 5.9%, where 4.4% comes from the acceptance and operation of the luminosity monitor and 4.0% from the calculation of the inelastic  $p\bar{p}$  cross-section [22].

A 3-level trigger system [5] selects events for further analysis offline. The first two levels of triggers consist of dedicated fast digital electronics analyzing a subset of the full detector data. The third level, applied to the full data from the detector for those events passing the first two levels, consists of a farm of computers that reconstruct the data and apply selection criteria for (typically) several hundred distinct triggers.

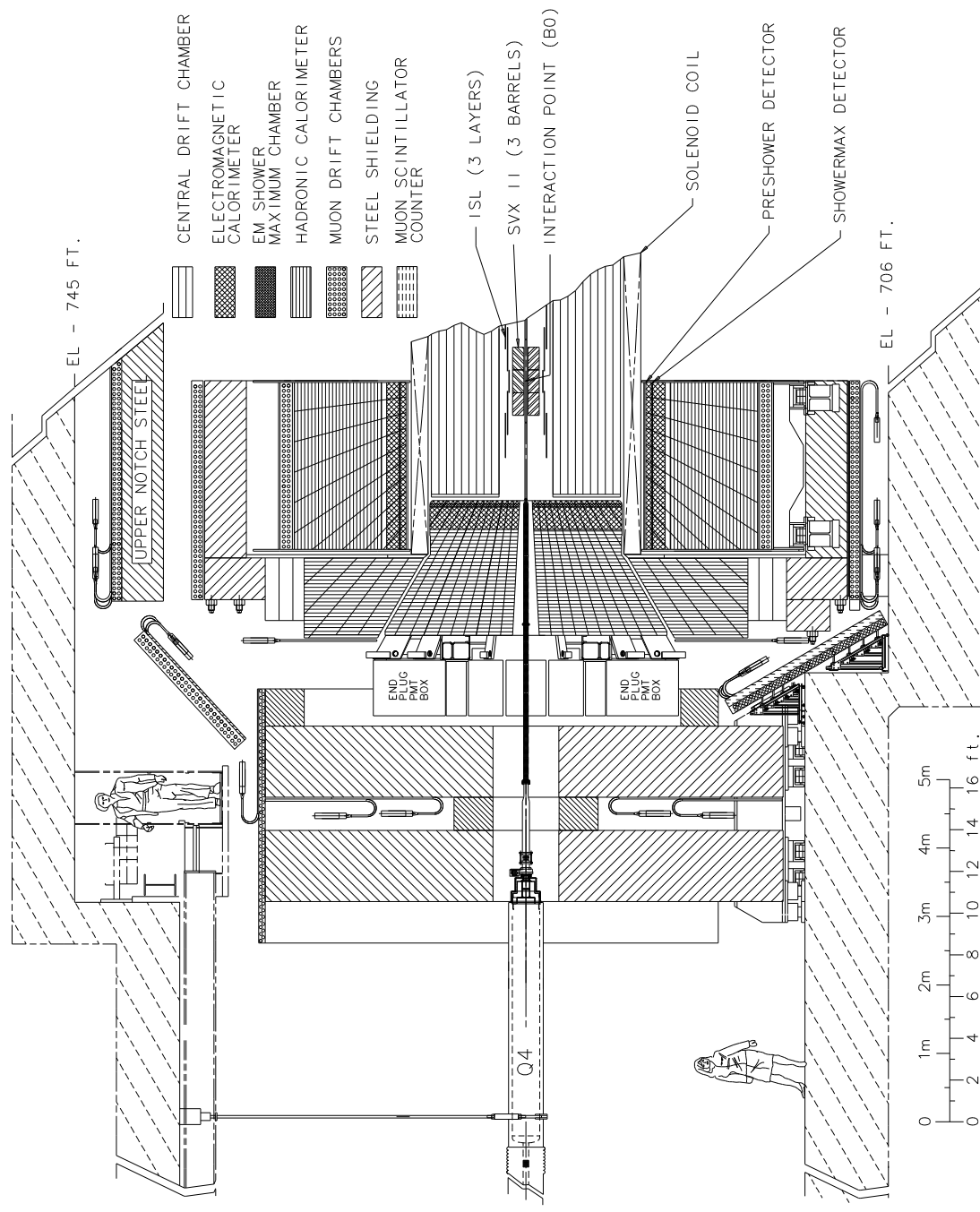


Figure 2.1: An elevation view of one half of the CDF Run II detector. The detector is approximately symmetric around the collision point.

## CHAPTER 3

### INTRODUCTION TO THE ANALYSIS STRATEGY

The measurement of the branching ratio of  $t \rightarrow Zc$  decay mode is designed to be similar to the measurement of the  $R$ -ratio between inclusive cross-section of  $W$ 's to  $Z$ 's. The ratio  $R$  is defined as:

$$R = \frac{\sigma(W)Br(W \rightarrow \ell\nu)}{\sigma(Z)Br(Z \rightarrow \ell^+\ell^-)}, \quad (3.1)$$

where  $\sigma(W)$  and  $\sigma(Z)$  are cross-sections of inclusively produced  $W$  and  $Z$  bosons. A measurement of the  $R$ -ratio is itself a precise test of lepton identification efficiencies, triggering, and Monte Carlo simulations. A measured  $R$ -ratio has smaller uncertainties than  $\sigma(W)$  and  $\sigma(Z)$  since some of the uncertainties (e.g. for integrated luminosity) completely cancel out. This makes  $R$  a valuable tool for precise comparisons between experimental and theoretical predictions for channels involving both  $W$  and  $Z$  bosons.

We estimate  $R$  for electrons and muons separately (see Chapter 8) since these particles rely on different detector subsystems. The agreement between the theoretical prediction and observed numbers is good [23]. This cross-check was performed before measuring the branching ratio  $Br(t \rightarrow Zc)$ .

The measurement of  $Br(t \rightarrow Zc)$  is designed as the measurement of the ratio between events with a  $Z$  boson and four jets to events with a  $W$  boson and four jets. The FCNC signal from  $t\bar{t}$  decays is expected to affect the rate of  $Z + 4$  jets events

primarily when the majority of the Standard Model  $t\bar{t}$  decays are contributing to events with a  $W$  and four jets. We subtract SM non- $t\bar{t}$  events from the event with a  $W$  or a  $Z$  boson and four jets so that the ratio is more sensitive to the FCNC signal. The ratio of  $Z + 4$  jets to  $W + 4$  jets increases in presence of FCNC events.

## CHAPTER 4

### EVENT SELECTION

The analysis uses events selected by the trigger system that contain either a central electron with  $E_T > 18$  GeV or a muon with  $p_T > 18$  GeV [11]. The electron dataset contains 75,466,634 events; the muon dataset contains 21,251,395 events. The integrated luminosity of each dataset is  $1.52 \text{ fb}^{-1}$ .

Both the observed and the simulated events are processed through the same selection criteria to identify electrons and muons, jets,  $W$  and  $Z$  bosons, missing transverse energy, and jets containing heavy flavor. Details of the selection criteria are provided below.

#### 4.1 Lepton Identification

We use standard CDF definitions for identification (ID) of electrons and muons, described below. The same lepton ID requirements are applied to events from data and Monte Carlo simulations.

The identification and triggering efficiencies for leptons are different for events in data and Monte Carlo though they demonstrate a very similar energy dependence. To eliminate this inconsistency we follow the CDF policy of using correction factors (‘scale factors’) to re-weight the MC events (see Section 4.1.3).

In order to maintain a high efficiency for  $Z$  bosons, for which we require two identified leptons, we define ‘tight’ and ‘loose’ selection criteria for both electrons and muons, as described below.

To reduce backgrounds to leptons from the decays of hadrons produced in jets, leptons are required to be “isolated”. The  $E_T$  deposited in the calorimeter towers in a cone in  $\eta - \varphi$  space [13] of radius  $R = 0.4$  around the lepton position is summed, and the  $E_T$  due to the lepton is subtracted. The remaining  $E_T$  is required to be less than 10% of the lepton  $E_T$  for electrons or  $p_T$  for muons.

#### 4.1.1 Electron Selection

An electron candidate passing the “tight” selection [24, 25] must have: a) a high-quality track with  $p_T > 0.5 \cdot E_T$ , unless  $p_T > 50$  GeV; b) a good transverse shower profile at shower maximum that matches the extrapolated track position; c) a lateral sharing of energy in the two calorimeter towers containing the electron shower consistent with that expected; and d) minimal leakage into the hadron calorimeter [26].

Additional central electrons are required to have  $E_T > 12$  GeV and to satisfy the tight central electron criteria but with a track requirement of only  $p_T > 10$  GeV (rather than  $0.5 \cdot E_T$ ), and no requirement on a shower maximum measurement or lateral energy sharing between calorimeter towers. The summary of the selection requirements for the central electrons is presented in Table A.2. Electrons in the end-plug calorimeters [27] ( $1.2 < |\eta| < 2.5$ ) are required to have  $E_T > 12$  GeV, minimal leakage into the hadron calorimeter, a “track” containing at least 3 hits in the silicon tracking system, and a shower transverse shape consistent with that expected, with a centroid close to the extrapolated position of the track [28]. The

full list of identification requirements for the plug electrons is presented in Table A.3. Any additional electrons in event are classified as “loose” leptons.

### 4.1.2 Muon Selection

A muon candidate passing the “tight” cuts [29] must have: a) a well-measured track in the COT with  $p_T > 20$  GeV; b) energy deposited in the calorimeter consistent with expectations [30]; c) a muon track [31] in both the CMU and CMP, or in the CMX, consistent with the extrapolated COT track [32]; and d) COT timing consistent with a track from a  $p\bar{p}$  collision [33].

Additional muons are required to have  $p_T > 12$  GeV and to satisfy the same criteria as for “tight” muons but with fewer hits required on the track, or, alternatively, for muons outside the muon system fiducial volume, a more stringent cut on track quality but no requirement that there be a matching track in the muon systems [34].

A detailed summary of muon selection criteria is presented in Table A.1 .

### 4.1.3 Corrections due to modeling of electrons and muons in the MC events

Following the standard treatment of lepton efficiencies in CDF, we re-weight Monte Carlo events to take into account the difference between the identification efficiencies [29, 35] measured in leptonic  $Z$  decays and those used in simulation [36]. We then make additional corrections for the difference in trigger efficiencies in simulated events and measured in data. Corrections to trigger efficiencies are typically 4% for tight electrons, 8% for tight muons that traverse both the CMU and CMP systems,

and 5% for muons in the CMX system. The full list of corrections is presented in Tables B.1 and B.2. The electron triggering is described in Ref. [37].

## 4.2 Jet Identification

Jets are reconstructed using the standard CDF cone clustering algorithm with a cone radius of  $R = 0.4$  and within  $|\eta| < 2.4$ . The jet energies are corrected for the eta-dependent response of the calorimeters and for the luminosity-dependent effect of multiple- $p\bar{p}$  interactions; the absolute jet energy scale is then set to match that from PYTHIA Monte Carlo dijet events [38]. The raw energy of the jets must be greater than 8 GeV and the corrected energy is required to be greater than 15 GeV. Jets that coincide with an identified electron or photon are removed; i.e. each calorimeter cluster can be associated with either a jet, an electron, or a photon which have mutually exclusive definitions to avoid any ambiguities.

## 4.3 Photon Identification

High- $p_T$  photons are not rare in hard-scattering events, and are precisely measured in the electromagnetic calorimeters, without the necessity of large energy corrections as for jets. Identifying photons as jets and then correcting them as jets can lead to mis-reconstructed missing transverse energy and other kinematic variables, and can be important in an analysis leading to small signal samples, as in this analysis.

Photon candidates [39] are required to have no track with  $p_T > 1$  GeV, and at most one track with  $p_T < 1$  GeV, pointing at the calorimeter cluster; good profiles in both transverse dimensions at shower maximum; and minimal leakage into the hadron calorimeter [26].

In addition, we require photons to be ‘isolated’ in a slightly more restrictive fashion than that for the leptons: the sum of the  $p_T$  of all tracks in the cone must be less than  $2.0 \text{ GeV} + 0.005 \times E_T$ . The photon selection criteria are summarized in Table C.1.

#### 4.4 Missing $E_T$ Reconstruction

Missing transverse energy ( $\cancel{E}_T$ ) is the negative two-dimensional vector sum of  $\vec{E}_T$  of all identified objects in the event: electrons (see Section 4.1), muons (see Section 4.1), photons (see Section 4.3), jets (see Section 4.2), and unclustered energy. The unclustered energy is calculated as a two-dimensional vector of raw calorimeter energy corrected for the energy deposited by identified jets, electrons, muons, and photons. Appropriate jet energy corrections (see Ref. [38]) are used for the identified jets for the  $\cancel{E}_T$  calculation; much smaller energy corrections are applied to electrons and photons.

#### 4.5 Additional Kinematic Variables Used In the Analysis

The kinematic structure of the events with  $W$  and  $Z$  bosons is studied using the distributions in the following variables:

- $H_T$  (Scalar sum of  $E_T$  of all reconstructed objects (electrons, muons, photons, jets, missing transverse energy, and unclustered energy)),
- Number of jets,
- $P_T(W)$  or  $P_T(Z)$  (transverse momentum of a  $W$  or a  $Z$  boson ),

- Rapidity,  $y$ , of the  $Z$ -boson,
- $E_T$  (transverse energy) of leptons (electrons and muons),
- Pseudo-rapidity ( $\eta$ ) of the leptons (+ and - separately for  $W$ 's)

## CHAPTER 5

### PRODUCTION OF $Z$ BOSONS WITH JETS

To be identified as a  $Z$ -boson a pair of opposite-sign electrons or muons must have a reconstructed invariant mass,  $M_{inv}(\ell^+\ell^-)$ , in the mass window from 66 GeV to 116 GeV. The selection of  $Z \rightarrow \ell^+\ell^-$  events requires two “tight” leptons or a “tight” and a “loose” lepton. The two leptons are required to be assigned to the same primary vertex. Figure 5.1 shows the distributions in invariant mass for electron and muon pairs.

The SM expectation for events with a  $Z$ -boson and jets is constructed using Monte Carlo simulations of SM electroweak processes such as the production of  $WW$ ,  $WZ$ ,  $ZZ$ , and  $Z \rightarrow \tau\tau$  (see Section 7).

The detection of  $Z$ -bosons is less sensitive to the lepton trigger efficiencies than the detection of  $W$ -bosons, since there are two leptons in each  $Z$  event.

$Z$ -bosons provide a good check on lepton ID efficiencies and energy scales of the leptons and jets, as one lepton serves to record the event and the other can be examined in an unbiased fashion.

Process	# of Generated events	# of Reconstructed events	$A * \epsilon$
$Z \rightarrow e^+e^-$	4043452	859332	0.2125
$Z \rightarrow \mu^+\mu^-$	3465140	467415	0.1349

Table 5.1: Summary of the acceptance-times-efficiency for inclusive  $Z$  production measured from the Monte Carlo samples.

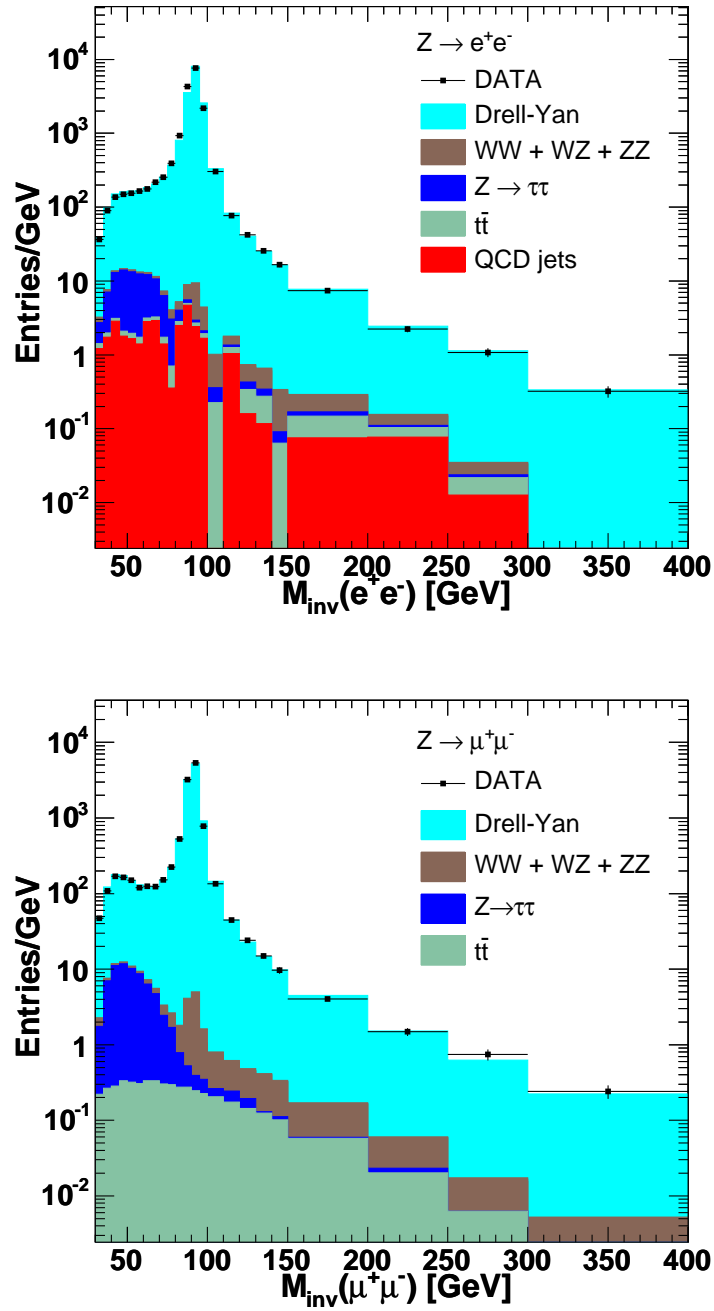


Figure 5.1: Distributions in the invariant mass,  $M_{inv}(\ell^+\ell^-)$ , for  $Z \rightarrow e^+e^-$  events (upper figure) and  $Z \rightarrow \mu^+\mu^-$  events (lower figure). Points represent observed data. The distributions expected from the Standard Model are shown as the stacked histograms.

Process	Observed	Expected “Z+jets”	Background Fraction
$Z \rightarrow e^+e^-$	82901	82641	0.4%
$Z \rightarrow \mu^+\mu^-$	53368	53237	0.25%

Table 5.2: Comparison of the numbers of observed  $Z$ +jets events versus expectations.

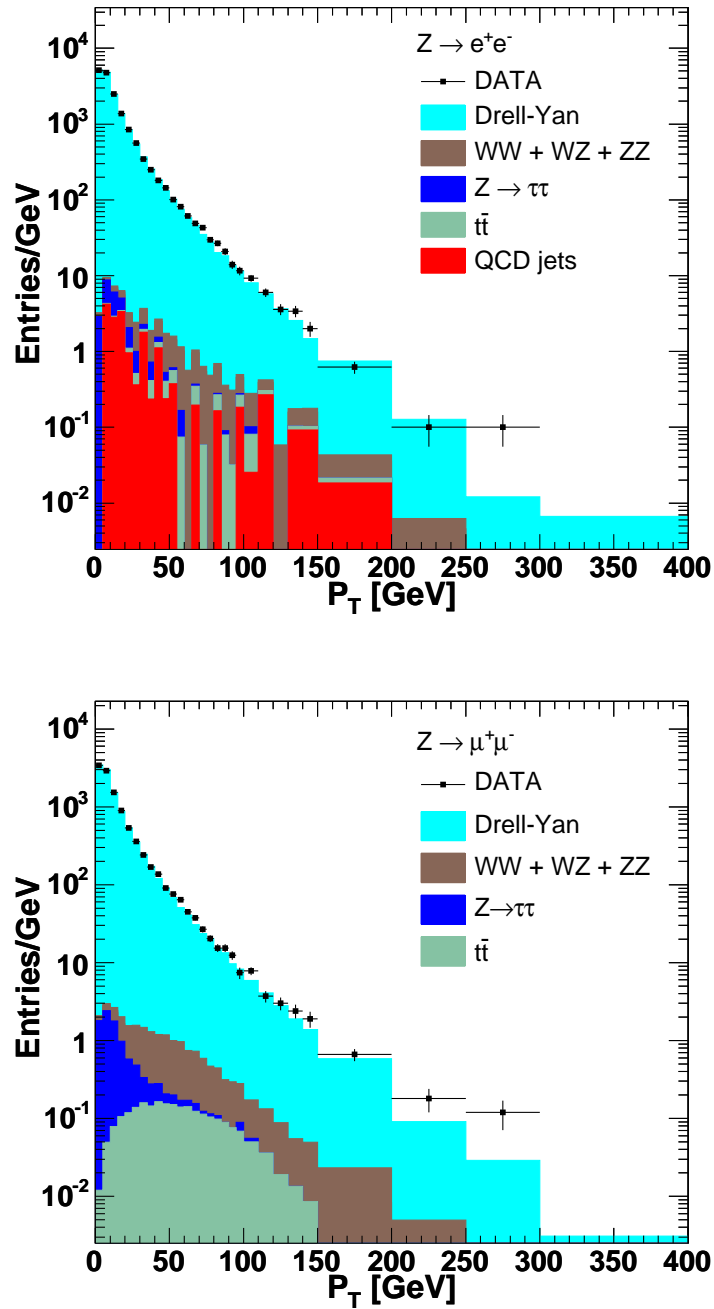


Figure 5.2: Distributions in transverse momentum,  $p_T$ , for  $Z \rightarrow e^+e^-$  events (upper figure) and  $Z \rightarrow \mu^+\mu^-$  events (lower figure). The distributions expected from the Standard Model are shown as stacked histograms. Points represent observed data. We have selected events with  $66 < M_{inv}(\ell^+\ell^-) < 116$  GeV for these histograms.

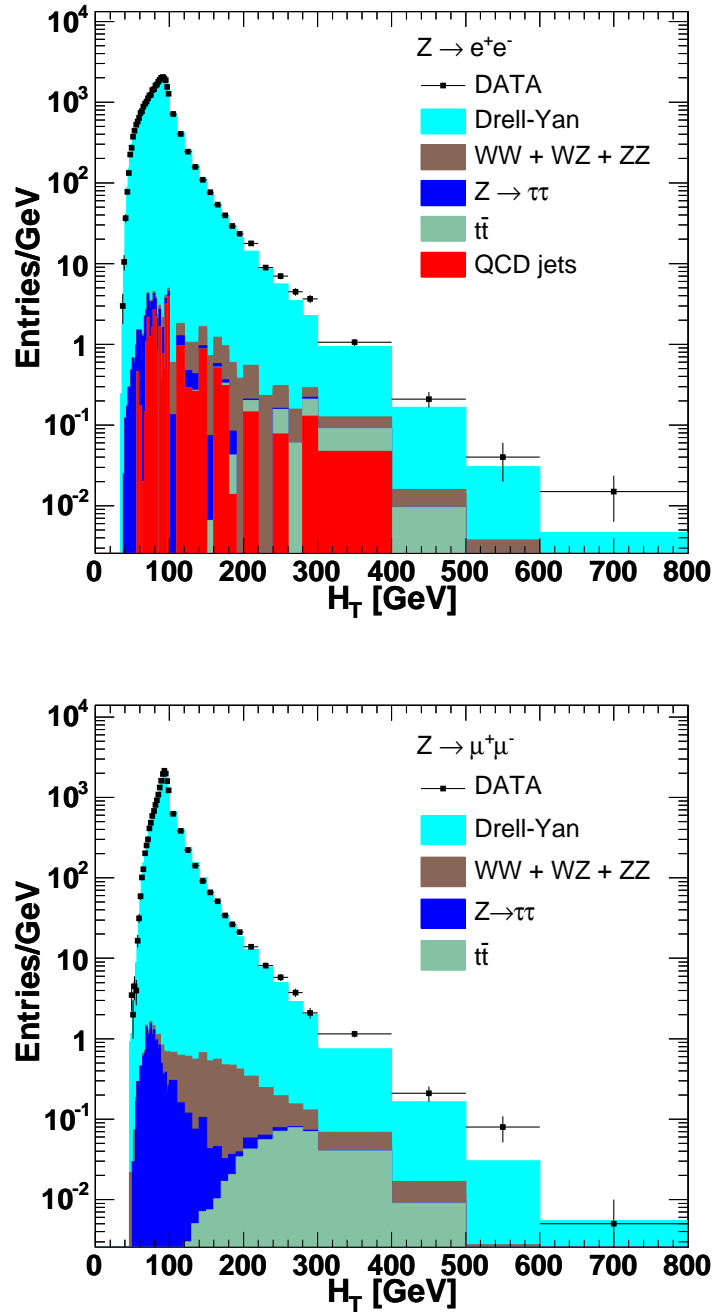


Figure 5.3: Distributions in total transverse energy,  $H_T$ , for  $Z \rightarrow e^+e^-$  events (upper figure) and  $Z \rightarrow \mu^+\mu^-$  events (lower figure). The distributions expected from the Standard Model are shown as stacked histograms. Points represent observed data. We have selected events with  $66 < M_{inv}(\ell^+\ell^-) < 116$  GeV for these histograms.

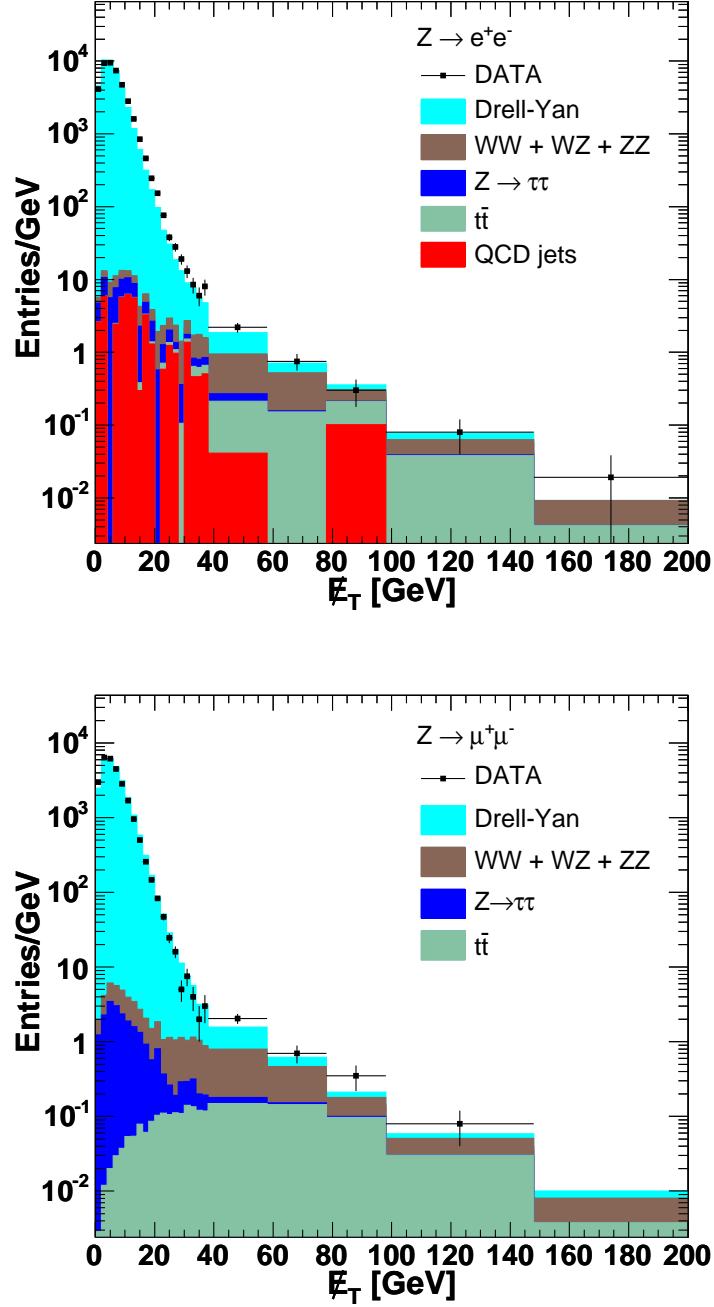


Figure 5.4: Distributions in missing transverse momentum,  $E_T$ , for  $Z \rightarrow e^+e^-$  events (upper figure) and  $Z \rightarrow \mu^+\mu^-$  events (lower figure). The distributions expected from the Standard Model are shown as stacked histograms. Points represent observed data. We have selected events with  $66 < M_{inv}(\ell^+\ell^-) < 116$  GeV for these histograms.

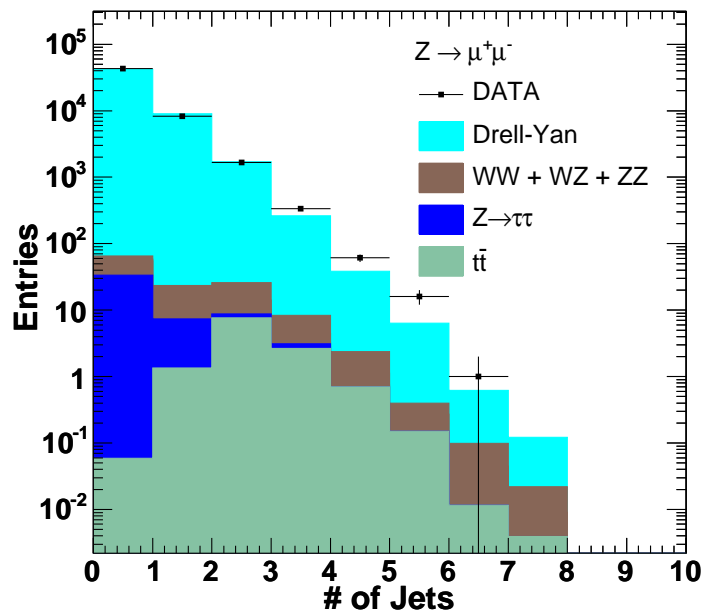
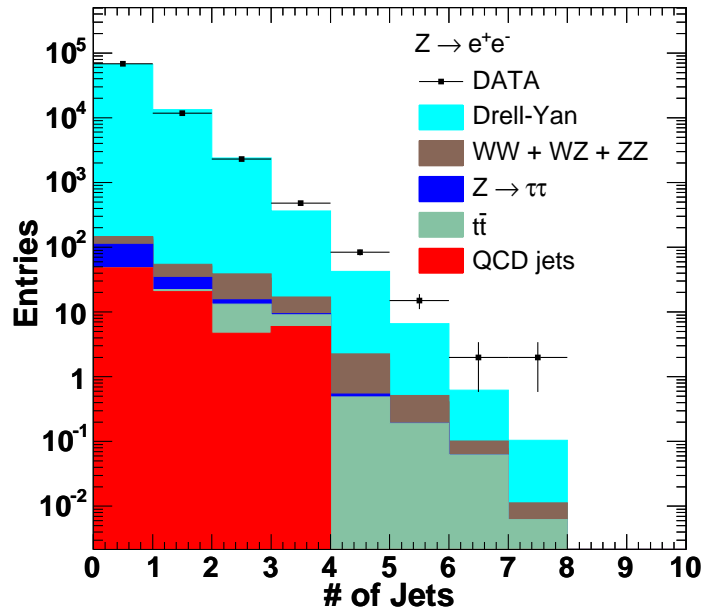


Figure 5.5: Distributions in number of jets for  $Z \rightarrow e^+e^-$  events (upper figure) and  $Z \rightarrow \mu^+\mu^-$  events (lower figure). The distributions expected from the Standard Model are shown as stacked histograms. Points represent observed data. We have selected events with  $66 < M_{inv}(\ell^+\ell^-) < 116$  GeV for these histograms.

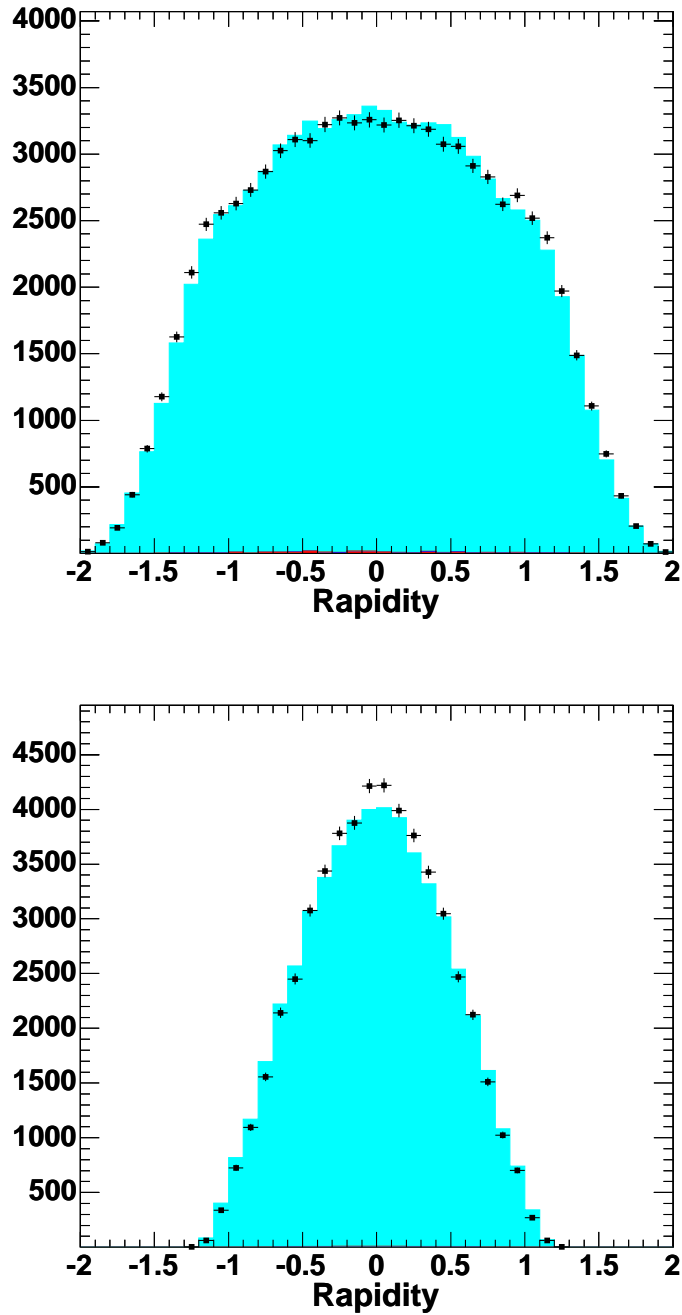


Figure 5.6: Distributions in rapidity of  $Z$ -bosons for  $Z \rightarrow e^+e^-$  events (upper figure) and  $Z \rightarrow \mu^+\mu^-$  events (lower figure). The distributions expected from the Standard Model are shown as stacked histograms. Points represent observed data. We have selected events with  $66 < M_{inv}(\ell^+\ell^-) < 116$  GeV for these histograms.

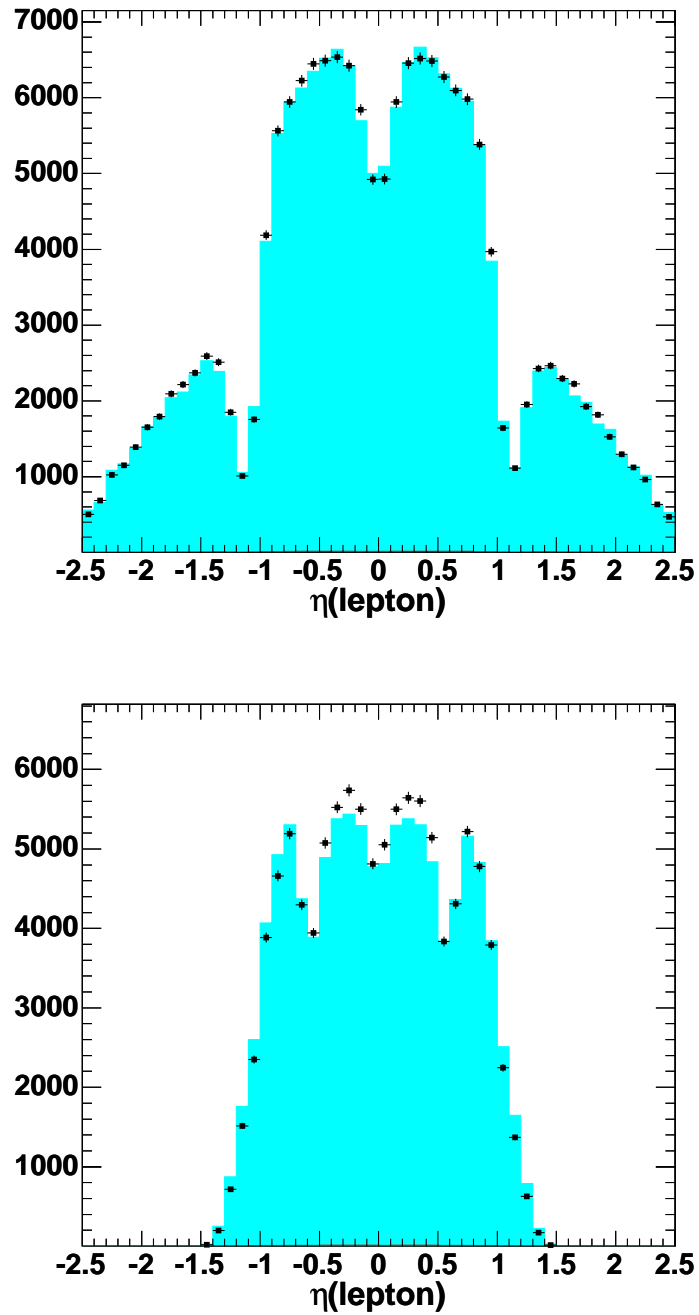


Figure 5.7: Distributions in pseudo rapidity,  $\eta$ , of the leptons (electrons or muons) observed in  $Z \rightarrow e^+e^-$  events (upper figure) and  $Z \rightarrow \mu^+\mu^-$  events (lower figure). The distributions observed from data are presented with points. The expected distributions are shown as stacked histograms.

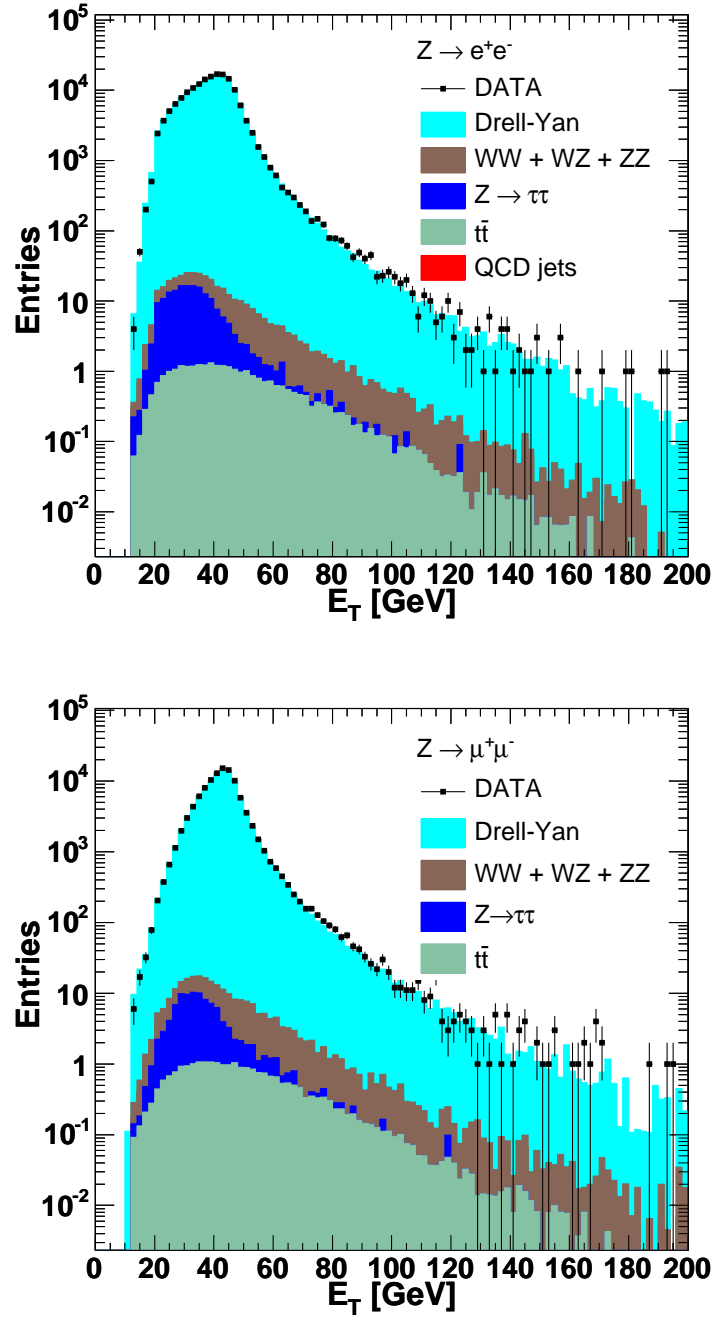


Figure 5.8: Distributions in transverse momentum,  $p_T$ , of the leptons observed in  $Z \rightarrow e^+e^-$  events (upper figure) and  $Z \rightarrow \mu^+\mu^-$  events (lower figure). Points represent observed data. Stacked histograms correspond to Standard Model predictions.

## CHAPTER 6

### PRODUCTION OF $W$ BOSONS WITH JETS

The selection of  $W \rightarrow \ell\nu$  events requires a “tight” central electron or a “tight” muon and  $\cancel{E}_T$  greater than 25 GeV. We require that each  $W$ -event has only one tight lepton, and no loose leptons. The transverse mass ( $M_{trans}(\ell\nu)$ ) reconstructed from the lepton and the missing transverse energy is required to be greater than 20 GeV. Figure 6.1 shows the measured and expected distributions in transverse mass for the  $W \rightarrow e\nu$  and  $W \rightarrow \mu\nu$  events.

The production of  $W$  bosons is used as a tool to check the efficiencies of lepton triggers and lepton identification. In addition the  $W$  sample provides a good validation of the reconstruction and modeling of missing transverse energy, since every event with a  $W$ -boson is expected to have intrinsic missing energy.

The SM backgrounds to events with  $W + \text{jets}$  (where  $W \rightarrow \ell\nu$ ) are estimated using the data and from MC simulations. The MC simulations are used to predict well-understood SM electroweak processes, such as  $Z \rightarrow \ell\ell$ ,  $WW$ ,  $WZ$ , and  $ZZ$ . Backgrounds that are largely instrumental, such as the misidentification of a QCD jet as a lepton from  $W$  decay, are predicted from the data. More details are provided in Section 7.

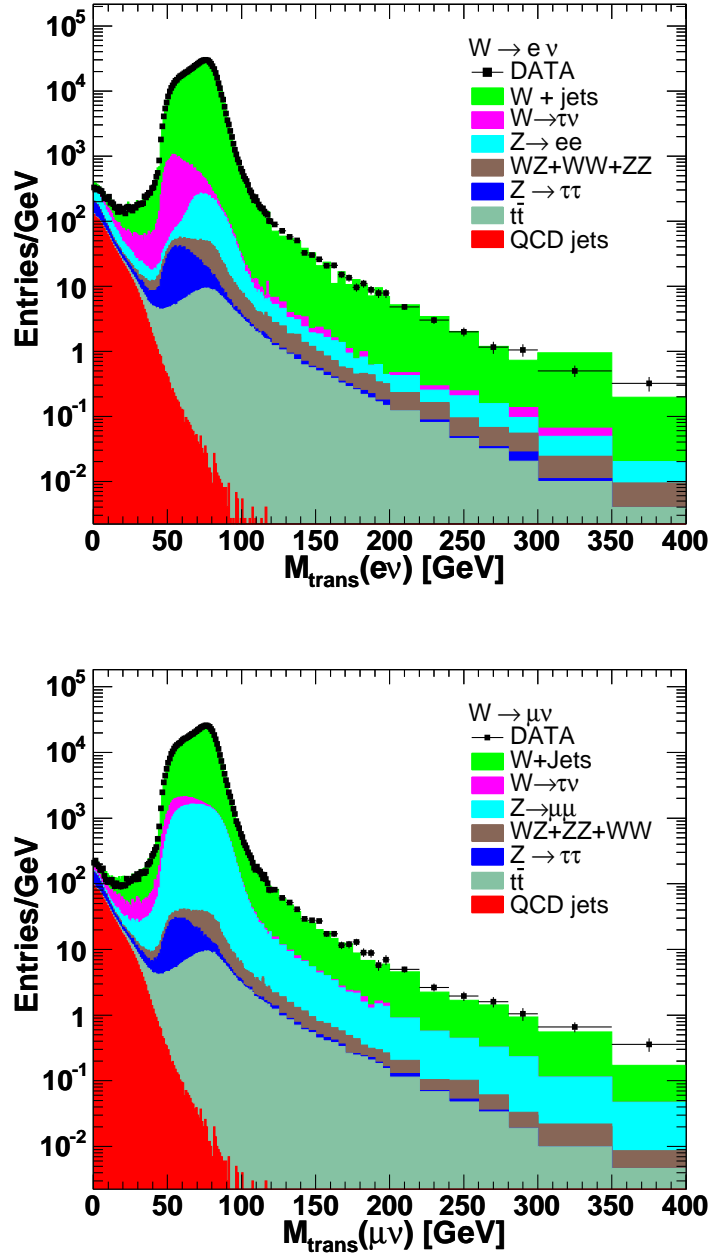


Figure 6.1: Distributions in transverse mass,  $M_{trans}(\ell\nu)$ , for  $W \rightarrow e\nu$  events (upper figure) and  $W \rightarrow \mu\nu$  events (lower figure). Observed data are presented with points. Predictions of the Standard Model are show with stacked histograms.

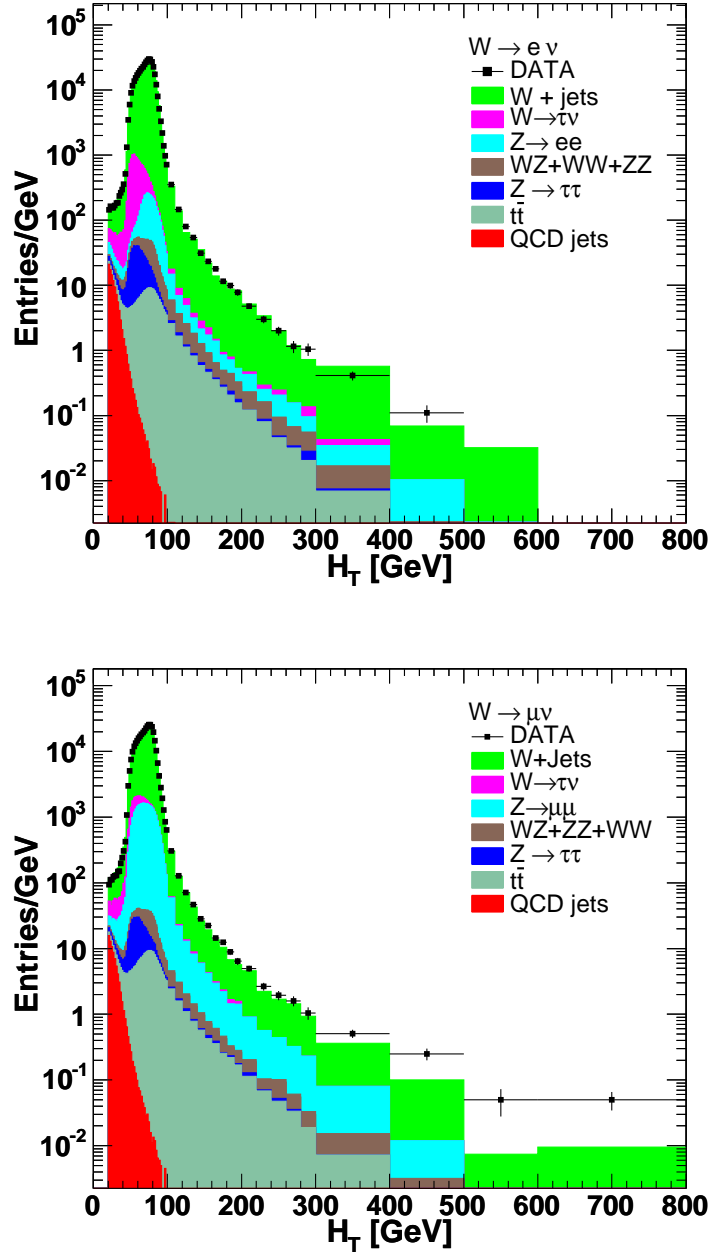


Figure 6.2: Distributions in total transverse energy,  $H_T$ , for  $W \rightarrow e\nu$  events (upper figure) and  $W \rightarrow \mu\nu$  events (lower figure), where  $M_{trans}(\ell\nu) > 20$  GeV. The discrepancy at large  $H_T$  in the wewk8m ( $W \rightarrow \mu\nu$ ) muon sample does not appear in the analogous plot for  $Z \rightarrow \mu^+\mu^-$ , and so has no effect on this analysis. Observed data are shown with points. The expected distributions are presented with stacked histograms.

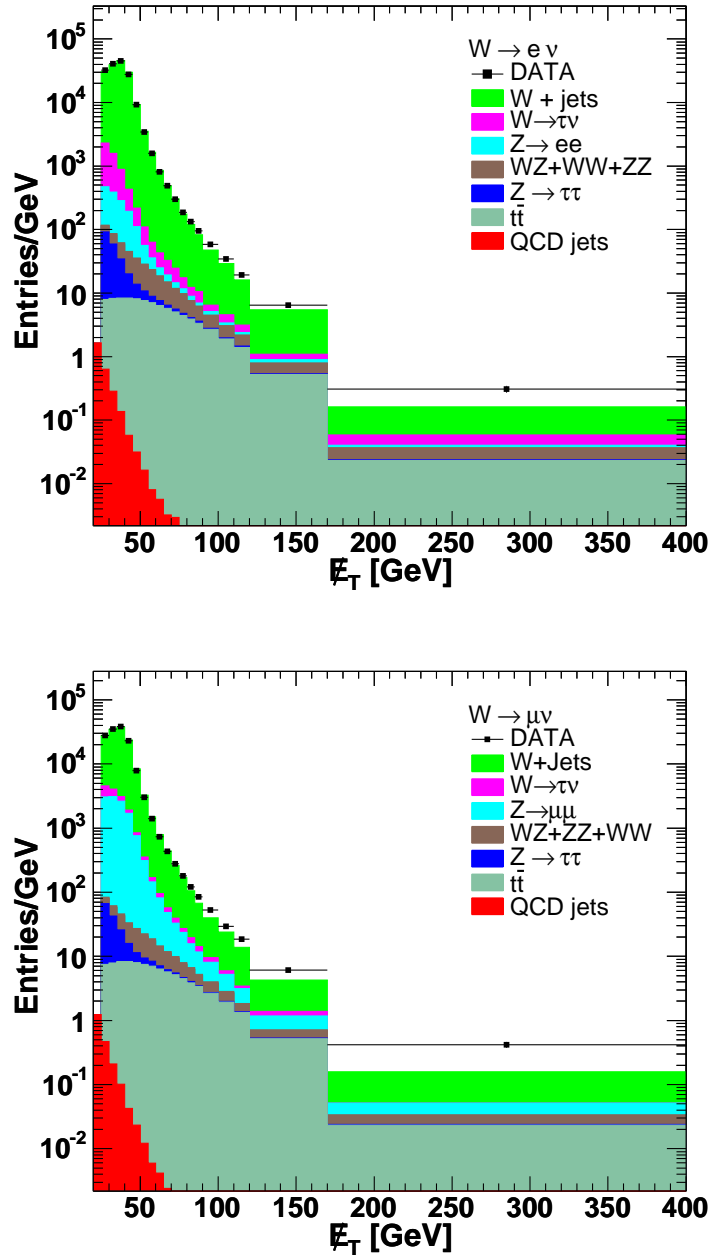


Figure 6.3: Distributions in missing transverse energy,  $E_T$ , for  $W \rightarrow e\nu$  events (upper figure) and  $W \rightarrow \mu\nu$  events (lower figure), where  $M_{trans}(\ell\nu) > 20$  GeV. Observed data are shown with points. The expected distributions are presented with stacked histograms.

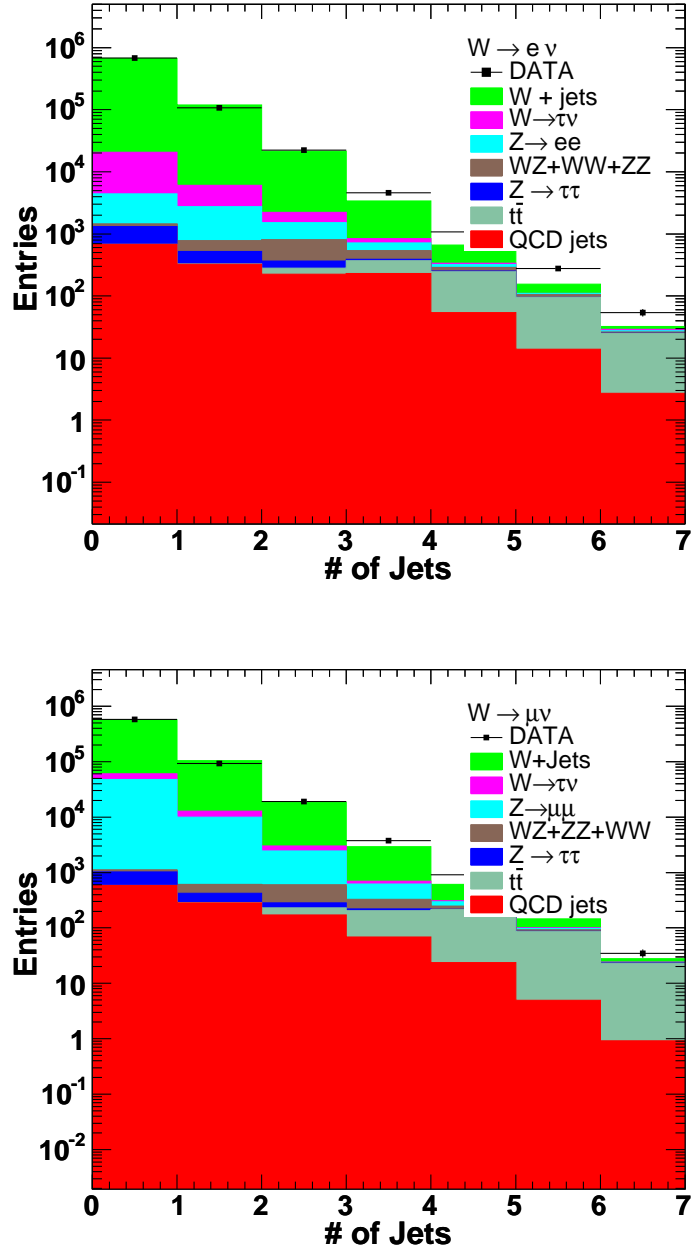


Figure 6.4: Distributions in number of jets,  $N_{jets}$ , for  $W \rightarrow e\nu$  events (upper figure) and  $W \rightarrow \mu\nu$  events (lower figure), where  $M_{trans}(\ell\nu) > 20$  GeV. Observed data are shown with points. The expected distributions are presented with stacked histograms.

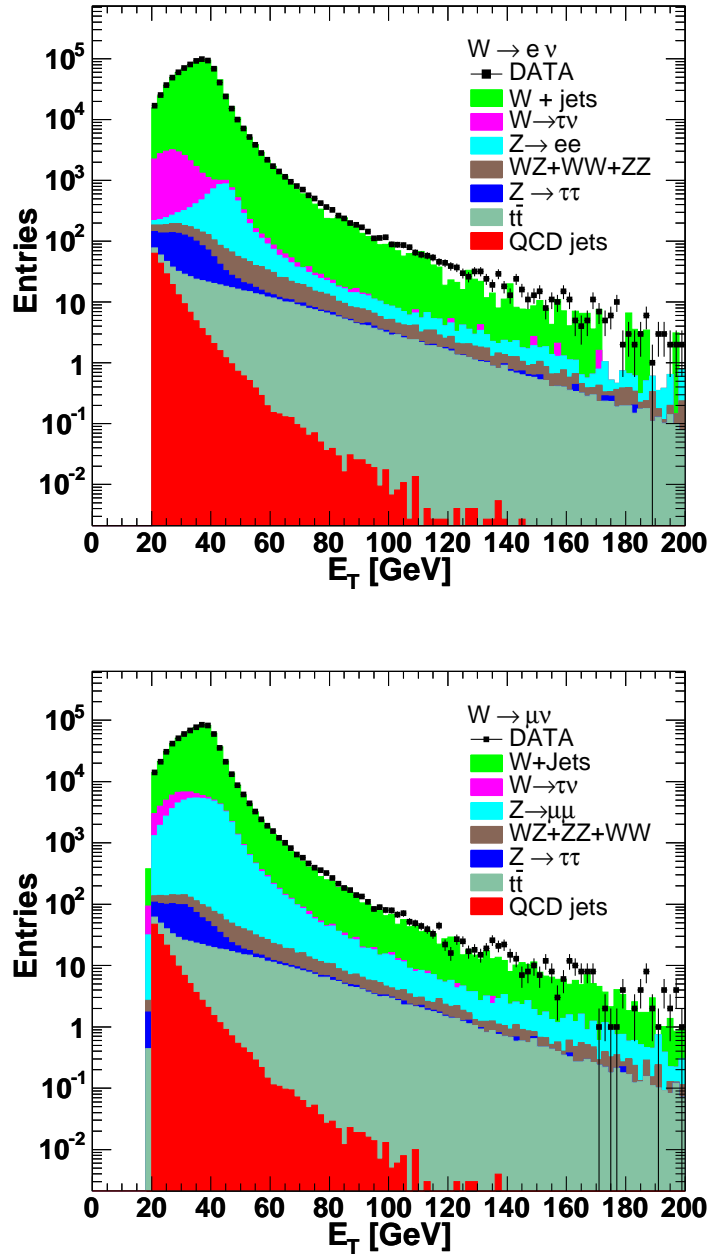


Figure 6.5: Distributions in transverse momentum,  $p_T$ , of the charged lepton in  $W \rightarrow e\nu$  events (upper figure) and  $W \rightarrow \mu\nu$  events (lower figure), where  $M_{trans}(\ell\nu) > 20$  GeV. Observed data are shown with points. The expected distributions are presented with stacked histograms.

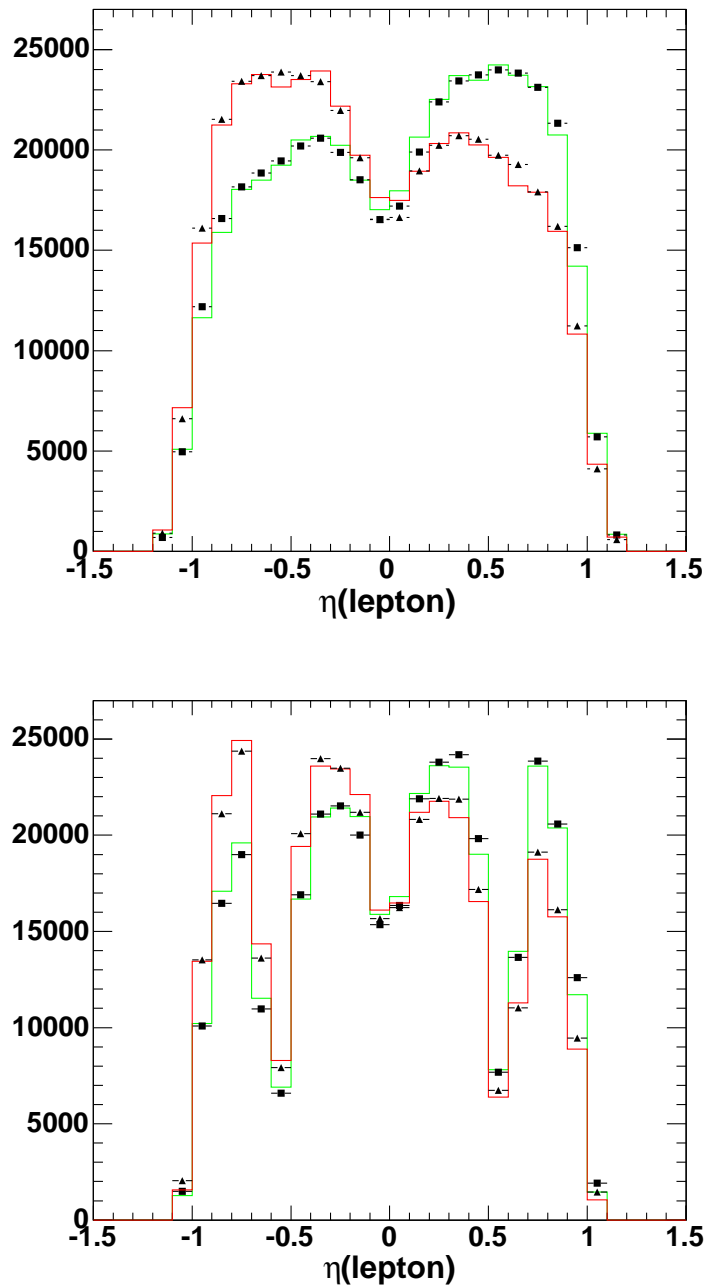


Figure 6.6: A further check of the lepton and  $\cancel{E}_T$  modeling of the simulations: Distributions in pseudo rapidity,  $\eta$ , of the leptons in  $W \rightarrow e\nu$  events (upper figure) and  $W \rightarrow \mu\nu$  events (lower figure). Positive-charge leptons are shown by squares (data) and the green line (SM simulations); negative-charge by triangles (data) and the red line (SM simulations).

Process	# of Generated events	# of Reconstructed events	$A * \epsilon$
$W \rightarrow e\nu$	1304237	250722	0.1922
$W \rightarrow \mu\nu$	5571556	833985	0.1497

Table 6.1: Summary of the acceptance-times-efficiency for inclusive  $W$  production measured from the Monte Carlo samples.

Process	Observed in Data	Expected from the SM	Background Fraction
$W \rightarrow e\nu$	814746	786005	3.5%
$W \rightarrow \mu\nu$	694651	618226	11%

Table 6.2: Summary of the numbers of inclusive  $W$  events observed in the data compared to Standard Model simulations. The Background fractions correspond to events where there are no real  $W$ -bosons.

# CHAPTER 7

## STANDARD MODEL CONTRIBUTIONS TO EVENTS WITH A $W$ OR A $Z$ BOSON AND JETS

### 7.1 Monte Carlo Simulations of the Standard Model Processes

The Standard Model expectations for the production of  $W$  and  $Z$  bosons are calculated from Monte Carlo simulations. We use PYTHIA to generate the processes “ $W$  + light jets” and “ $Z$  + light jets” processes and ALPGEN for generation of the heavy flavor processes  $W$  + HF jets and  $Z$  + HF jets. We use MADGRAPH [40] to generate tree-level diagrams for FCNC signal events. A complete list of the MC datasets used in the analysis is presented in Table D.1.

The datasets for the  $W$  and  $Z$  + light jets signatures are produced using a customized version of PYTHIA in which the  $p_T^Z$  spectrum of the  $Z$ -bosons has been tuned to CDF Run I data for  $0 < p_T^Z < 20$  GeV, a tuned underlying-event [41], and a requirement that  $M(\ell^+\ell^-) > 30$  GeV. The  $W$  and  $Z$  + heavy flavor jets samples are produced with a version of ALPGEN that has built-in matching of the number of jets from showering and matrix-element production, and are hadronized with PYTHIA [42].

The MC contributions from the SM leading-order processes are combined into inclusive samples using weights proportional to the cross-sections of each contribution.

These summed MC samples are then compared to the observed events in the electron and muon decay modes of  $W$ - and  $Z$ -bosons separately.

## 7.2 Electroweak Backgrounds

Several SM processes other than Drell-Yan production of  $W$ 's and  $Z$ 's contribute to the  $W$  and  $Z$  leptonic signatures we use in the analysis, in particular  $Z \rightarrow \tau^+\tau^-$ ,  $W^+W^-$ ,  $WZ$ ,  $ZZ$ ,  $W \rightarrow \tau\nu$ , and  $t\bar{t} \rightarrow WbWb$ . These processes are estimated from corresponding MC samples, generated using PYTHIA.

## 7.3 Fake $Z$ Background from Hadron Jets Misidentified as Leptons

This background consists of events in which one or more leptons are “fake”, i.e. jets misidentified as leptons. We assume that in the samples with a vector boson and two-or-more jets, the true lepton and the fake lepton making up the  $Z$  in the background events have no charge correlation. As the number of fake  $Z$  bosons is small (see below), we use the number of same sign lepton pairs to estimate the hadron jet background in the  $\gamma^*/Z \rightarrow \ell^+\ell^-$  sample.

The  $Z \rightarrow \mu^+\mu^-$  sample, which requires  $66 \text{ GeV} < M_{inv}(\ell\ell) < 116 \text{ GeV}$ , contains only 8 events with muons of the same sign out of 53,358 total events in the sample. The fake muon background is consequently negligibly small.

Same-sign electron pairs have a significant source from  $e^+e^-$  pair-production by photon conversions. The observed number of same-sign electron pairs in the  $Z \rightarrow e^+e^-$  sample is corrected for the predicted number of  $e^+e^-$  pairs mis-reconstructed as  $e^+e^+$  or  $e^-e^-$  using MC predictions for  $Z \rightarrow e^+e^-$  production.

We observe 398 same-sign electron pairs and 82,901  $e^+e^-$  pairs. We remove the contribution of real  $\gamma^*/Z \rightarrow e^+e^-$  events from the number of observed events by subtracting the number of observed  $e^+e^-$  events scaled by the fraction of same-sign to opposite-sign events in the Monte-Carlo samples for  $Z \rightarrow e^+e^-$ . The 78 same-sign electron pairs are used to estimate the hadron jet background in the  $Z \rightarrow e^+e^-$  sample (see Figure 5.1).

## 7.4 Fake $W$ backgrounds from Hadron jets

Jet production, which has a much higher cross-section than  $W$  or  $Z$  boson production, produces events which mimic the leptonic decay of a  $W$ -boson by a mis-measured jet ‘faking’ a tight isolated lepton and large missing energy ( $\cancel{E}_T$ ).

To estimate the non- $W$  background coming from hadron jets we use a data-derived model for non- $W$  events. The number of fake  $W$  bosons is estimated separately for electrons and muons by fitting the observed distributions in  $\cancel{E}_T$  with templates from real  $W$  decays and modeled non- $W$  events. The distributions in  $\cancel{E}_T$  are fitted over the range  $0 < \cancel{E}_T < 60$  GeV using events that contain one tight lepton, and no other leptons, with transverse mass  $M_{trans}(\ell\cancel{E}_T) > 20$  GeV (see Figures 7.1 and 7.2). The non- $W$  events are modeled by taking electrons which pass all the selection (see Tables A.2 and A.3) criteria except those on the quality of the calorimeter shower (labeled anti-selected-electrons in Figures 7.1 and 7.2). The fractions of non- $W$  events are estimated separately for events with 0, 1, 2, 3, and  $\geq 4$  jets in the final state by propagating the distribution of the modeled non- $W$  events into the region with  $\cancel{E}_T > 25$  GeV. The estimated fractions of non- $W$  events for each jet multiplicity are summarized in Table 7.1.

Jet Multiplicity	0 jets	1 jet	2 jets	3 jets	$\geq 4$ jets
$W \rightarrow e\nu + \text{jets}$	0.6%	1.9%	7%	14%	20%
$W \rightarrow \mu\nu + \text{jets}$	0.1%	0.3%	0.9%	1.8%	2.6%

Table 7.1: Fractions of non- $W$  events in events with one tight lepton and no other leptons, and with  $\cancel{E}_T > 25$  GeV and  $M_{trans}(\ell + \cancel{E}_T) > 20$  GeV.

A systematic uncertainty of 26% is assigned on the fractions of non- $W$  events, derived from the level of agreement between the shape of the data-derived non- $W$  sample and the shape of  $\cancel{E}_T$  distribution of fake electrons in data.

## 7.5 Cosmic Ray Backgrounds

High-energy cosmic muons traverse the CDF detector at a significant rate, and if they intersect the beam-line can be reconstructed as  $\mu^+\mu^-$  pairs. Because cosmic rays are uncorrelated in time with the  $p\bar{p}$  collisions, and one “leg” (segment of a cosmic track) is earlier than the other, in some cases only one track is reconstructed, mimicking a  $W \rightarrow \mu\nu$  event. We remove cosmic ray events with an algorithm that finds the missing hits and fits the two tracks of the  $\mu^+\mu^-$  pair to a single arc composed of an incoming track segment and an outgoing segment, consistent in time evolution with a through-going track [33]. The algorithm also removes cosmic rays from events where only one muon is reconstructed as a  $W \rightarrow \mu\cancel{E}_T$  decay. It searches for hits in the COT chamber within a narrow road along a predicted trajectory opposite to the identified muon. Finally, the algorithm performs a simultaneous fit of the hits of the muon track and the hits in the predicted trajectory with a single helix to determine consistency with the cosmic-ray hypothesis.

An independent estimate of the number of cosmic muons in the Z-boson sample that have survived the cosmic-ray filter can be made from the distribution  $|\vec{P}(\mu^+\mu^-)|$

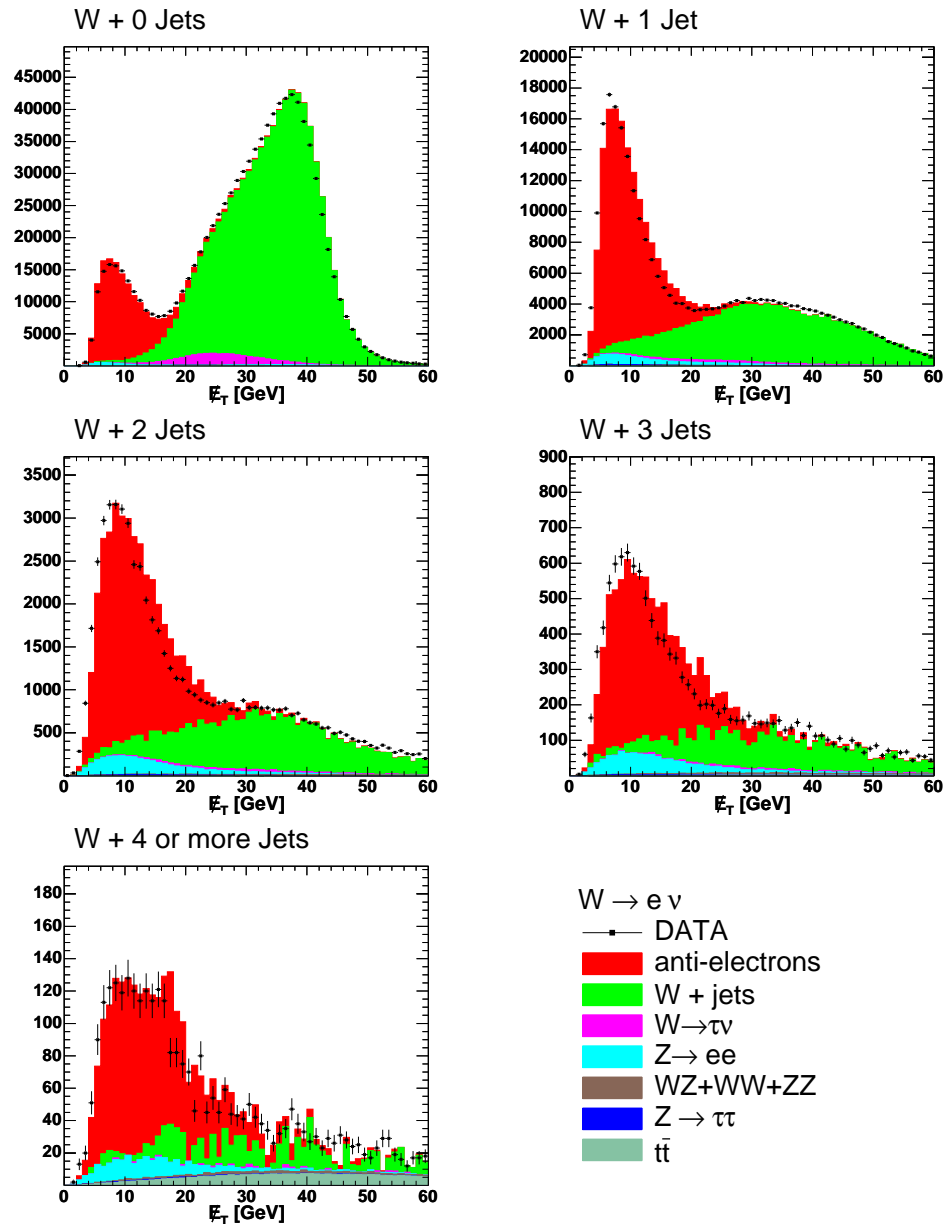


Figure 7.1: Distributions in missing transverse energy,  $\cancel{E}_T$ , for  $W \rightarrow e \nu$  events with 1, 2, 3, and 4 or more jets, where  $M_{trans}(\ell \nu)$  is more than 20 GeV and  $\cancel{E}_T$  is not required to be greater than 25 GeV. The observed distributions are compared to those from SM expectations and non- $W$  events (labeled “anti-selected-electron” in text) in order to estimate the QCD background.

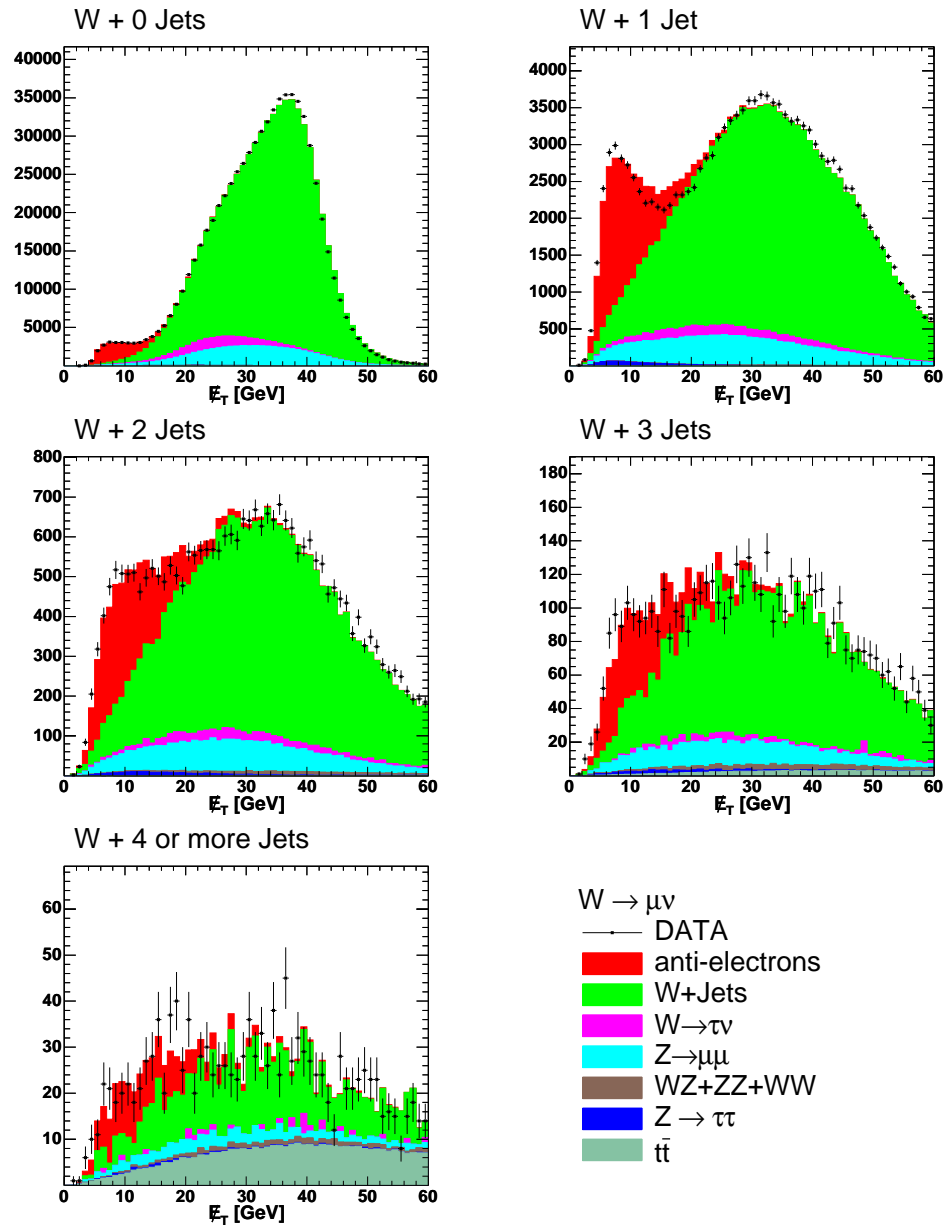


Figure 7.2: Distributions in missing transverse energy,  $\cancel{E}_T$ , for  $W \rightarrow \mu\nu$  events with 1, 2, 3, and 4 or more jets, where  $M_{trans}(\ell\nu)$  is more than 20 GeV and  $\cancel{E}_T$  is not required to be greater than 25 GeV. The observed distributions are compared to those from SM expectations and non- $W$  events (labeled anti-selected-electron in text) in order to estimate the QCD background.

of the muon pair. This is an elegant way of combining the usual back-to-back and momentum balance criteria for the two muons into a single distribution, as cosmic  $\mu^+\mu^-$  pairs have a very narrow peak at  $|\vec{P}(\mu^+\mu^-)| = 0$  GeV, while real  $Z \rightarrow \mu^+\mu^-$  decays occupy only a small area in the 3-dimensional phase space near  $|\vec{P}(\mu^+\mu^-)|=0$ . Using the  $|\vec{P}(\mu^+\mu^-)|$  distribution as an estimator, the most probable number of cosmic ray events in the sample surviving the cosmic filter is zero, as is shown in Figure 7.3.

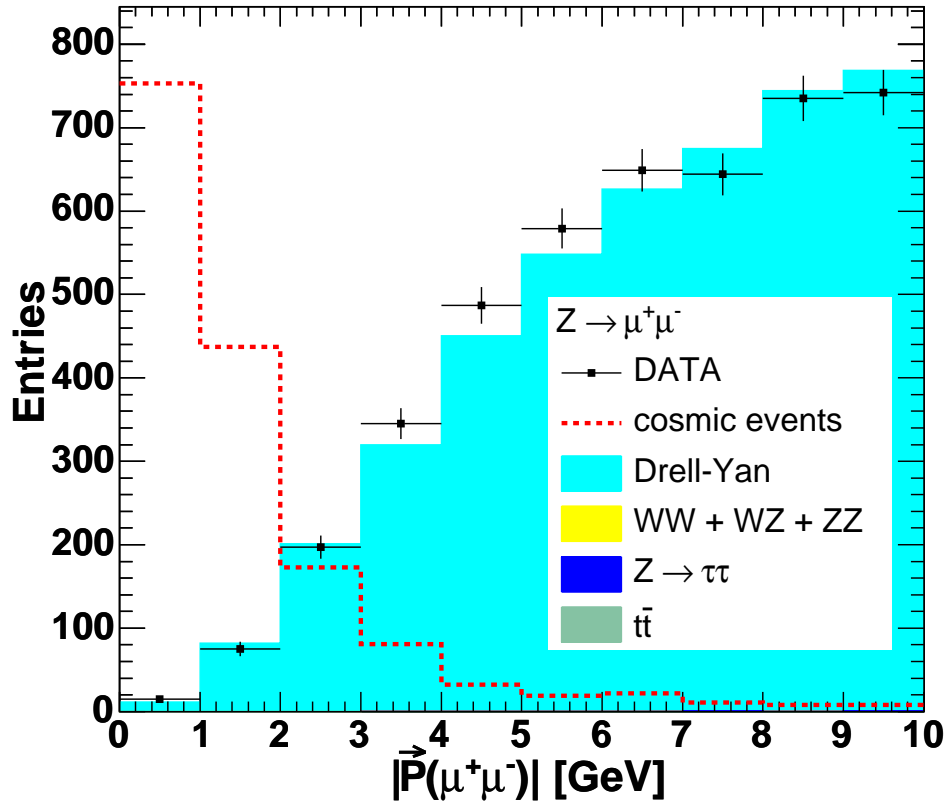


Figure 7.3: The distribution  $|\vec{P}(\mu^+\mu^-)|$  of muon pairs from  $Z$ -boson candidates (solid), expected events from MC simulations (stacked histogram), and from a cosmic ray sample (dashed). Cosmic ray muons produce a very narrow peak at  $|\vec{P}(\mu^+\mu^-)| = 0$  GeV, while real  $Z \rightarrow \mu^+\mu^-$  decays occupy only a small area in the 3-dimensional phase space near  $|\vec{P}(\mu^+\mu^-)| = 0$ . The most probable number of cosmic ray events in the search sample is zero.

## CHAPTER 8

### USING R AS A PRECISE CHECK OF THE MONTE CARLO SIMULATIONS

The Monte Carlo simulation of a dataset extending over years, with changing detector and accelerator conditions, is an exceptionally complex task, involving large quantities of time-dependent conditions stored in databases. Small errors in book-keeping or in properly specifying which data to use in the code are common and exceptionally difficult to detect. To validate the modeling of the lepton identification, acceptances, and triggering we use a calibration that is predicted to better than 1.5% and is directly sensitive to errors affecting overall efficiencies for leptons and  $\cancel{E}_T$ . We measure the ratio  $R$  of inclusively produced  $W$  and  $Z$  bosons in their respective leptonic decay channels [43].

The ratio  $R$  is defined as:

$$R = \frac{\sigma(W) * Br(W \rightarrow \ell\nu)}{\sigma(Z) * Br(Z \rightarrow \ell^+\ell^-)}, \quad (8.1)$$

where  $\sigma(W)$  and  $\sigma(Z)$  are cross-sections of inclusively produced  $W$  and  $Z$  bosons. The measured cross-sections are proportional to the numbers of events and inversely proportional to the integrated luminosity of the dataset. The luminosity thus does not contribute directly to the measured  $R$ -ratio. We note that the search for  $t \rightarrow Zc$ , described in Chapter 10, is based on a similar measurement of ratios.

The ratio  $R$  has been calculated at NNLO by Stirling et al., and is predicted to be  $10.67 \pm 0.15$  [44], providing a precise check of lepton acceptances, efficiencies, and the  $W$  and  $Z$  boson selection criteria both in data and MC simulations. We measure  $R = 10.52$  using electrons and  $10.46$  using muons. The biggest disagreement between the theoretical prediction and a measured value is less than 2%, negligible in comparison to the other systematic uncertainty on the  $t \rightarrow Zc$  measurement.

## CHAPTER 9

### TAGGING OF HEAVY FLAVOR JETS

We identify decays of bottom and charm quarks (Heavy Flavor, HF) with an algorithm that identifies displaced secondary vertexes within a jet. The primary vertex is identified by fitting all tracks in the event to a vertex constrained to lie on the beam-line. Jets with  $E_T > 15$  GeV are checked for good quality tracks with hits in the COT and the silicon detector. The secondary vertex can be reconstructed with at least two of those tracks and the distance between the primary and the secondary vertexes along the jet direction can be calculated. The jet is considered to contain a HF quark (“b-tagged”) if the significance of this distance is greater than  $7.5\sigma$ . The algorithm has an efficiency of approximately 50% to tag a b-jet, depending on the  $E_T$  of the jet, in a  $t\bar{t}$  event. More details of the algorithm are available in Ref. [45].

To model the multiple SM sources of tagged events, we use control samples selected from the data to estimate mistag rates (i.e. the number of tags coming from the falsely tagged jets), and Monte Carlo simulated samples to get the contribution from SM physics processes with true heavy flavor jets.

The mistag rate is estimated by applying the mistag parametrization to each event in a data sample that has all the desired characteristics except a b-tag (called the “pre-tag” sample). The parametrization gives each jet a probability to be falsely tagged based on the jet  $E_T$ ,  $\eta$ , and number of tracks of good quality in the jet. The calculation of the rate is performed in the following steps:

1. We identify all jets with  $E_T > 10$  GeV and  $|\eta| < 2.4$  that are not identified as electrons or photons (this is important since we have at least one lepton in each event).
2. We apply the mistag parameterization to this list of jets.
3. We loop through jets satisfying the selection requirements and find the probability for each jet to be tagged. These probabilities are combined into a probability of the event to have at least one b-tag.

The contribution from real HF jets is estimated by applying the tagging algorithm to  $Z$ +HF and  $W$ +HF MC samples. Events with at least one b-tag are selected. Each selected event is weighted by a standard CDF “scale-factor”  $(1 - (1 - 0.95)^{N_{tags}})$  [45], where  $N_{tags}$  is the number of b-tagged jets in the event, to take into account the difference in the tagging efficiencies between data and simulation.

## CHAPTER 10

### OVERVIEW OF THE FCNC ANALYSIS

The top pair production process provides the most sensitivity to the FCNC decays  $t \rightarrow Zc$ , since the Standard Model backgrounds to single top production are overwhelming. Assuming that the  $Br(t \rightarrow Zc) > 0$ , a  $t\bar{t}$  pair can decay to  $WbWb$ ,  $WbZc$ , or  $ZcZc$  with decay rates proportional to  $(1 - Br(t \rightarrow Zc))^2$ ,  $2Br(t \rightarrow Zc) \cdot (1 - Br(t \rightarrow Zc))$ , and  $Br(t \rightarrow Zc)^2$ , respectively.  $W$ - and  $Z$ - bosons are identified well only via their leptonic decay modes, which have small branching fractions ( $\sim 11\%$  at  $3\%$  respectively). To keep acceptances high we require one of the bosons from the  $t\bar{t}$  pair to decay leptonically and the other hadronically. We consider two final states which have significant contributions from decays of  $t\bar{t}$  pairs:  $\ell^+\ell^-cjjb$ , (i.e.  $p\bar{p} \rightarrow t\bar{t} \rightarrow ZcWb \rightarrow \ell^+\ell^-cjjb$ ) and  $\ell\nu bjbb$  (i.e.  $p\bar{p} \rightarrow t\bar{t} \rightarrow WbWb \rightarrow \ell\cancel{E}_Tbjbb$ ), where:  $\ell$  is a lepton ( $e$  or  $\mu$ ),  $j$  is a jet,  $\nu$  is a neutrino, inferred via missing transverse energy ( $\cancel{E}_T$ ),  $b$  and  $c$  are ‘‘heavy-flavor’’ jets formed by hadronization of a bottom-quark or a charm-quark, respectively. The decay channels above have at least one charged lepton in the final state, allowing a single dataset containing both channels to be formed from an inclusive high-Pt lepton ( $e$  or  $\mu$ ) trigger.

To avoid large systematic uncertainties we analyze simultaneously two final states from decays of top pairs:  $p\bar{p} \rightarrow t\bar{t} \rightarrow ZcWb \rightarrow \ell^+\ell^-cjjb$  and  $p\bar{p} \rightarrow t\bar{t} \rightarrow WbWb \rightarrow \ell\cancel{E}_Tbjbb$ . This is done by comparing the number of expected events from SM  $t\bar{t}$  decays and SM backgrounds to the number of observed events in each final state. The contributions from  $t\bar{t}$  decays depend on two numbers:  $Br(t \rightarrow Zc)$  and  $N_{t\bar{t}} =$

$\sigma(p\bar{p} \rightarrow t\bar{t}) \cdot \int L dt$ , where  $\sigma(p\bar{p} \rightarrow t\bar{t})$  is the cross-section of top pair production at CDF and  $\int L dt$  is the integrated luminosity.

Additional discrimination against SM backgrounds is achieved by requiring at least one of the four jets in the final state to be consistent with originating from a heavy-flavor quark (b or c quark).

The unknown structure of the FCNC coupling is fully described via polarization of the  $Z$  boson produced in  $t \rightarrow Z$  decay. The polarization of the  $Z$  boson is the only parameter which affects the acceptance of FCNC top decays. We vary the value of the longitudinal polarization of the  $Z$ -bosons from 0.0 to 1.0 to cover the whole face space of FCNC couplings. The final result is presented as a function of the longitudinal polarization of  $Z$ -bosons.

We reconstruct the invariant mass of the top quark,  $M_{top}$ , in events with two leptons and four jets assuming that the events are  $t\bar{t}$  FCNC decays. The distribution of  $M_{top}$  provides additional separation between Standard Model backgrounds and the FCNC signal.

# CHAPTER 11

## MEASURING TOP QUARK PAIR PRODUCTION IN EVENTS WITH A $W$ BOSON AND FOUR JETS

The measurement of the FCNC branching ratio relies on two datasets (see Section 3):  $\ell^+\ell^- + 4jets$  and  $\ell\cancel{E}_T + 4jets$ , where  $\ell^+\ell^-$  and  $\ell\cancel{E}_T$  are consistent with decays of a  $Z$ -boson or a  $W$ -boson (see Sections 5 and 6), respectively. In this section we focus only on the  $\ell\cancel{E}_T + 4jets$  events, where the majority of events come from  $t\bar{t} \rightarrow WbWb$  decays. At least one of the four jets in the final state is required to be identified as heavy flavor (HF) decay by the secondary vertex identification algorithm. The estimate of SM production of “W+HF” events (e.g.  $W + b\bar{b}$ ) requires normalization of three key components:  $t\bar{t}$ ;  $W + b\bar{b}$ ,  $W + c\bar{c}$ ,  $W + c$ ; and “non- $W$ ” background events, which arise from mis-measured jet events.

### 11.1 Estimating the Relative Contributions from $t\bar{t}$ ; the $W$ +HF Processes $W + b\bar{b}$ , $W + c\bar{c}$ , and $W + c$ ; and non- $W$ Background

The dominant SM contribution to the  $W$ +4-jet bin with one jet identified as heavy flavor (a “b-tag”) is SM  $t\bar{t}$  production. The production of  $W$  with heavy flavor,  $W + b\bar{b}$ ,  $W + c\bar{c}$ , and  $W + c$ , however, dominate production in the  $W$ +2 jet bin. We consequently use the spectrum in the number of jets in  $W$ +HF production to

estimate the contribution from  $t\bar{t}$  alone in an iterative process. We take the top pair production cross-section to be  $\sigma(t\bar{t}) = 7.6$  pb [46].

We initially assume that the fraction of non- $W$  events is negligible. We determine the normalization of the Standard Model contribution to the “ $W$ +HF” processes “ $W + b\bar{b}$ ”, “ $W + c$ ” and “ $W + c\bar{c}$ ” by rescaling the respective cross-sections to match the total number events observed in the  $W + 2jets$  bin. We assume that the overall normalization of “ $W + b\bar{b} + jets$ ”, “ $W + c\bar{c} + jets$ ”, and “ $W + c + jets$ ” can be corrected by a single scale factor which is the same for the electron and muon channels.

We then use this normalization of the “ $W$ +HF” samples to estimate the remaining contribution from fake  $W$ ’s, as described in detail below in Section 11.2.

We then repeat the calculation of the fraction of real “ $W$ +HF” events now using the estimate of fake  $W$ ’s. We find that the  $W$ +HF processes are rescaled by a factor of  $0.97 \pm 0.09$  to match the number of events in the  $W + 2jets$  bin. The final jet multiplicity distributions for the  $W + HF$  sample are shown in Figure 11.3. We find good agreement for 2 or more jets in the  $W$ +HF sample.

The motivation for normalizing to the two-jet multiplicity bin is based on the matrix-element structure of associated heavy flavor production in  $W$  and  $Z$  events. The real problem is that different diagrams contribute differently to the  $N=1$  and the  $N=2$  jet multiplicity bins; taking into account the (large, particularly for charm) NLO corrections is tricky since the corrections differ significantly for the different processes. In contrast, the radiation of additional jets and jet matching procedures are fairly well understood and have been studied elsewhere quite carefully. As we do not use the 1-jet bin we avoid all these issues by normalizing to the 2nd jet bin.

A consistency check using top-pair production rate (assuming that there is no FCNC [47]) can be made by computing the difference between the observed and the

expected non- $t\bar{t}$  events in the  $W+4\text{jets}$  bin. To illustrate this we scale  $\sigma(t\bar{t} \rightarrow WbWb)$  to match the calculated difference in the  $W + 4\text{jets}$  bin. The scale factor is found to be  $1.17 \pm 0.09$ , consistent with the SM expectation. The  $H_T$ -distributions [48] with the rescaled  $\sigma(t\bar{t} \rightarrow WbWb)$  agree well with those of top-pair decays (see Figure 11.4).

## 11.2 Fake $W$ backgrounds in the $t\bar{t}$ Sample

The number of fake  $W$  bosons is estimated by fitting the  $\cancel{E}_T$ -distribution for each jet multiplicity bin in events with one tight lepton and  $M_{trans}(\ell\cancel{E}_T)$  higher than 20 GeV, where the transverse mass  $M_{trans}(\ell\cancel{E}_T)$  is calculated for the lepton and  $\cancel{E}_T$  (this is done to match kinematic properties of the events). The fitted distributions of  $\cancel{E}_T$  are shown in Figures 11.1 and 11.2. Basically, we repeat the same thing we have done earlier for the inclusive  $W$ -bosons (see Section 7.4). The fractions of the fake  $W$ -events obtained after applying the  $\cancel{E}_T$ -cut ( $\cancel{E}_T > 25$  GeV) are presented in Table 11.1.

Jet Multiplicity	1 jet	2 jets	3 jets	$\geq 4$ jets
$W \rightarrow e\nu + \text{jets}$	2.0%	4.9%	7.6%	4.7%
$W \rightarrow \mu\nu + \text{jets}$	0.3%	0.9%	1.3%	–%

Table 11.1: Fractions of the non- $W$  QCD events in events with a tight lepton ( $e$  or  $\mu$ ),  $\cancel{E}_T > 25$  GeV,  $M_{trans}(\ell\cancel{E}_T) > 20$  GeV, and at least one B-tagged jet. (The fit for  $W \rightarrow \mu\nu + 4$  jets returned 0 events due to the low statistics of the sample. In any case this number should be comparable with the one for inclusive  $W$ 's so we take 2.6% for the tagged sample.)

The acceptance and efficiency calculated from the MC for the “ $W + 4$  jets” bin are presented in Tables 11.2. The number of events observed and the expected number from all processes except  $t\bar{t}$  production are given in Table 11.3.

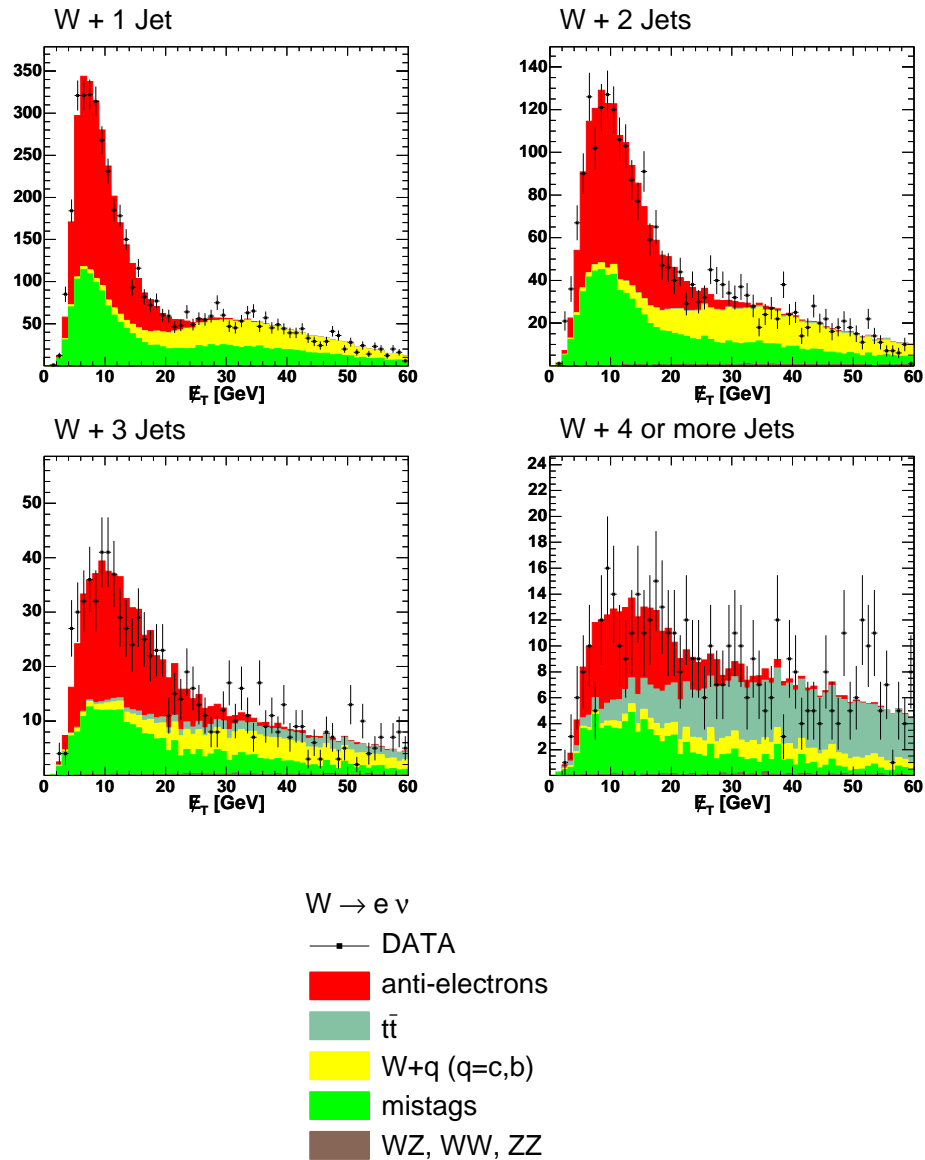


Figure 11.1: Distributions in missing transverse energy,  $\cancel{E}_T$ , for  $W \rightarrow e\nu$  events with 1, 2, 3, and 4 or more jets, where  $M_{trans}(\ell\cancel{E}_T)$  is more than 20 GeV,  $\cancel{E}_T$  is not required to be greater than 25 GeV, and at least one jet is b-tagged. The observed distributions are compared to those from SM expectations and non- $W$  events (labeled “anti-electron” in text) in order to estimate the QCD background. We let the overall normalization float.

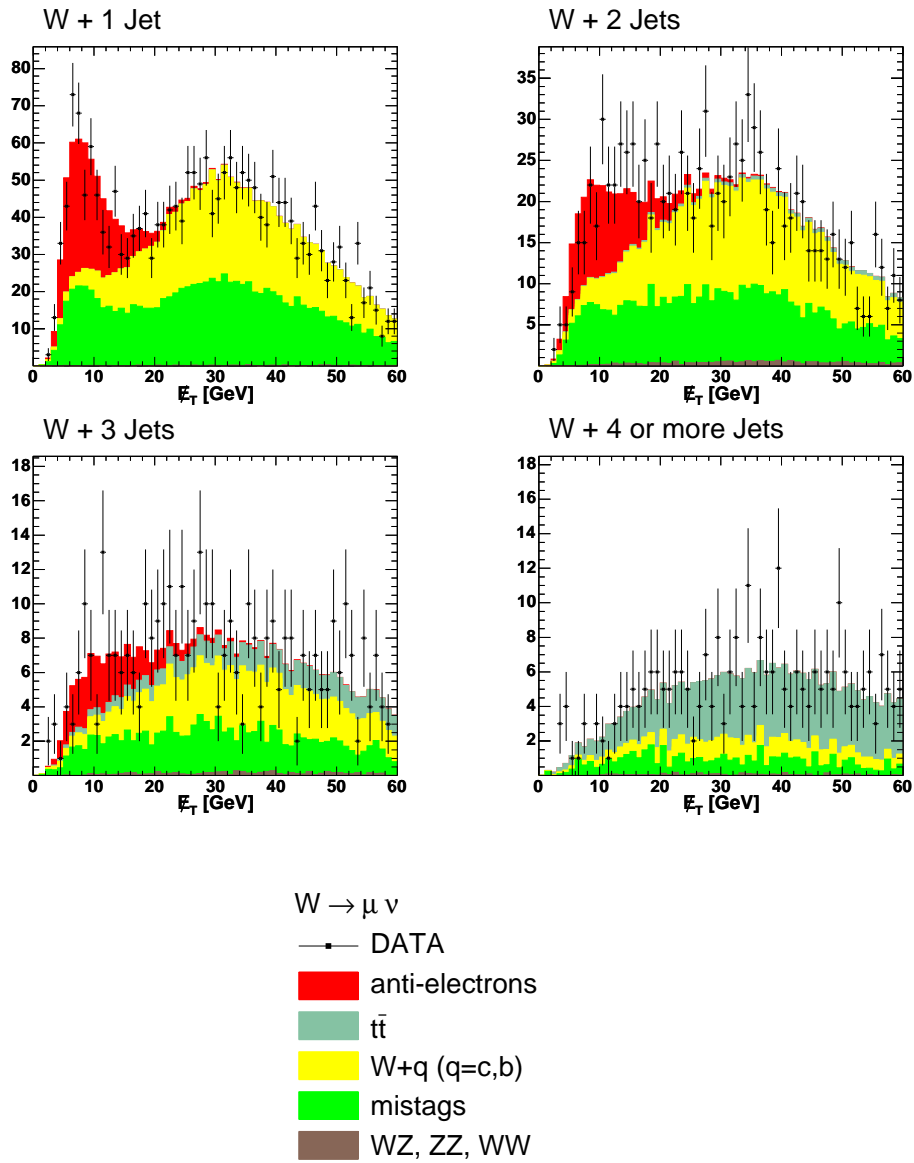


Figure 11.2: Distributions in missing transverse energy,  $\cancel{E}_T$ , for  $W \rightarrow \mu\nu$  events with 1, 2, 3, and 4 or more jets, where  $M_{trans}(\ell\cancel{E}_T)$  is more than 20 GeV,  $\cancel{E}_T$  is not required to be greater than 25 GeV, and at least one jet is b-tagged. The observed distributions are compared to those from SM expectations and non- $W$  events (labeled “anti-electron” in text) in order to estimate the QCD background. We let the overall normalization float.

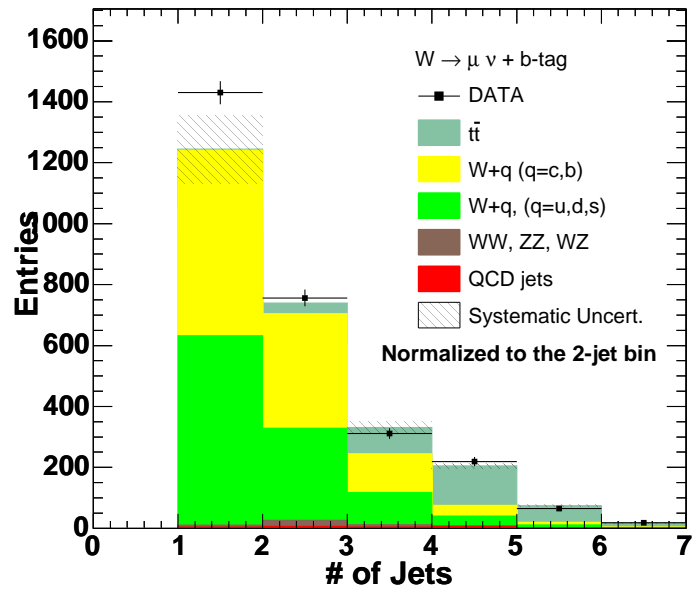
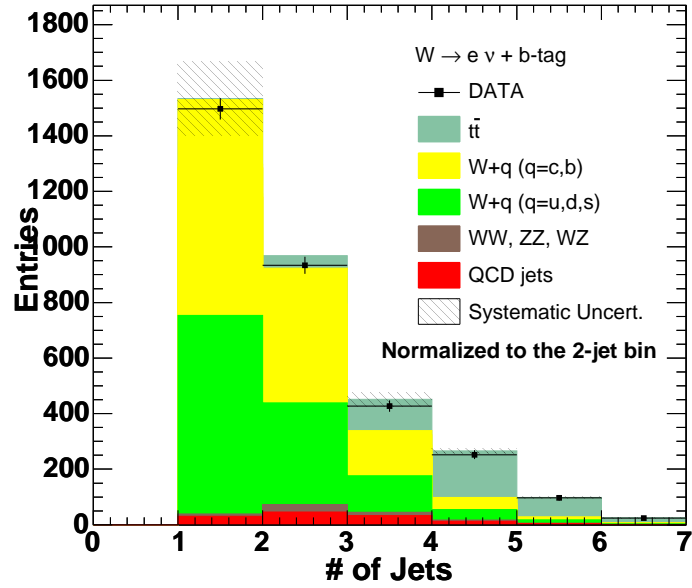


Figure 11.3: The measured distributions (points) in the number of jets in  $W \rightarrow e\nu$  events (upper figure) and  $W \rightarrow \mu\nu$  events (lower figure) with at least one b-tagged jet and  $M_{trans} > 20$  GeV, compared to SM expectations (stacked histogram).

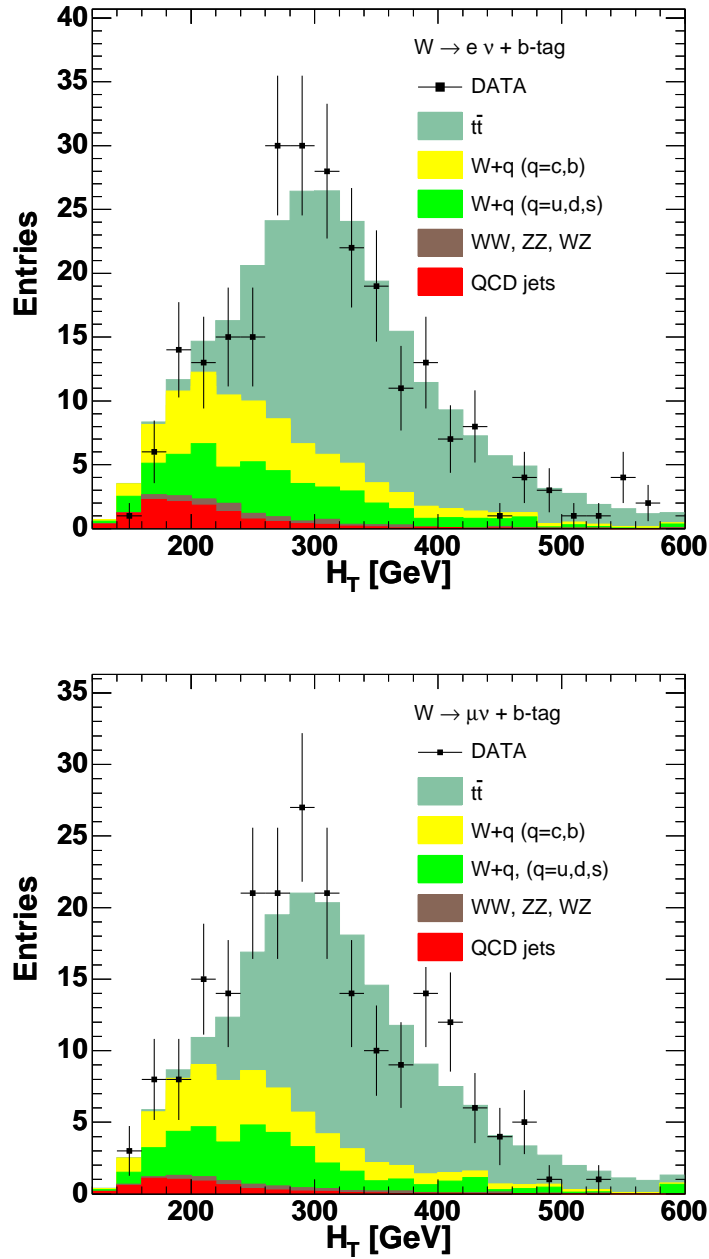


Figure 11.4: The measured distribution (points) in total transverse momentum,  $H_T$ , in events with a b-tagged jet and  $M_{trans}(\ell \cancel{E}_T) > 20$  GeV, compared to SM expectations (stacked histogram), for the  $W \rightarrow e\nu$  events (upper figure) and the  $W \rightarrow \mu\nu$  events (lower figure).

Process	$A_{WW \rightarrow \ell \cancel{E}_T}$
$t\bar{t} \rightarrow WbWb \rightarrow e \cancel{E}_T + bj\bar{j}b$	0.0128
$t\bar{t} \rightarrow WbWb \rightarrow \mu \cancel{E}_T + bj\bar{j}b$	0.00994

Table 11.2: The acceptance times efficiency for inclusive  $t\bar{t} \rightarrow WbWb$  production measured from the Monte Carlo samples.

Final state	Observed	Background (non- $t\bar{t}$ )
$e + \cancel{E}_T + 4jets$	252	98.7
$\mu + \cancel{E}_T + 4jets$	219	75.2

Table 11.3: Summary of the numbers of “ $W + 4$  jets” events. At least one jet in each event is required to be B-tagged.

# CHAPTER 12

## THE CONTRIBUTION FROM FCNC DECAYS OF TOP QUARK PAIRS TO EVENTS WITH $W/Z$ BOSONS AND JETS

### 12.1 Acceptances for $t\bar{t}$ decays

We use a modified version of the MADGRAPH Monte Carlo event generator [49] to produce tree-level diagrams for the  $t\bar{t} \rightarrow ZcWb$  and  $t\bar{t} \rightarrow ZcZc$  processes, which are then hadronized using PYTHIA.

In order to calculate the rates of expected events for the two final states  $\ell^+\ell^- + 4jets$  and  $\ell\cancel{E}_T + 4jets'$ , we need to introduce a notation for the acceptances multiplied by efficiencies,  $(A * \epsilon)_Y$ , for the decay chains “Y” of  $t\bar{t}$  pairs. Acceptance  $(A * \epsilon)_Y$  is a fraction of  $t\bar{t}$  events observed in the corresponding final state. The acceptances  $(A * \epsilon)_Y$  include combinatoric factors and the corresponding branching fractions for decays of  $W$ 's and  $Z$ 's:  $\text{Br}(W \rightarrow \ell\cancel{E}_T)$ ,  $\text{Br}(W \rightarrow qq')$ ,  $\text{Br}(Z \rightarrow \ell\ell)$ , and  $\text{Br}(Z \rightarrow q\bar{q})$ .

The acceptances  $(A * \epsilon)_Y$  depend on the FCNC branching ratio  $\text{Br}(t \rightarrow Zc)$ . We divide the acceptances by polynomials dependent on  $\text{Br}(t \rightarrow Zc)$  to factor out the terms independent of the FCNC the branching ratio:

$$A_{ZZ \rightarrow \ell\ell} = \frac{(A * \epsilon)_{t\bar{t} \rightarrow ZcZc \rightarrow \ell^+\ell^- + 4 jets}}{\text{Br}(t \rightarrow Zc)^2}, \quad (12.1)$$

$$A_{WZ \rightarrow \ell\ell} = \frac{(A * \epsilon)_{t\bar{t} \rightarrow ZcWb \rightarrow \ell^+\ell^- + 4 jets}}{\text{Br}(t \rightarrow Zc) \cdot (1 - \text{Br}(t \rightarrow Zc))}, \quad (12.2)$$

$$A_{WZ \rightarrow \ell \cancel{E}_T} = \frac{(A * \epsilon)_{t\bar{t} \rightarrow ZcWb \rightarrow \ell\nu + 4 \text{ jets}}}{Br(t \rightarrow Zc) \cdot (1 - Br(t \rightarrow Zc))} + \frac{(A * \epsilon)_{t\bar{t} \rightarrow ZcWb \rightarrow \ell \cancel{E}_T + 4 \text{ jets}}}{Br(t \rightarrow Zc) \cdot (1 - Br(t \rightarrow Zc))}, \quad (12.3)$$

$$A_{WW \rightarrow \ell \cancel{E}_T} = \frac{(A * \epsilon)_{t\bar{t} \rightarrow WbWb \rightarrow \ell\nu + 4 \text{ jets}}}{(1 - Br(t \rightarrow Zc))^2}, \quad (12.4)$$

and

$$A_{ZZ \rightarrow \ell \cancel{E}_T} = \frac{(A * \epsilon)_{t\bar{t} \rightarrow ZcZc \rightarrow \ell \cancel{E}_T + 4 \text{ jets}}}{Br(t \rightarrow Zc)^2}. \quad (12.5)$$

The values of  $A_Y$  are determined using simulated samples where all the  $t\bar{t}$  pairs decay exclusively to only one of the intermediate states:  $WbZc$ ,  $ZcZc$ , or  $WbWb$ . The acceptance  $A_{WZ \rightarrow \ell \cancel{E}_T}$  includes two decay chains since the missing energy,  $\cancel{E}_T$ , can be produced via decay  $W \rightarrow \ell\nu$  or by mis-identifying  $Z \rightarrow \ell\ell$  decay of the  $Z$ -boson.

## 12.2 Properties of the FCNC $t \rightarrow Zc$ coupling

We note that the helicity structure of a possible  $t \rightarrow Zc$  vertex is model-dependent. We cover the full range of possible helicities so as to be assumption-independent.

The kinematic properties of  $t \rightarrow Zc$  decay are reflected by the angular distributions of the decay products. This affects the total acceptance for the FCNC events since the isolation requirement is placed on all the identified jets and leptons. For example, the final state of the  $t \rightarrow Zc \rightarrow \ell^+\ell^-c$  decay chain can be fully described by introducing an angle  $\theta^*$ , taken to be the angle between the direction of the top-quark (anti-top-quark) and the positive (negative) lepton in the rest frame of the  $Z$ -boson. The angular distribution of  $\theta^*$  has the following general form:

$$f(\theta^*) = a_0 \cdot f_0(\theta^*) + a_1 \cdot f_1(\theta^*) + a_2 \cdot f_2(\theta^*), \quad (12.6)$$

where  $a_0$ ,  $a_1$ , and  $a_2$  are constants which depend on the polarization of the  $Z$ -boson and whose sum is one ( $a_0 + a_1 + a_2 = 1$ ). The functions  $f_i(\theta^*)$  are given by:

$$f_0(\theta^*) = \frac{3}{4}(1 - \cos^2(\theta^*)), \quad (12.7)$$

$$f_1(\theta^*) = \frac{3}{8}(1 + \cos(\theta^*))^2, \quad (12.8)$$

and

$$f_2(\theta^*) = \frac{3}{8}(1 - \cos(\theta^*))^2. \quad (12.9)$$

The angular distribution of decay products of the  $t \rightarrow Wb \rightarrow \ell\nu b$  decay is parametrized with the same function  $f(\theta^*)$  by taking appropriate values of the  $a_i$ . In the case of  $t \rightarrow Wb$  decay the coefficients  $a_0$ ,  $a_1$ , and  $a_2$  are the fractions of longitudinal, left-handed, and right-handed helicities of the  $W$ -boson, respectively. However, the  $Z$ -boson, unlike the  $W$ -boson, has both right-handed and left-handed couplings. Consequently, while the coefficient  $a_0$  is simply the fraction of the longitudinally polarized  $Z$  bosons, the coefficients  $a_1$  and  $a_2$  are linear functions of the fractions of left-handed and right-handed helicities of the  $Z$  boson.

The distribution of  $\cos(\theta^*)$  resulting from an arbitrary FCNC coupling can always be described by choosing appropriate values for the constants  $a_i$ . The acceptances of the FCNC top quark decays  $A_Y$  depend on the angular distributions of the decay products since we require the isolation in cone of 0.4 for all the identified leptons and jets. In consequence, the acceptances are functions of  $a_0$  and  $a_1$  (i.e.  $A_Y = A_Y(a_0, a_1)$  and  $a_2 = 1 - a_0 - a_1$ ). The top quark decay is symmetric with respect to the charge of the fermion ( $\ell\bar{\ell}$  or  $q\bar{q}$ ), and therefore the acceptances calculated for decays of right-handed  $Z$  bosons and left-handed bosons decays are identical. This means that the

acceptances  $A_Y$  can be fully parametrized with the fraction of longitudinally polarized  $Z$  bosons (i.e.  $A_Y = A_Y(a_0, 1 - a_0) = A_Y(a_0)$ ).

We compute each acceptance  $A_Y$  for five values of the fraction of longitudinally polarized  $Z$  bosons using Monte Carlo simulated events. This allows us to calculate the acceptances  $A_Y$  for any fraction  $a_0$  by interpolating the acceptances  $A_Y$  between the points measured. The acceptance  $A_{WW \rightarrow \ell \bar{\nu}_T}$  is a constant since it does not have any FCNC vertexes. The other acceptances,  $A_{ZZ \rightarrow \ell \ell}$ ,  $A_{WZ \rightarrow \ell \ell}$ ,  $A_{WZ \rightarrow \ell \bar{\nu}_T}$ , and  $A_{ZZ \rightarrow \ell \bar{\nu}_T}$  have linear or quadratic dependences on the fraction of the longitudinal helicity of the  $Z$ -bosons:

$$A_{ZZ \rightarrow \ell \ell}(a_0) = a_0^2 \cdot A_{ZZ \rightarrow \ell \ell}^{long} + 2 \cdot a_0 \cdot (1 - a_0) \cdot A_{ZZ \rightarrow \ell \ell}^{corr} + (1 - a_0)^2 \cdot A_{ZZ \rightarrow \ell \ell}^{left}, \quad (12.10)$$

$$A_{WZ \rightarrow \ell \ell}(a_0) = a_0 \cdot A_{WZ \rightarrow \ell \ell}^{long} + (1 - a_0) \cdot A_{WZ \rightarrow \ell \ell}^{left}, \quad (12.11)$$

$$A_{WZ \rightarrow \ell \bar{\nu}_T}(a_0) = a_0 \cdot A_{WZ \rightarrow \ell \bar{\nu}_T}^{long} + (1 - a_0) \cdot A_{WZ \rightarrow \ell \bar{\nu}_T}^{left}, \quad (12.12)$$

and

$$A_{ZZ \rightarrow \ell \bar{\nu}_T}(a_0) = a_0^2 \cdot A_{ZZ \rightarrow \ell \bar{\nu}_T}^{long} + 2 \cdot a_0 \cdot (1 - a_0) \cdot A_{ZZ \rightarrow \ell \bar{\nu}_T}^{corr} + (1 - a_0)^2 \cdot A_{ZZ \rightarrow \ell \bar{\nu}_T}^{left}, \quad (12.13)$$

where  $A_Y^{long}$  are measured for the longitudinally-polarized component of the  $Z$ -decays,  $A_Y^{left}$  are for the left-handed component, and the value of  $A_Y^{corr}$  is obtained using FCNC events where the  $Z$ -bosons are mixed with 50% left-handed and 50% longitudinal polarizations. The acceptance  $A_{ZZ \rightarrow \ell \ell}$  has a quadratic dependence on  $a_0$  since it accounts for the two FCNC decays of the top and anti-top quarks. The numerical values of the acceptances are tabulated in Chapters 11 and 13.

# CHAPTER 13

## MEASURING THE CONTRIBUTIONS FROM FCNC AND SM PROCESSES IN EVENTS WITH A $Z$ -BOSON AND FOUR JETS

At this stage we consider only events which have two leptons consistent with a  $Z$ -boson and at least one B-tagged jet. We use the jet multiplicity distribution (see Figure 13.1) to constrain the number of not-top  $Z+4$ jet events. We do this by scaling the whole “ $Z+HF$ ” component to the number of (observed - mis-tagged)  $Z+2$  jets events in the electron and muon modes simultaneously. The number of events with a fake  $Z$ -boson is less than 0.5% and we neglect it.

The FCNC signal contribution is divided into two parts,  $ZcWb$  and  $ZcZc$ , since the b-tagging rates are different. We summarize the acceptance and the efficiency measurements for the  $Z + 4$  jets channel in Tables 13.2, 13.1, 13.3, and 13.4. The case when a leptonic decay of a  $Z$ -boson fakes the leptonic decay of a  $W$ -boson is taken into account in Tables 13.3 and 13.4.

The  $M_{top}$ -dependent acceptances  $A_{ZZ \rightarrow \ell\ell}^{(i)}$  and  $A_{WZ \rightarrow \ell\ell}^{(i)}$  are obtained by multiplying the cumulative acceptance  $A_j$  by the fraction of events contributing to the  $i$ 'th bin of the top mass distribution:

$$A_Y^{(i)} = A_Y \cdot \frac{N_i}{\sum_k N_k}. \quad (13.1)$$

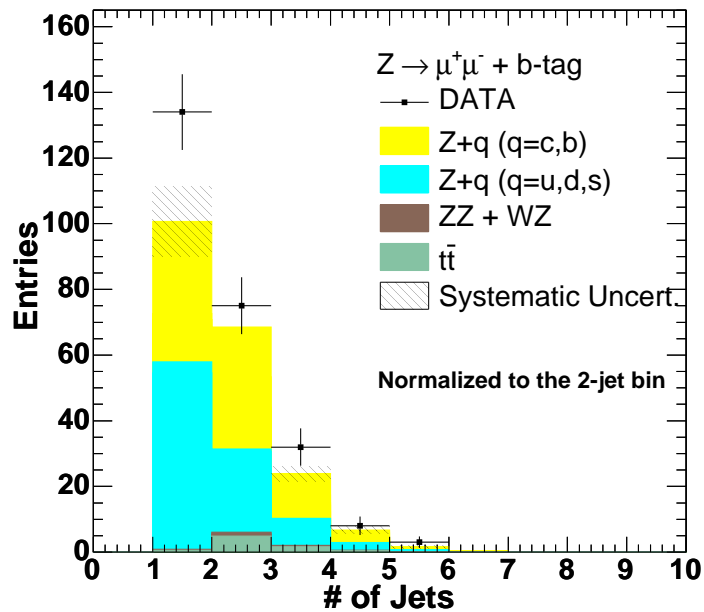
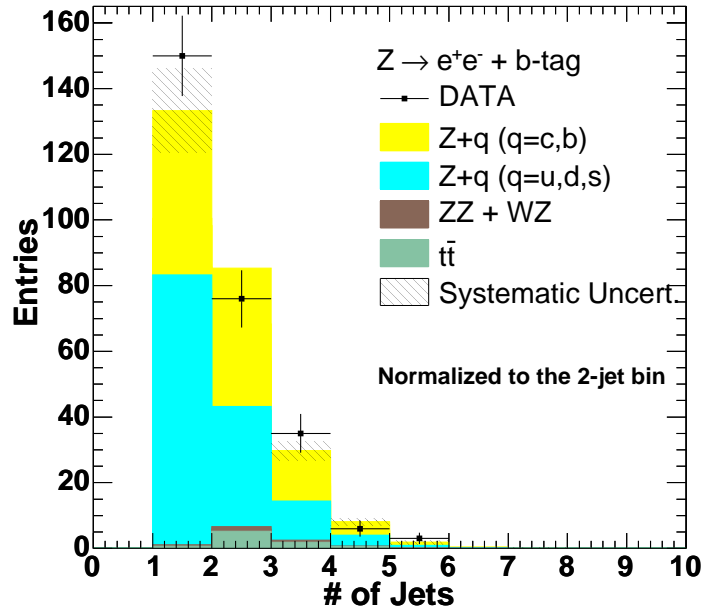


Figure 13.1: The measured distribution (points) in the number of jets in events with a  $Z$  and a b-tag, compared to SM expectations (stacked histogram), for the electron channel (upper figure) and the muon channel (lower figure). We normalize to the average of the  $Z \rightarrow e^+e^-$  and  $Z \rightarrow \mu^+\mu^-$  2-jet bins. The 1-jet bin is not used in this measurement.

Process	$A_{ZZ \rightarrow \ell\ell}$
Longitudinal fraction is $a_0=0.00$	
$t\bar{t} \rightarrow ZcZc \rightarrow e^+e^- + 4jets$	0.00185
$t\bar{t} \rightarrow ZcZc \rightarrow \mu^+\mu^- + 4jets$	0.00178
Longitudinal fraction is $a_0=0.50$	
$t\bar{t} \rightarrow ZcZc \rightarrow e^+e^- + 4jets$	0.00203
$t\bar{t} \rightarrow ZcZc \rightarrow \mu^+\mu^- + 4jets$	0.00192
Longitudinal fraction is $a_0=1.00$	
$t\bar{t} \rightarrow ZcZc \rightarrow e^+e^- + 4jets$	0.00222
$t\bar{t} \rightarrow ZcZc \rightarrow \mu^+\mu^- + 4jets$	0.00205

Table 13.1: The acceptance times efficiency for the dilepton signature from inclusive FCNC decay of  $t\bar{t} \rightarrow ZcZc \rightarrow l^+l^- + ccjj$  for different values of the longitudinal fraction of  $Z$  bosons, for electron pairs and muon pairs separately. The SM branching ratios for the  $Z \rightarrow l^+l^-$  decays are included. Note that this channel depends on the square of the FCNC branching ratio for the  $Z$ , and so its contribution is suppressed relative to that from the case where only one  $Z$  decays by FCNC (see Table 13.2).

Process	$A_{WZ \rightarrow \ell\ell}$
Longitudinal fraction is $a_0=0.00$	
$t\bar{t} \rightarrow ZcWb \rightarrow e^+e^- + 4jets$	0.00275
$t\bar{t} \rightarrow ZcWb \rightarrow \mu^+\mu^- + 4jets$	0.00267
Longitudinal fraction is $a_0=1.00$	
$t\bar{t} \rightarrow ZcWb \rightarrow e^+e^- + 4jets$	0.00313
$t\bar{t} \rightarrow ZcWb \rightarrow \mu^+\mu^- + 4jets$	0.00293

Table 13.2: Summary of the acceptance times efficiency for the dilepton signature from inclusive FCNC decays of  $t\bar{t} \rightarrow ZcWb \rightarrow l^+l^- + cjjb$ , for different values of the longitudinal fraction of  $Z$  bosons, for electron pairs and muon pairs separately. Note that the FCNC branching ratio enters only to the first power, and so this would be the dominant contribution to the FCNC signal.

### 13.1 Fitting the Top Mass

We reconstruct the value of  $M_{top}$  for each candidate event that contains at least two leptons consistent with a  $Z$ -boson and at least four jets. The procedure is similar to that of the CDF top mass measurement (see Ref. [50]). The value of  $M_{top}$  is determined by minimizing a value of  $\chi^2$ .

Process	$A_{WZ \rightarrow \ell \cancel{E}_T}$
Longitudinal fraction is $a_0=0.00$	
$t\bar{t} \rightarrow WbZc \rightarrow e\nu + bjjc$	0.00927
$t\bar{t} \rightarrow WbZc \rightarrow e\cancel{E}_T + cjjb$	0.00179
$t\bar{t} \rightarrow WbZc \rightarrow \mu\nu + bjjb$	0.007915
$t\bar{t} \rightarrow WbZc \rightarrow \mu\cancel{E}_T + bjjb$	0.002180
Longitudinal fraction is $a_0=1.00$	
$t\bar{t} \rightarrow WbZc \rightarrow e\nu + bjjc$	0.00967
$t\bar{t} \rightarrow WbZc \rightarrow e\cancel{E}_T + cjjb$	0.00185
$t\bar{t} \rightarrow WbZc \rightarrow \mu\nu + bjjc$	0.00817
$t\bar{t} \rightarrow WbZc \rightarrow \mu\cancel{E}_T + bjjc$	0.00227

Table 13.3: Summary of the acceptance times efficiency for the contribution to the single lepton +  $\cancel{E}_T$  signature from the inclusive FCNC decays of  $t\bar{t} \rightarrow WbZc \rightarrow \ell\cancel{E}_T + cjjb$  (i.e. the decay of a  $Z$  boson is mis-identified as the decay of a  $W$  boson) and  $t\bar{t} \rightarrow WbZc \rightarrow \ell\nu + bjjc$ . Standard model branching ratios are included. The acceptance  $A_{WZ \rightarrow \ell\cancel{E}_T}$  is the sum of acceptances for the both decay modes which contribute to the signature of  $\ell + \cancel{E}_T + 4jets$ .

The  $\chi^2$  includes all the top-specific corrections and energy resolutions used in the single lepton top mass measurement. The reconstructed top mass agrees well with the generated one. The difference between the reconstructed and the generated masses does not contribute to the final result and we neglect it.

The value of  $M_{top}$  is calculated by minimizing the  $\chi^2$  distribution, which is based on the assumption that the event is  $p\bar{p} \rightarrow t\bar{t} \rightarrow Z + 4jets \rightarrow \ell^+\ell^- + 4jets$ . The minimization takes into account every combination of the jets in the event since we do not know the true jet-parton assignments. The top mass distribution obtained for  $t\bar{t} \rightarrow ZcZc \rightarrow \ell^+\ell^- + 4jets$  decays does not differ significantly from that of  $WbZc$  decay. The exact formula for the  $\chi^2$  has the following structure:

$$\chi^2(M_{top}) = \sum_{\ell_1, \ell_2, jets} \frac{(\hat{E}t_i - Et_i)^2}{\sigma_i^2} + \sum_{x,y} \frac{(\hat{E}t_i^{uncl} - Et_i^{uncl})^2}{\sigma_i^2} +$$

Process	$A_{ZZ \rightarrow \ell \cancel{E}_T}$
Longitudinal fraction is $a_0=0.00$	
$t\bar{t} \rightarrow ZcZc \rightarrow e + \cancel{E}_T + 4jets$	0.000873
$t\bar{t} \rightarrow ZcZc \rightarrow \mu + \cancel{E}_T + 4jets$	0.00127
Longitudinal fraction is $a_0=0.50$	
$t\bar{t} \rightarrow ZcZc \rightarrow e + \cancel{E}_T + 4jets$	0.000858
$t\bar{t} \rightarrow ZcZc \rightarrow \mu + \cancel{E}_T + 4jets$	0.00132
Longitudinal fraction is $a_0=1.00$	
$t\bar{t} \rightarrow ZcZc \rightarrow e + \cancel{E}_T + 4jets$	0.000838
$t\bar{t} \rightarrow ZcZc \rightarrow \mu + \cancel{E}_T + 4jets$	0.00137

Table 13.4: The acceptance times efficiency for the contribution to the single lepton +  $\cancel{E}_T$  signature from the inclusive FCNC decay of  $t\bar{t} \rightarrow ZcZc \rightarrow \ell + \cancel{E}_T + cjjc$ , where the di-leptonic decay of at least one  $Z$  boson has been mis-identified as the decay of a  $W$  boson. Standard model branching ratios are included. Note that this channel depends on the square of the FCNC branching ratio for the  $Z$ , and so its contribution is suppressed relative to that from the case where only one  $Z$  decays by FCNC (see Table 13.3).

$$\begin{aligned}
& \frac{(M(j_1j_2) - M_W)^2}{\Gamma_W^2} + \frac{(M(l^+l^-) - M_Z)^2}{\Gamma_Z^2} + \\
& \frac{(M(W + j) - M_{top})^2}{\Gamma_{top}^2} + \frac{(M(Z + j) - M_{top})^2}{\Gamma_{top}^2}. \quad (13.2)
\end{aligned}$$

The first term contains the fitted transverse energies of the leptons and four jets within the corresponding experimental resolutions. The second term includes the x- and y- components of the unclustered energy. The formula also contains terms for the reconstructed masses of the  $W$ ,  $Z$ , and the two top-quarks.

We process all the “ $Z+4jets$ ” events in data and simulations with the same top mass fitting algorithm so that we can compare the  $M_{top}$  distributions to set the limit (see Figure 13.2). The  $\chi^2$  function we use does not have the proper shape since each term in the sum should be distributed as a squared Gaussian with the mean of 1. The observed distributions are shown in Figure 13.3.

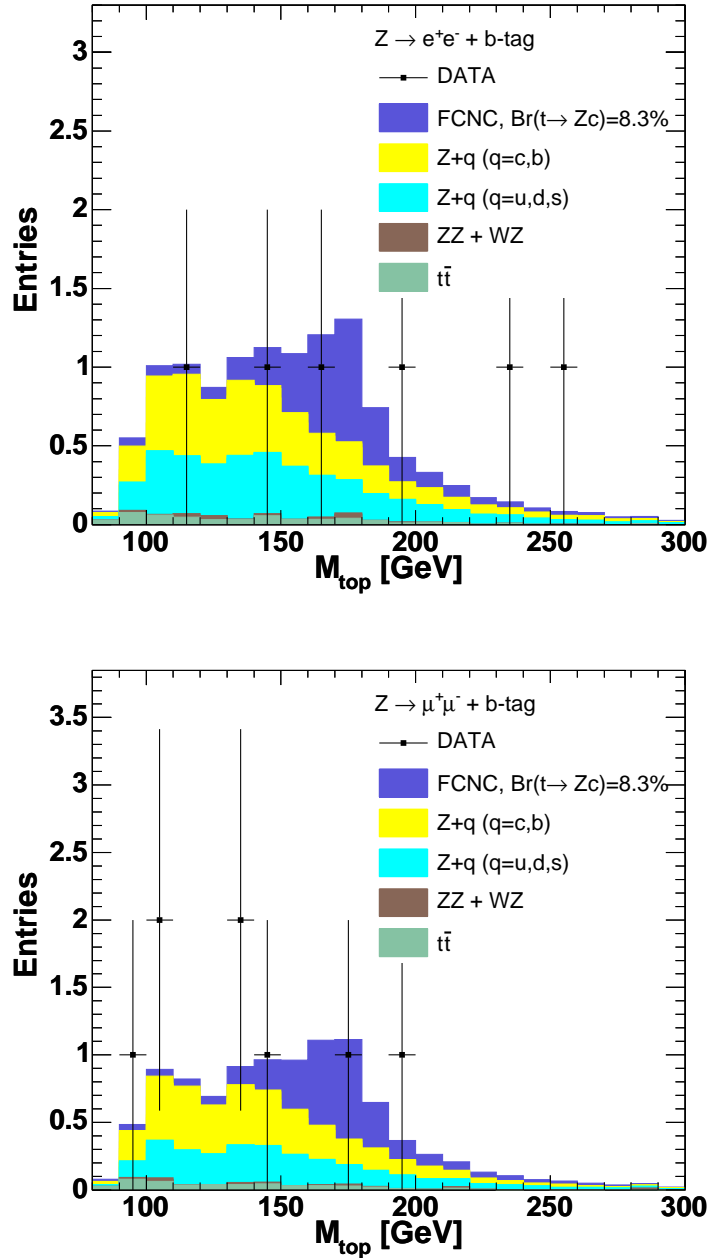


Figure 13.2: The measured distribution (points) in the fitted top mass in events with a  $Z$  and four jets with at least one b-tagged jet, compared to the SM expectations (stacked histogram), for  $Z \rightarrow e^+e^-$  events (upper figure) and  $Z \rightarrow \mu^+\mu^-$  events (lower figure).

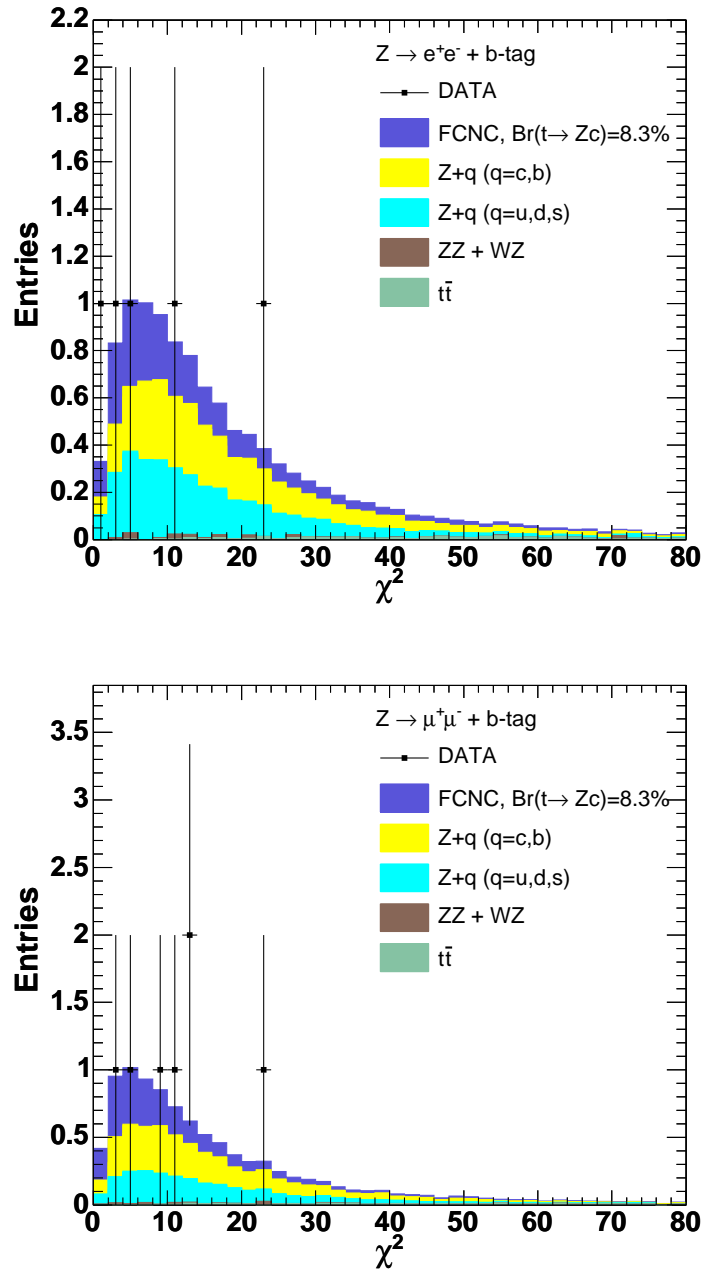


Figure 13.3: The measured distribution (points) in the fitted top  $\chi^2$  in events with a  $Z$  and four jets with at least one B-tagged jet, compared to the SM expectations (stacked histogram), for the electron channel (upper figure) and for the muon channel (lower figure).

## CHAPTER 14

### SYSTEMATIC UNCERTAINTIES

We discuss separately the systematic uncertainties involving the acceptances and backgrounds in the following two subsections.

#### 14.1 Systematic Uncertainties on the Acceptances

The uncertainties on the five acceptances used in determining the limit,  $A_Y$ , defined in Chapter 3, are summarized in Table 14.1. For each of the  $A_Y$  the effect of uncertainties in the jet energy scale, initial and final state radiation, lepton identification efficiencies, parton distribution functions, and the identification (‘tagging’) of bottom quarks and charmed quarks have been taken into account.

To estimate the systematic uncertainty from each of these sources, we vary each of the parameters listed below by one standard deviation ( $\pm\sigma$ ) and recalculate the acceptances  $A_Y$ . The effect of the uncertainty for each of the sources is correlated among the  $A_Y$ , and these correlations are taken into account in the limit-setting procedure.

Of the two acceptances that contribute to the signatures containing two charged leptons,  $A_{ZZ\rightarrow\ell\ell}$  and  $A_{WZ\rightarrow\ell\ell}$ ,  $A_{WZ\rightarrow\ell\ell}$  dominates as it depends linearly on the FCNC branching ratio of the  $Z$  boson, while the contribution corresponding to  $A_{ZZ\rightarrow\ell\ell}$  enters as the square. In a similar fashion, the single lepton +  $\cancel{E}_T$  signature is dominated by the SM decay of the top pair into  $W^+W^-b\bar{b}$ , with an acceptance

Source	$\frac{\delta(A_{ZZ\rightarrow\ell\ell})}{A_{ZZ\rightarrow\ell\ell}}$	$\frac{\delta(A_{WZ\rightarrow\ell\ell})}{A_{WZ\rightarrow\ell\ell}}$	$\frac{\delta(A_{WZ\rightarrow\ell\cancel{E}_T})}{A_{WZ\rightarrow\ell\cancel{E}_T}}$	$\frac{\delta(A_{WW\rightarrow\ell\cancel{E}_T})}{A_{WW\rightarrow\ell\cancel{E}_T}}$	$\frac{\delta(A_{ZZ\rightarrow\ell\cancel{E}_T})}{A_{ZZ\rightarrow\ell\cancel{E}_T}}$
JES	2.5%	2.6%	2.7%	2.4%	6.4%
ISR	0.5%	0.5%	0.5%	0.5%	0.5%
FSR	0.6%	0.6%	0.6%	0.6%	0.6%
PDFs	0.9%	0.9%	0.9%	0.9%	0.9%
b-jet ID	3.4%	3.6%	3.6%	3.9%	3.4%
c-jet ID	9.7%	3.5%	3.5%	1.4%	10.0%
ID of $e$ 's	1.6%	1.6%	-0.1%	-0.1%	-0.1%
or					
ID of $\mu$ 's	2.8%	2.8%	0.9%	0.9%	0.9%
Total	$10.6\% \oplus \sigma_\ell$	$5.8\% \oplus \sigma_\ell$	$5.8\% \oplus \sigma_\ell$	$4.9\% \oplus \sigma_\ell$	$12.4\% \oplus \sigma_\ell$

Table 14.1: Summary table of the relative systematic uncertainties on the acceptances. Correlations are taken into account in the calculation of the limit. The abbreviation  $\sigma_\ell$  stands for the systematic uncertainty due to lepton identification and triggering. The lepton-related systematic uncertainties should be added separately depending to the final state used.

$A_{WW\rightarrow\ell\cancel{E}_T}$ , as there is no FCNC branching ratio in the rate. The process described by  $A_{WZ\rightarrow\ell\cancel{E}_T}$  is suppressed by a single factor of the FCNC branching ratio, while that described by  $A_{ZZ\rightarrow\ell\cancel{E}_T}$  is quadratic, and hence makes a very small contribution.

The largest systematic uncertainties in the dominant processes in the dilepton and single-lepton modes are the uncertainties in the efficiency for identifying b-quarks and c-quarks. For b-quarks, we lower the Monte Carlo acceptances by factor of  $0.95 \pm 0.05$ , found from comparing data and Monte Carlo [51]. The uncertainty on the acceptance is found by varying the normalization by  $\pm 1 \sigma$  and recalculating the tagging efficiency.

For c-quarks, we assume that the b-tagging scale factor for a jet with a charm-quark decay is the same as that for a jet with a bottom-quark decay, i.e. the MC predicted efficiency needs to be multiplied by 0.95. However, there are no direct measurements of this hypothesis with the CDF-II detector. To estimate the uncertainty, we follow the prescription used previously in the top cross-section measurement [52],

and recalculate the acceptances using a normalization factor of 0.80 rather than 0.95 for b-tags caused by decays of c-quarks in the MC.

The next largest contribution to the systematic uncertainties is from uncertainties in the calibration of jet energies [53]. The systematic uncertainties are positively correlated for all the  $A_Y$ . We note that this is almost certainly an over-estimate, as changing the jet-energy-scale by  $\pm 1 \sigma$  at the low jet threshold we use would change the spectrum in the number of jets observed outside of theoretical predictions [54].

The contributions from lepton identification and trigger efficiencies are limited by the precision check of the R-ratio (see Section 8). We assume that the reconstruction and the triggering efficiencies of electrons and muons are not correlated, but acceptances of  $W$ 's and  $Z$ 's decaying to leptons of the same flavor are correlated. This means that  $A_{ZZ \rightarrow \ell\ell}$  would be mis-estimated by the same percentage as  $A_{WZ \rightarrow \ell\ell}$  for leptons of the same flavor. The same principle is true for  $A_{WZ \rightarrow \ell \cancel{E}_T}$ ,  $A_{WW \rightarrow \ell \cancel{E}_T}$ , and  $A_{ZZ \rightarrow \ell \cancel{E}_T}$ .

The observed R-ratios (see Chapter 8) agree with the NNLO predictions to within 2%. However the cross-section  $\sigma(Z \rightarrow \mu^+ \mu^-)$  differs from the NNLO prediction by 2.8% (this is the largest discrepancy). A simple explanation of why the uncertainty in the R-ratio is smaller than that on an individual cross-section is that the  $\sigma(W \rightarrow l\nu)$  is proportional to the product of efficiencies of the high- $p_T$  lepton trigger and lepton reconstruction, but  $\sigma(Z \rightarrow l^+ l^-)$  is proportional only to the square of the efficiency of the lepton reconstruction. The uncertainty for the  $W$  then is linear in the uncertainties on both the reconstruction and the trigger, while the uncertainty for the  $Z$  is dominated by twice the uncertainty on the acceptance. The uncertainty on R, the ratio of  $W$  to  $Z$ , thus depends on both the uncertainty on the reconstruction and the uncertainty on the trigger. If the reconstruction uncertainty is the larger,

then  $R$  will be better measured than the individual cross-sections. This is the case in the muon channel.

The systematic uncertainties in the  $A_Y$  due to lepton identification and triggering are estimated using deviations between the measured cross-sections of inclusive  $W$ 's and  $Z$ 's, used in calculating the ratio  $R$ , from their theoretical values:

$$\frac{\Delta\sigma(Z \rightarrow \ell\ell)}{\sigma(Z \rightarrow \ell\ell)} = -\frac{\delta(A_{ZZ \rightarrow \ell\ell})}{A_{ZZ \rightarrow \ell\ell}} = -\frac{\delta(A_{WZ \rightarrow \ell\ell})}{A_{WZ \rightarrow \ell\ell}} \quad (14.1)$$

and

$$\begin{aligned} \frac{\Delta\sigma(W \rightarrow \ell\cancel{E}_T)}{\sigma(W \rightarrow \ell\cancel{E}_T)} &= -\frac{\delta(A_{WZ \rightarrow \ell\cancel{E}_T})}{A_{WZ \rightarrow \ell\cancel{E}_T}} \\ &= -\frac{\delta(A_{WW \rightarrow \ell\cancel{E}_T})}{A_{WW \rightarrow \ell\cancel{E}_T}} \\ &= -\frac{\delta(A_{ZZ \rightarrow \ell\cancel{E}_T})}{A_{ZZ \rightarrow \ell\cancel{E}_T}} \end{aligned} \quad (14.2)$$

The uncertainty on the integrated luminosity does not contribute at the first order to the measurement of  $\text{Br}(t \rightarrow Zc)$  since it's positively correlated between  $\sigma(W \rightarrow \ell\cancel{E}_T)$  and  $\sigma(Z \rightarrow \ell\ell)$ . Only negatively correlated uncertainties affect the measurement of  $\text{Br}(t \rightarrow Zc)$ .

The deviation of the measured  $R$  ratio is

$$\begin{aligned} \frac{\Delta R}{R} &= \Delta \left( \frac{\sigma(W \rightarrow \ell\cancel{E}_T)}{\sigma(Z \rightarrow \ell\ell)} \right) / \left( \frac{\sigma(W \rightarrow \ell\cancel{E}_T)}{\sigma(Z \rightarrow \ell\ell)} \right) \\ &= \frac{\Delta\sigma(W \rightarrow \ell\cancel{E}_T)}{\sigma(W \rightarrow \ell\cancel{E}_T)} - \frac{\Delta\sigma(Z \rightarrow \ell\ell)}{\sigma(Z \rightarrow \ell\ell)}. \end{aligned} \quad (14.3)$$

Therefore the connection between the deviation in the  $R$ -ratio and the uncertainties

of the  $A_Y$  is as following:

$$\begin{aligned} \frac{\Delta R}{R} &= \sigma \left( \frac{A_{WZ \rightarrow \ell\ell}}{A_{WW \rightarrow \ell\cancel{E}_T}} \right) / \left( \frac{A_{WZ \rightarrow \ell\ell}}{A_{WW \rightarrow \ell\cancel{E}_T}} \right) \\ &= \frac{\delta(A_{WZ \rightarrow \ell\ell})}{A_{WZ \rightarrow \ell\ell}} - \frac{\delta(A_{WW \rightarrow \ell\cancel{E}_T})}{A_{WW \rightarrow \ell\cancel{E}_T}}. \end{aligned} \quad (14.4)$$

We treat  $\frac{\delta(A_{WZ \rightarrow \ell\cancel{E}_T})}{A_{WW \rightarrow \ell\cancel{E}_T}}$  and  $\frac{\delta(A_{WZ \rightarrow \ell\ell})}{A_{WZ \rightarrow \ell\ell}}$  as negatively correlated as it is the most conservative case. Also this treatment insures the constraint from the  $R$ -ratio.

Contributions from other sources are significantly smaller than those from heavy flavor identification and jet-energy scale. The effect of initial and final radiation (ISR and FSR) on  $A_{WW \rightarrow \ell\cancel{E}_T}$  was studied in Ref. [52]. We expect that FSR will contribute to the uncertainties in the other three  $A_Y$  in the same way since we require four jets in the final state for all four channels and the samples are triggered on leptons. The ISR error should also contribute identically to the uncertainties of the four acceptances  $A_Y$ . The uncertainties are 0.5% for ISR and 0.6% for FSR, and they are 100% correlated across all  $A_Y$ .

The uncertainties arising from parton distribution functions (PDF). can also propagate into the acceptance. However, the dominant effect is on the production of the  $t\bar{t}$  pairs and not the decays. The effect of the uncertainties was also studied in Ref. [52]. The total uncertainty is 0.9% and is 100% correlated for the four  $A_Y$ .

The uncertainty on the top quark mass is now close to 1% [55]. This will introduce an uncertainty similar to, but much smaller than and correlated with, that from the jet energy scale, and so we consider it included in the (conservatively estimated) uncertainty on the jet energy scale.

## 14.2 Systematic Uncertainties of the Backgrounds

The sensitivity of this search for a  $Z$ -boson and a charm quark coming from top decay depends strongly on the understanding of the SM  $W$ -boson and  $Z$ -boson production in conjunction with heavy flavor ( $W/Z$ +HF). We summarize the systematic uncertainties of backgrounds in both the single lepton and di-lepton signatures (the terms  $B_{\ell \cancel{E}_T}$  and  $B_{\ell^+\ell^-}$  in Equations 15.3 and 15.2) in Table 14.2, and discuss them below.

Source of Systematic Uncertainty	$\ell + \cancel{E}_T + 4 \text{ jets}$	$\ell^+\ell^- + 4 \text{ jets}$
Radiation of extra jets	20%	20%
Parametrization of mistag rates	15%	15%
Background normalization	2.5%	8%

Table 14.2: The relative systematic uncertainties on the backgrounds for 4-jet semi-leptonic and dilepton final states of  $t\bar{t}$  pairs. The contributions from Monte Carlo and Mistags are (conservatively) taken to be correlated in the computation of the limit. The normalization uncertainties are contributed from the finite statistics of the 2-jet bin in  $W$ +HF and  $Z$ +HF samples.

The largest uncertainty in the background comes from modeling the production of  $W$ -bosons and  $Z$ -bosons accompanied by heavy-flavor and additional jets. The  $Z$ +HF and  $W$ +HF backgrounds are modeled by ALPGEN [56], and hadronized with PYTHIA [57]. The predictions suffer from uncertainties in the modeling procedure. In particular, the expected number of events in the “ $W/Z + 4 \text{ jets}$ ” category enters directly into the calculation for the final result. To make an estimate of the uncertainty on the expected number of  $W/Z$ +HF events, we assume that there is a set of parameters which allows ALPGEN to model data perfectly. A deviation from the “ideal set” can be estimated using inclusive  $Z + \text{jets}$  events with jet multiplicity below three. A comparison between data and ALPGEN simulations is shown in Figures 14.1 and 14.2.

The observed deviation on radiation of one extra jet in the inclusive sample is less than 5%. We assume independent gluon emission, and so take 10% as the estimate of the uncertainty on this ALPGEN prediction for the radiation of 2 extra jets in the inclusive sample. However, the slopes of the N-jet distribution are predicted to be different in the inclusive and HF samples, with the factors for each additional jet being 5.0 and 2.7 in the inclusive and b-tagged samples, respectively. The ratio of 5.0 to 2.7 makes a relative difference of 1.85 between radiating an extra jet in inclusive and tagged samples. We consequently increase the 10% deviation by a factor of 2 (rounding 1.85 up), to 20%.

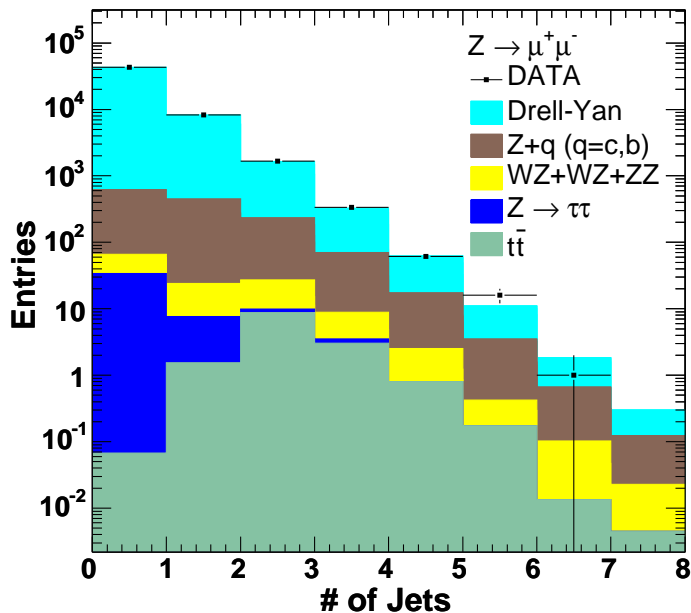


Figure 14.1: The measured distribution (points) in the number of jets in events with an inclusive decay of  $Z \rightarrow \mu^+ \mu^-$ , compared to SM expectations (stacked histogram). The “Z+Jets” processes (Drell-Yan,  $Z+b$ , and  $Z+c$ ) are modeled with ALPGEN.

The sensitivity of the limit to the number of 4-jet  $Z$ +HF events was calculated by performing a set of pseudo-experiments with different levels of the systematic

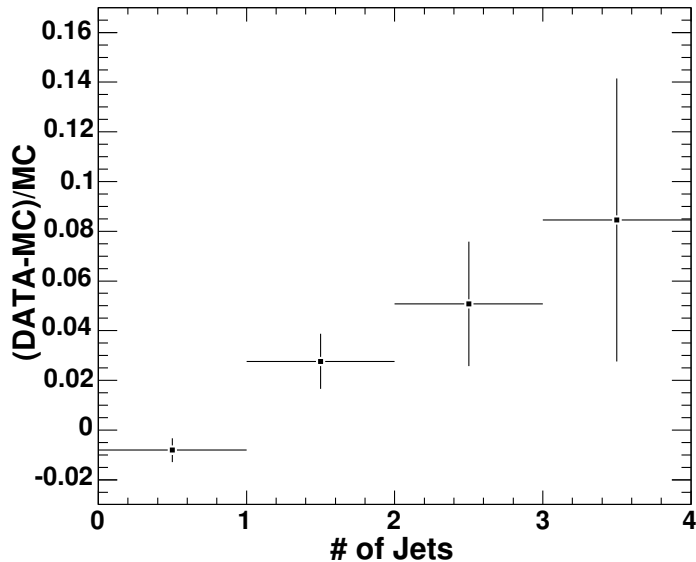


Figure 14.2: The ratio between the measured distribution (DATA) and the SM expectations (MC) in the number of jets in events with an inclusive decay of  $Z \rightarrow \mu^+ \mu^-$ . The “ $Z$ +jets” processes (Drell-Yan,  $Z$ +b, and  $Z$ +c) contribution to the SM expectations are modeled with ALPGEN.

uncertainties of the backgrounds. The limit was calculated with this systematic uncertainty set to zero, set to 20% (nominal), and set to 40%. The respective shifts in the limit are -0.1%, zero (by construction), and +0.1%, respectively. The weak dependence is caused by the measurement technique; we measure a ratio of top quark events between  $Z + 4$  jets and  $W + 4$  jets final states. An increase in the number of background events leads to a decrease in the  $t\bar{t}$  cross-section measured with  $W + 4$  jets events. Simultaneously it leads to a decrease in the upper limit on the number of FCNC signal events in the  $Z + 4$  jets final state.

The method of predicting misidentified heavy flavor (mistag rates) by applying a parameterization of the rate for a light-quark jet or gluon jet being mis-identified as jet from a charm or bottom quark to jets in a sample before heavy flavor identification

contributes a significant systematic uncertainty to the background estimates. We vary the mistag probability calculated by the standard CDF algorithm used in the measurement of the top quark cross-section [58] jet-by-jet by  $\pm 15\%$  (i.e. a factor of 0.85 or 1.15) to estimate the contribution to the uncertainty.

A smaller contribution to the uncertainty is due to the overall normalization of the predicted SM boson+HF contribution. The normalizations of the background distributions from  $W$ +HF and  $Z$ +HF events are treated as independent, and are normalized to match the number of observed events in the  $W$ +HF+2 jets and  $Z$ +HF+2 jets channels, respectively, as discussed in detail in Chapters 11 and 13. The finite statistics of the 2-jet bin of the data contributes an uncertainties of 2.5% and 8% to the single lepton and di-lepton signatures, respectively.

The 6% uncertainty of the measured luminosity affects only processes that are normalized absolutely. These processes are  $WW$ ,  $WZ$ , and  $ZZ$  production. The contribution from the uncertainty from luminosity to the final result consequently is negligible ( $< 0.1\%$ ).

## CHAPTER 15

### STATISTICAL EVALUATION OF THE LIMITS ON $\text{BR}(T \rightarrow ZC)$

At this point we have all the ingredients needed to evaluate limits on the FCNC branching ratio  $Br(t \rightarrow Zc)$ . The branching ratio is evaluated by comparing the numbers of expected and observed events in two final states, “ $\ell^+\ell^- + 4jets$ ” and “ $\ell\cancel{E}_T + 4jets$ ”, using Poisson statistics. The numbers of observed events are denoted as  $N_{\ell\cancel{E}_T}$  and  $N_{\ell^+\ell^-}$  for final states “ $\ell\cancel{E}_T + 4jets$ ” and “ $\ell^+\ell^- + 4jets$ ”, respectively, the numbers of expected events are denoted as  $E_{\ell\cancel{E}_T}$  and  $E_{\ell^+\ell^-}$ .

To avoid large systematic uncertainties we simultaneously analyze two final states from decays of top pairs:  $p\bar{p} \rightarrow t\bar{t} \rightarrow ZcWb \rightarrow \ell^+\ell^-cjbb$ , and  $p\bar{p} \rightarrow t\bar{t} \rightarrow WbWb \rightarrow \ell\cancel{E}_Tbjbb$ . This is done by comparing the number of expected events from SM  $t\bar{t}$  decays and SM backgrounds to the number of observed events in each final state. The contributions from  $t\bar{t}$  decays depend on two numbers:  $Br(t \rightarrow Zc)$  and  $N_{t\bar{t}} = \sigma(p\bar{p} \rightarrow t\bar{t}) \cdot \int L dt$ , where  $\sigma(p\bar{p} \rightarrow t\bar{t})$  is the cross-section of top pair production at CDF and  $\int L dt$  is the integrated luminosity. We treat these two numbers,  $Br(t \rightarrow Zc)$  and  $N_{t\bar{t}}$ , as free parameters in the calculation of the limit on the FCNC branching ratio. The result of the comparison is presented as a likelihood which is a two-dimensional function of  $Br(t \rightarrow Zc)$  and  $N_{t\bar{t}}$ . We use the likelihood distribution to estimate limits on the FCNC branching ratio  $Br(t \rightarrow Zc)$  using a Bayesian approach.

For simplicity, let us consider the case in which we observe only two numbers of events:  $N_{\ell\cancel{E}_T}$  and  $N_{\ell^+\ell^-}$ , by applying some set of selection requirements. Later we

will show how to generalize this approach to be used with more categories of selected events. This is be done since we will consider events with electrons and muons separately and we use a binned distribution of  $M_{top}$  for “ $\ell^+\ell^- + 4jets$ ” events.

We assume that the top quark has only the two decay channels  $Wb$  and  $Zc$ , and so  $\text{Br}(t \rightarrow Wb) + \text{Br}(t \rightarrow Zc) = 1$ . The number of expected  $t\bar{t}$  pairs is

$$N_{t\bar{t}} = \sigma(p\bar{p} \rightarrow t\bar{t}) \cdot \int L dt, \quad (15.1)$$

where  $\sigma(p\bar{p} \rightarrow t\bar{t})$  can be taken *a priori* since it is independent of any FCNC physics.

The expected numbers of events in each of the decay modes are estimated as follows, where we use the notation  $B_Z = \text{Br}(t \rightarrow Zc)$ :

$$\begin{aligned} E_{\ell\cancel{E}_T} = & B_{\ell\cancel{E}_T} + N_{t\bar{t}} \cdot \{(1 - B_Z)^2 \cdot A_{WW \rightarrow \ell\cancel{E}_T} + \\ & B_Z(1 - B_Z) \cdot (A_{WZ \rightarrow \ell\cancel{E}_T}) + \\ & B_Z^2 \cdot A_{ZZ \rightarrow \ell\cancel{E}_T}\} \end{aligned} \quad (15.2)$$

and

$$\begin{aligned} E_{\ell^+\ell^-} = & B_{\ell^+\ell^-} + N_{t\bar{t}} \cdot \{A_{WZ \rightarrow \ell\ell} \cdot B_Z + \\ & (A_{ZZ \rightarrow \ell\ell} - A_{WZ \rightarrow \ell\ell}) \cdot B_Z^2\}. \end{aligned} \quad (15.3)$$

In the formulas above  $B_{\ell\cancel{E}_T}$  and  $B_{\ell^+\ell^-}$  are non-top SM contributions (backgrounds) to final states “ $\ell\cancel{E}_T + 4jets$ ” and “ $\ell^+\ell^- + 4jets$ ”, respectively;  $A_Y$  is acceptance for a decay mode “Y” (see Section 10).

The limit on the ratio  $Br(t \rightarrow Zc)$  is estimated using probability density (i.e. likelihood) function defined as:

$$L(B_Z, N_{t\bar{t}}) = P(N_{\ell\cancel{\nu}_T}, N_{\ell+\ell-} | B_Z, N_{t\bar{t}}) \quad (15.4)$$

i.e.

$$L(B_Z, N_{t\bar{t}}) = P(N_{\ell\cancel{\nu}_T} | E_{\ell\cancel{\nu}_T}) \cdot P(N_{\ell+\ell-} | E_{\ell+\ell-}), \quad (15.5)$$

where

$$P(N|E) = \frac{E^N e^{-E}}{N!} \quad (15.6)$$

is a Poisson distribution. The likelihood  $L(B_Z, N_{t\bar{t}})$  is defined in the physical region of the two free parameters  $N_{t\bar{t}} \geq 0$  and  $0 \leq B_Z \leq 1$ .

The complete set of systematic uncertainties is included in the likelihood function by using a numerical integration technique. The correlations between the uncertainties are taken into account.

To discriminate the FCNC signal from the expected SM background, we use the distribution in the reconstructed top-quark mass,  $M_{top}$ , for “Z+4jets” events. Events from the signal process should form a distinguishable peak at the top quark mass. We combine probabilities for each bin of the reconstructed top-quark mass distribution

$$\prod_i P(N_{\ell+\ell-}^i | E_{\ell+\ell-}^i), \quad (15.7)$$

where the index  $i$  refers to the  $i$ th bin of the distribution in the top mass. This requires calculating the acceptances  $A_{ZZ \rightarrow \ell\ell}^{(i)}$  and  $A_{WZ \rightarrow \ell\ell}^{(i)}$  for each bin of the reconstructed top quark mass histogram.

We note that the electron and muon decay modes of the top quarks are treated

separately up to this point of the analysis in order to better understand the systematics of both. The two channels are then included together in the final likelihood function  $L(B_Z, N_{t\bar{t}})$ .

The likelihood function is used to construct a posterior probability density  $P(B_Z|\text{DATA})$ , where DATA refers to the numbers of observed events,  $\mathbf{N}_{\ell\cancel{E}_T}$  and  $\mathbf{N}_{\ell+\ell-}$ , in all the categories (electrons, muons, and the binned  $M_{top}$  distributions). The posterior probability density function is converted into a limit on the FCNC branching ratio  $Br(t \rightarrow Zc)$  with a Bayesian approach.

## 15.1 Numerical Computation of the Likelihood Distribution Function

The observed distribution of the likelihood (computed for  $t \rightarrow Zc$  decays where the  $Z$ -bosons are 100% longitudinally polarized) is presented in Figure 15.1.

A likelihood distribution is calculated for each given value of helicity of the  $t \rightarrow Zc$  coupling since the acceptances  $A_Y$  vary for different structures of the FCNC coupling.

## 15.2 Computation of the Posterior $P(Br(t \rightarrow Zc)|\text{DATA})$

The posterior probability density functions  $P(B_Z|\text{DATA})$  are computed from the likelihood functions  $L(B_Z, N_{t\bar{t}})$  using a Bayesian approach as follows:

$$P(\text{DATA}|B_Z) = \int_0^\infty L(B_Z, N_{t\bar{t}}) \cdot \pi_0(N_{t\bar{t}}) dN_{t\bar{t}} \quad (15.8)$$

$$P(B_Z|\text{DATA}) = \frac{P(\text{DATA}|B_Z) \cdot \pi_1(B_Z)}{\int_0^1 P(\text{DATA}|B_Z) \cdot \pi_1(B_Z) dB_Z}, \quad (15.9)$$

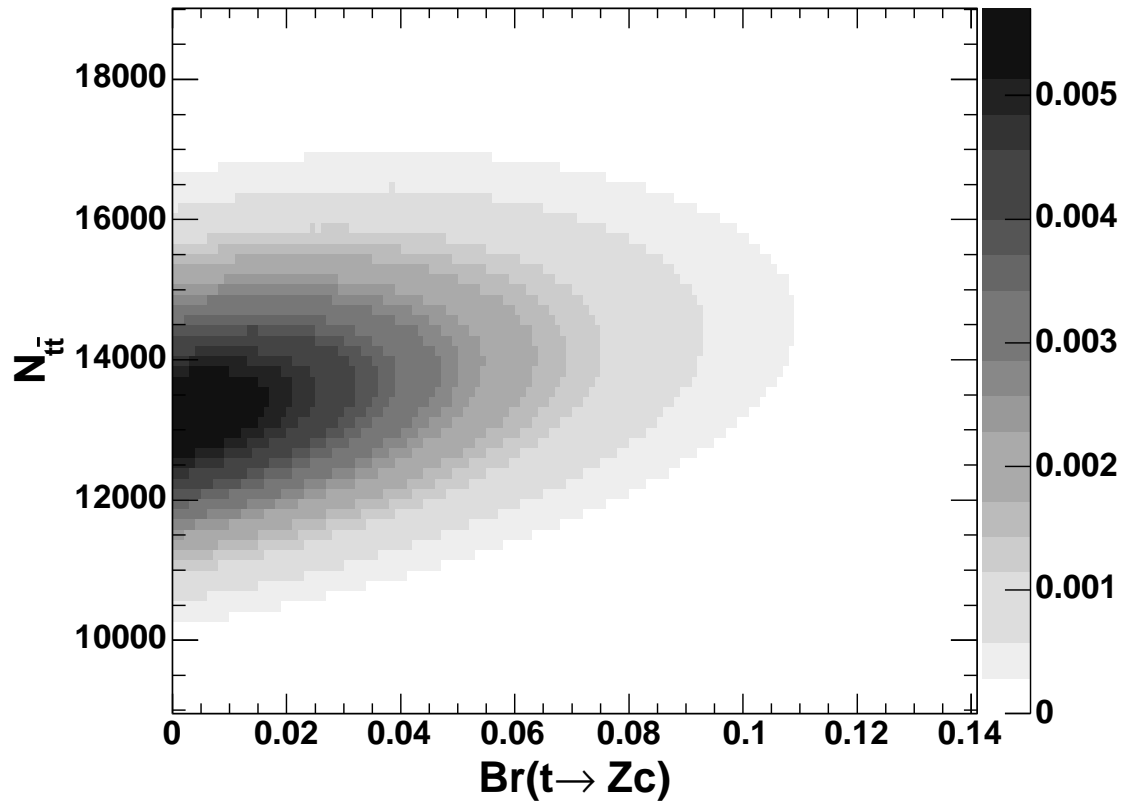


Figure 15.1: The likelihood distribution  $L(B_Z, N_{t\bar{t}})$  calculated as a function of  $N_{t\bar{t}}$  and  $Br(t \rightarrow Zc)$ . The distribution shown is for FCNC decays of  $t \rightarrow Zc$  with 100% longitudinally polarized  $Z$ -bosons.

where  $\pi_0(N_{t\bar{t}})$  is the *a priori* probability density function of  $N_{t\bar{t}}$  and  $\pi_1(B_Z)$  is the *a priori* distribution of  $B_Z$  which is flat in the physical region (it is 1.0 for  $0 \leq B_Z \leq 1$  and zero everywhere else). The distribution of  $\pi_0(N_{t\bar{t}})$  represents the prior knowledge of the top pair production cross-section,  $\sigma(p\bar{p} \rightarrow t\bar{t})$ .

We consider two choices of the  $\pi_0(N_{t\bar{t}})$  prior distribution: “Flat” and “Gaussian”. The “Flat” distribution does not contain any information regarding the theoretical predictions of  $\sigma(p\bar{p} \rightarrow t\bar{t})$ , being just a constant. The “Gaussian” distribution is derived using the theoretical estimates of top pair production cross-section  $\sigma(p\bar{p} \rightarrow t\bar{t})$  [59] and the integrated luminosity. The theoretical estimate of the top pair production cross-section is presented as a function of top quark mass  $M_{top}$ . The measured top-quark mass is  $170.9 \pm 1.8$  GeV [55]. The luminosity is  $1.52 \text{ fb}^{-1}$  and it comes with an uncertainty of 6%. The “Gaussian” prior allows us to take into account the theoretical FCNC-independent knowledge of  $\sigma(p\bar{p} \rightarrow t\bar{t})$ .

The distribution for  $P(B_Z|\text{DATA})$ , calculated for 100% longitudinally polarized  $Z$ -bosons, is shown in Figure 15.2.

### 15.3 Computation of the Upper Limits on $Br(t \rightarrow Zc)$

We use the posterior function  $P(B_Z|\text{DATA})$  to calculate the upper limit  $B_Z^{lim}$  on  $Br(t \rightarrow Zc)$  (i.e.  $B_Z$ ) by solving the equation:

$$\beta = \int_0^{B_Z^{lim}} P(B_Z|\text{DATA}) dB_Z, \quad (15.10)$$

where  $\beta$  is 0.95 (95% C.L). The upper limits versus helicity of the  $Z$ -boson are summarized in Table 16.1.

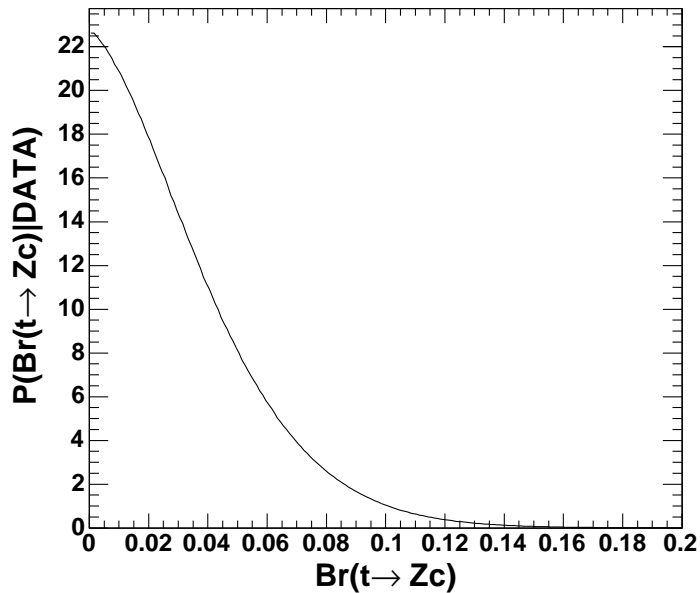


Figure 15.2: The distribution for  $P(B_Z|\text{DATA})$ , calculated for 100% longitudinally polarized  $Z$ -bosons.

We perform statistical cross-checks of the measured upper limits using pseudo-experiments. Each pseudo-experiment is a set of numbers given to the likelihood machinery (i.e. it is two distributions of  $M_{top}$ , for  $Z \rightarrow e^+e^-$  and  $Z \rightarrow \mu^+\mu^-$ , and numbers of  $e\nu + 4jets$  and  $\nu\nu + 4jets$  events). The pseudo-experiments are generated randomly assuming that there is no contribution from FCNC processes (i.e. by setting  $Br(t \rightarrow Zc)=0$ ). The expected upper limit for 100% longitudinally polarized  $Z$ 's on  $Br(t \rightarrow Zc)$  is  $8.7 \pm 2.6$  %, consistent with the observed limit of 8.3%.

## CHAPTER 16

### CONCLUSIONS AND RESULTS

Taking into account systematic uncertainties on Monte Carlo simulations,  $b$ -tagging, mistag modeling, and lepton identification, etc., we find an upper limit at 95% C.L. on the branching ratio of  $t \rightarrow Zc$  of 8.3% for FCNC decays where the  $Z$ -bosons are 100% longitudinally polarized.

To be assumption-independent we parametrize the limit on  $Br(t \rightarrow Zc)$  as a function of the fraction of longitudinally polarized  $Z$ -bosons. The parametrization allows us to cover the full range of all possible helicity structures of the  $t \rightarrow Zc$  vertex. The upper limits are calculated at 95% C.L. for five fractions of longitudinally polarized  $Z$ 's using  $1.52 \text{ fb}^{-1}$  of data. The results are presented in Table 16.1 for both the ‘‘Gaussian’’ and the ‘‘flat’’ priors. The limits vary between 8.3 and 9.0% for the ‘‘Gaussian’’ prior depending on the polarisation of the  $Z$ -boson and are about 1% less restrictive for the ‘‘flat’’ prior.

Longitudinal Fraction	0.00	0.25	0.50	0.75	1.0
Gaussian prior	9.0%	8.8%	8.6%	8.5%	8.3%
Flat prior	10.2%	10.0%	9.7%	9.5%	9.2%

Table 16.1: The upper limits on the FCNC branching ratio  $Br(t \rightarrow Zc)$  in % as a function of the longitudinal fraction of the  $Z$ -bosons in the FCNC coupling ( $t \rightarrow Zc$ ) at 95% CL. The limits labeled ‘‘Gaussian prior’’ use as input the theoretical cross-section of  $\sigma(p\bar{p} \rightarrow t\bar{t})$ ; the limits labeled ‘‘Flat prior’’ are theory-independent.

## APPENDIX A

### DETAILS OF LEPTON SELECTION CRITERIA

Variable	Tight	Loose
$P_T$ , GeV	$> 20$	$> 12$
$E_{EM}$ , GeV	$< 2 + \max(0, p-100) * 0.0115$	$< 2 + \max(0, p-100) * 0.0115$
$E_{HAD}$ , GeV	$< 6 + \max(0, p-100) * 0.028$	$< 6 + \max(0, p-100) * 0.028$
$isolation/P_T$	$< 0.1$	$< 0.1$
#SL with $\geq 5$ hits	$\geq 3$ stereo and axial	$\geq 3$ axial and $\geq 2$ stereo
$\chi_{COT}^2/DOF$	$< 3$	$< 4$
$ Z0 $ , cm	$< 60$	$< 60$
$\Delta X_{CMU}$ , cm	$< 7$	
$\Delta X_{CMP}$ , cm	$< 7^a$	
$\Delta X_{CMX}$ , cm	$< 6$ for run $> 150144$	
COT exit radius	$> 140$ cm	
Muon Detector	CMUP or CMX	
Cosmic Filter	On	On
Fiducial Requirements	Yes	

*a.* We use a wider cut than the default of 5.0 cm since the MC does not reproduce the distribution of  $\Delta X_{CMP}$  well enough.

Table A.1: Summary of the muon identification cuts. "DOF" stands for degrees of freedom (i.e. the number of COT hits - 5).

Variable	Tight	Loose
$E_T$ , GeV	$> 20$	$> 12$
Track $P_T$ , GeV	$> 10$	$> 10$
Track $Z_0$ , cm	$< 60$	$< 60$
$E/P$	$< 2$ or $P_T > 50$ GeV	
charge signed $\Delta X$ , cm	$< 1.5$ and $> -3.0$	
# of SI with $\geq 5$ hits	$\geq 3$ axial and $\geq 2$ stereo	$\geq 3$ axial and $\geq 2$ stereo
Conversion Filter	On	On
$Had/EM$	$< 0.055 + 0.00045 \cdot E$	$< 0.055 + 0.00045 \cdot E$
Lshr	$< .2$	
$\chi_{strip}^2$	$< 10$	
Calorimeter Iso./ $E_T$	$< .1$	$< .1$
Fiducial Requirements	$X_{CES} < 21.5$ cm and $9 < Z_{CES} < 230$ cm	$X_{CES} < 21.5$ cm and $9 < Z_{CES} < 230$ cm

Table A.2: Summary of the central (CEM) electron identification cuts.

Variable	Cut
Type	Phoenix
$E_T$ , GeV	$> 12$
$ \eta_{det} $	$1.2 <  \eta_{det}  < 2.5$
Track type	phoenix
Track $Z_0$ , cm	$< 60$
SVX Hits	$> 2$
$Had/EM$	$< 0.05$
$\chi_{tree}^2$	$< 10$
Frac. Cal. Iso.	$< .1$
PES 5X9 U	$> 0.65$
PES 5X9 V	$> 0.65$
PEM fit towers	$\neq 0$

Table A.3: Summary of the plug (PEM) electron identification cuts.

**APPENDIX B**  
**CORRECTIONS TO IDENTIFICATION EFFICIENCIES,**  
**ACCEPTANCES, AND TRIGGER EFFICIENCIES FOR**  
**ELECTRONS AND MUONS**

Type	Scale Factor
CEM Tight	$0.983 \pm 0.002(stat.) \pm 0.003(syst.)$
CEM Loose	$1.000 \pm 0.001(stat.) \pm 0.003(syst.)$
PEM	$0.937 \pm 0.003(stat.) \pm 0.003(syst.)$
Tight CMUP Muon	$0.9257 \pm 0.005$
Tight CMX Muon (Arches)	$0.9927 \pm 0.006$
Tight CMX Muon (MS + KS)	$0.9159 \pm 0.092$
Loose (Stubbles) Muon	$1.036 \pm 0.01$

Table B.1: Summary of the lepton scale factors. The Monte Carlo efficiencies are *multiplied* by these to match those in the data.

Trigger	Efficiency
ELECTRON_CENTRAL18	$0.9585(7) * (1 - 89593 * exp(-0.7127 * E_T))$ , where $E_T$ is of the trigger electron
MUON_CMUP18	$0.917 \pm 0.003$
MUON_CMX18 (Arches)	$0.953 \pm 0.003$
MUON_CMX18 (MS+KS)	$0.759 \pm 0.010$

Table B.2: Summary of the lepton trigger efficiencies. The Monte Carlo events are re-weighted to correct for the trigger inefficiencies.

## APPENDIX C

### PHOTON IDENTIFICATION CRITERIA

Variable	Cut
Corrected Et, GeV	$> 25$
CES x and z Fiducial	Ces $ X  < 21$ cm, $9 < \text{Ces }  Z  < 230$ cm
Had/Em	$< 0.125 \parallel < 0.055 + 0.00045 * \text{ECorr}$
Cone 0.4 IsoEtCorr (new correction- see notes)	EtCorr $<20$ : $< 0.1*\text{EtCorr}$ EtCorr $>20$ : $< 2.0+0.02*(\text{EtCorr}-20.0)$
Chi2 (Strips+Wires)/2.0	$< 20$
N track (N3D)	$\geq 1$
Track Pt	$< 1+0.005*\text{EtCorr}$ GeV
Cone 0.4 Track Iso	$< 2.0+0.005*\text{EtCorr}$
2nd CES cluster $E*\sin(\theta)$ (both strip and wire E individually)	EtCorr $<18$ : $< 0.14*\text{EtCorr}$ EtCorr $>18$ : $< 2.4+0.01*\text{EtCorr}$

Table C.1: Summary of cuts for selection of Central Photons.

## APPENDIX D

### LIST OF SIMULATED DATASETS

Table D.1: The Monte Carlo-simulated samples used for the SM backgrounds in the analysis. Variable  $K$  is a scale factor; it is a ratio between LO and NLO cross-sections.

Process	Dataset ID	Generator	$\sigma$ (pb)
$W \rightarrow e\nu + \text{jets}$	wtop1i	Pythia	2687
$W \rightarrow \mu\nu + \text{jets}$	wewk8m	Pythia	2687
$W \rightarrow \tau\nu + \text{jets}$	wewkat	Pythia	2687
WW	wtop1w	Pythia	13.25
WZ	wtop1z	Pythia	3.96
ZZ	ztopcz	Pythia	1.39
$Z \rightarrow e^+e^- + \text{jets}$	ztop7i	Pythia	251.3
$Z \rightarrow e^+e^- + \text{jets}$	ztopbi	Pythia	251.3
$Z \rightarrow \mu^+\mu^- + \text{jets}$	zewk9m	Pythia	251.3
$Z \rightarrow \tau\tau + \text{jets}$	ztop4i	Pythia	251.3
$t\bar{t} \rightarrow WbWb$	ttop75	Pythia	7.6
$W^+ + bb + 0\text{p}, W \rightarrow e\nu$	btop0w	Alpgen + Pythia	2.98
$W^+ + b\bar{b} + 1\text{p}, W \rightarrow e\nu$	btop1w	Alpgen + Pythia	0.888
$W^+ + b\bar{b} + 2\text{p}, W \rightarrow e\nu$	btop2w	Alpgen + Pythia	0.287
$W^+ + bb + 0\text{p}, W \rightarrow \mu\nu$	btop5w	Alpgen + Pythia	2.98
$W^+ + b\bar{b} + 1\text{p}, W \rightarrow \mu\nu$	btop6w	Alpgen + Pythia	0.889
$W^+ + b\bar{b} + 2\text{p}, W \rightarrow \mu\nu$	btop7w	Alpgen + Pythia	0.286
$W^+ + c\bar{c} + 0\text{p}, W \rightarrow e\nu$	ctop0w	Alpgen + Pythia	5.00
$W^+ + c\bar{c} + 1\text{p}, W \rightarrow e\nu$	ctop1w	Alpgen + Pythia	1.79
$W^+ + c\bar{c} + 2\text{p}, W \rightarrow e\nu$	ctop2w	Alpgen + Pythia	0.628
$W^+ + c\bar{c} + 0\text{p}, W \rightarrow \mu\nu$	ctop5w	Alpgen + Pythia	5.00
$W^+ + c\bar{c} + 1\text{p}, W \rightarrow \mu\nu$	ctop6w	Alpgen + Pythia	1.79
$W^+ + c\bar{c} + 2\text{p}, W \rightarrow \mu\nu$	ctop7w	Alpgen + Pythia	0.628
$W^+ + c + 0\text{p}, W \rightarrow e\nu$	stopw0	Alpgen + Pythia	17.1
$W^+ + c + 1\text{p}, W \rightarrow e\nu$	stopw1	Alpgen + Pythia	3.39
$W^+ + c + 2\text{p}, W \rightarrow e\nu$	stopw2	Alpgen + Pythia	0.507
$W^+ + c + 3\text{p}, W \rightarrow e\nu$	stopw3	Alpgen + Pythia	0.083

Continued on the next page

Table D.1, continued

Process	Dataset ID	Generator	$\sigma$ (pb)
$W^+ + c + 0p, W \rightarrow \mu\nu$	stopw5	Alpgen + Pythia	17.1
$W^+ + c + 1p, W \rightarrow \mu\nu$	stopw6	Alpgen + Pythia	3.39
$W^+ + c + 2p, W \rightarrow \mu\nu$	stopw7	Alpgen + Pythia	0.507
$W^+ + c + 3p, W \rightarrow \mu\nu$	stopw8	Alpgen + Pythia	0.083
$Z + b\bar{b} + 0p, Z \rightarrow e^+e^-$	ztopb0	Alpgen + Pythia	0.511
$Z + b\bar{b} + 1p, Z \rightarrow e^+e^-$	ztopb1	Alpgen + Pythia	0.134
$Z + b\bar{b} + 2p, Z \rightarrow e^+e^-$	ztopb2	Alpgen + Pythia	0.0385
$Z + b\bar{b} + 0p, Z \rightarrow \mu^+\mu^-$	ztopb5	Alpgen + Pythia	0.511
$Z + b\bar{b} + 1p, Z \rightarrow \mu^+\mu^-$	ztopb6	Alpgen + Pythia	0.134
$Z + b\bar{b} + 2p, Z \rightarrow \mu^+\mu^-$	ztopb7	Alpgen + Pythia	0.0385
$Z + c\bar{c} + 0p, Z \rightarrow e^+e^-$	ztopc0	Alpgen + Pythia	1.08
$Z + c\bar{c} + 1p, Z \rightarrow e^+e^-$	ztopc1	Alpgen + Pythia	0.331
$Z + c\bar{c} + 2p, Z \rightarrow e^+e^-$	ztopc2	Alpgen + Pythia	0.107
$Z + c\bar{c} + 0p, Z \rightarrow \mu^+\mu^-$	ztopc5	Alpgen + Pythia	1.08
$Z + c\bar{c} + 1p, Z \rightarrow \mu^+\mu^-$	ztopc6	Alpgen + Pythia	0.332
$Z + c\bar{c} + 2p, Z \rightarrow \mu^+\mu^-$	ztopc7	Alpgen + Pythia	0.107
$Z \rightarrow \mu^+\mu^- + 0p$	ztopp5	Alpgen + Pythia	$K^*158$
$Z \rightarrow \mu^+\mu^- + 1p$	ztopp6	Alpgen + Pythia	$K^*21.6$
$Z \rightarrow \mu^+\mu^- + 2p$	ztopzt	Alpgen + Pythia	$K^*3.46$
$Z \rightarrow \mu^+\mu^- + 3p$	ztop8p	Alpgen + Pythia	$K^*0.548$
$Z \rightarrow \mu^+\mu^- + 4p$	ztop9p	Alpgen + Pythia	$K^*0.0992$
$t\bar{t} \rightarrow ZcWb$	texo0w	Madgraph + Pythia	
$t\bar{t} \rightarrow ZcZc$	texo0z	Madgraph + Pythia	

**APPENDIX E**  
**SUMMARY TABLE OF ACCEPTANCES AND**  
**EFFICIENCIES**

Number of Interest	Electrons	Muons
Integrated Luminosity	1.52 fb <sup>-1</sup>	1.52 fb <sup>-1</sup>
Total Number of events	75466634	21351395
Number of observed $W \rightarrow \ell\nu$ decays	814746	694651
Fraction of background in $W \rightarrow \ell\nu$ decays	3.5%	11%
Acceptance times efficiency for $W \rightarrow \ell\nu$ decays	0.1922	0.1497
Number of observed $Z \rightarrow \ell\ell$ decays	82901	53368
Fraction of background in $Z \rightarrow \ell\ell$ decays	0.4%	0.25%
Acceptance times efficiency for $Z \rightarrow \ell\ell$ events	0.2125	0.1349
Number of observed $W + 4$ jets (with a $b$ -tag) events	252	219
Number of background events in the $W + 4$ jets decays	98.7	75.2
Acceptance for $t\bar{t} \rightarrow WbWb \rightarrow \ell\nu bj\bar{j}b$ , $A_{WW \rightarrow \ell\nu}$	0.01279	0.00994
Tagging efficiency for $\ell\nu bj\bar{j}b$ , $A_{WW \rightarrow \ell\nu}$	0.678	0.683
Number of observed $Z + 4$ jets (with a $b$ -tag) events	6	8
Number of background events in the $Z + 4$ jets decays	8.4	6.9
Acceptance for $t\bar{t} \rightarrow ZcWb \rightarrow \ell\ell c j\bar{j}b$ , $A_{ZW \rightarrow \ell\ell}$	0.003125	0.00293
Tagging efficiency for $\ell\ell c j\bar{j}b$ , $A_{ZW \rightarrow \ell\ell}$	0.49	0.54

Table E.1: Summary of the numbers of interest for electron and muon datasets. The table includes acceptances, efficiencies, numbers of background events, and numbers of observed events.

**APPENDIX F**  
**LIST OF EVENTS WITH A Z-BOSON AND FOUR JETS**

Run/Event: 184466/383360, $M_{top} = 142.88$ , $\chi^2 = 110.59$			
Identified Object	$p_T$	$\eta$	$\phi$
tight CEM electron	89.94	0.43	4.78
loose CEM electron	37.80	0.84	2.47
jet	53.88	0.13	0.87
b-tagged jet	50.12	1.43	3.48
jet	18.97	-1.29	4.97
jet	16.73	-1.09	4.52
$\cancel{E}_T$	93.11		0.92
$H_T$	376.66		
Z-boson, $M_{inv}(\ell\ell) = 109.43$	70.16	0.93	-1.91

Table F.1: Summary of event number 184466/383360. The event contains a  $Z$  boson and four jets.

Run/Event: 183097/3797423, $M_{top} = 169.09$ , $\chi^2 = 10.61$			
Identified Object	$p_T$	$\eta$	$\phi$
tight CEM electron	91.04	0.01	3.82
tight CEM electron	74.23	-0.13	5.10
jet	99.32	-0.17	1.09
jet	45.66	-0.40	0.52
b-tagged jet	44.42	0.48	2.41
jet	15.94	-1.86	4.13
$\cancel{E}_T$	6.32		0.57
$H_T$	374.40		
Z-boson, $M_{inv}(\ell\ell) = 98.67$	133.05	-0.07	-1.90

Table F.2: Summary of event number 183097/3797423. The event contains a  $Z$  boson and four jets.

Run/Event: 203509/331412, $M_{top} = 196.39$ , $\chi^2 = 1.85$			
Identified Object	$p_T$	$\eta$	$\phi$
tight CEM electron	110.41	-0.07	4.05
tight CEM electron	90.15	0.75	4.47
jet	124.05	-0.11	0.93
b-tagged jet	46.90	0.65	1.75
jet	20.67	1.94	6.17
jet	21.53	-1.27	1.71
$\cancel{E}_T$	10.88		1.88
$H_T$	422.09		
Z-boson, $M_{inv}(\ell\ell) = 93.98$	196.11	0.34	-2.04

Table F.3: Summary of event number 203509/331412. The event contains a  $Z$  boson and four jets.

Run/Event: 221532/2166426, $M_{top} = 111.30$ , $\chi^2 = 5.36$			
Identified Object	$p_T$	$\eta$	$\phi$
tight CEM electron	42.78	-0.41	1.26
PEM electron	36.14	-1.38	4.73
b-tagged jet	76.40	0.49	3.59
jet	19.40	-0.27	0.44
jet	15.70	-1.21	1.46
jet	15.27	-1.10	5.98
$\cancel{E}_T$	6.81		5.92
$H_T$	224.29		
Z-boson, $M_{inv}(\ell\ell) = 92.34$	13.65	-2.62	0.02

Table F.4: Summary of event number 221532/2166426. The event contains a  $Z$  boson and four jets.

Run/Event: 222322/2329377, $M_{top} = 237.83$ , $\chi^2 = 3.89$			
Identified Object	$p_T$	$\eta$	$\phi$
tight CEM electron	66.61	0.87	3.87
tight CEM electron	32.69	0.83	0.33
jet	113.45	-0.42	1.91
b-tagged jet	88.24	0.80	4.70
jet	50.93	-1.21	0.35
jet	17.19	-0.28	1.24
$\cancel{E}_T$	18.44		4.23
$H_T$	385.13		
Z-boson, $M_{inv}(\ell\ell) = 91.46$	38.72	1.64	-2.07

Table F.5: Summary of event number 222322/2329377. The event contains a  $Z$  boson and four jets.

Run/Event: 222801/1282328, $M_{top} = 253.63$ , $\chi^2 = 23.52$			
Identified Object	$p_T$	$\eta$	$\phi$
tight CEM electron	92.08	0.58	1.75
PEM electron	40.66	1.24	3.15
b-tagged jet	94.24	0.73	5.78
jet	39.92	0.26	3.03
jet	27.81	-2.06	4.80
jet	17.64	-2.27	5.53
$\cancel{E}_T$	4.34		3.07
$H_T$	315.19		
Z-boson, $M_{inv}(\ell\ell) = 91.60$	108.00	0.99	2.15

Table F.6: Summary of event number 222801/1282328. The event contains a  $Z$  boson and four jets.

Run/Event: 196368/115764, $M_{top} = 108.28$ , $\chi^2 = 22.98$			
Identified Object	$p_T$	$\eta$	$\phi$
tight CMUP muon	45.22	0.15	-2.63
loose muon	44.64	0.37	0.42
jet	40.52	-0.53	4.87
jet	25.05	-0.30	3.31
jet	24.56	-0.75	0.92
b-tagged jet	20.61	-0.85	6.10
$\cancel{E}_T$	10.94		2.03
$H_T$	210.06		
Z-boson, $M_{inv}(\ell\ell) = 90.27$	4.28	2.41	-1.24

Table F.7: Summary of event number 196368/115764. The event contains a  $Z$  boson and four jets.

Run/Event: 192987/336742, $M_{top} = 139.97$ , $\chi^2 = 9.73$			
Identified Object	$p_T$	$\eta$	$\phi$
tight CMUP muon	119.04	0.41	-2.54
loose muon	51.36	0.02	-1.35
b-tagged jet	47.66	-0.12	0.84
jet	33.99	-1.39	0.30
jet	24.04	0.75	1.94
jet	18.52	0.15	1.88
$\cancel{E}_T$	38.98		0.83
$H_T$	346.27		
Z-boson, $M_{inv}(\ell\ell) = 93.02$	145.94	0.34	-2.21

Table F.8: Summary of event number 192987/336742. The event contains a  $Z$  boson and four jets.

Run/Event: 203190/7183703, $M_{top} = 191.38$ , $\chi^2 = 13.44$			
Identified Object	$p_T$	$\eta$	$\phi$
tight CMUP muon	69.10	0.31	1.86
loose muon	30.96	-0.38	-0.47
b-tagged jet	80.19	0.38	4.07
jet	69.84	1.19	0.47
jet	24.06	-1.78	3.43
jet	17.76	-0.63	3.42
$\cancel{E}_T$	13.67		4.76
$H_T$	315.14		
Z-boson, $M_{inv}(\ell\ell) = 91.15$	52.76	0.19	1.42

Table F.9: Summary of event number 203190/7183703. The event contains a  $Z$  boson and four jets.

Run/Event: 178684/2540865, $M_{top} = 179.84$ , $\chi^2 = 10.34$			
Identified Object	$p_T$	$\eta$	$\phi$
tight CMUP muon	74.57	0.07	-2.02
loose muon	56.33	0.49	2.88
jet	81.35	-0.70	1.78
jet	42.01	0.29	6.28
b-tagged jet	31.05	1.44	6.24
jet	17.97	1.12	5.51
$\cancel{E}_T$	14.36		5.14
$H_T$	316.01		
Z-boson, $M_{inv}(\ell\ell) = 87.02$	101.57	0.33	-2.60

Table F.10: Summary of event number 178684/2540865. The event contains a  $Z$  boson and four jets.

Run/Event: 151974/194905, $M_{top} = 142.57$ , $\chi^2 = 2.44$			
Identified Object	$p_T$	$\eta$	$\phi$
tight CMX muon	48.26	-0.66	-0.57
tight CMUP muon	43.84	-0.18	2.58
jet	46.87	-2.00	3.47
jet	26.80	0.97	1.16
b-tagged jet	17.58	0.69	6.23
jet	15.69	0.22	5.64
$\cancel{E}_T$	7.04		1.89
$H_T$	219.26		
Z-boson, $M_{inv}(\ell\ell) = 94.71$	4.43	-2.94	-0.64

Table F.11: Summary of event number 151974/194905. The event contains a  $Z$  boson and four jets.

Run/Event: 164352/57731, $M_{top} = 133.40$ , $\chi^2 = 5.30$			
Identified Object	$p_T$	$\eta$	$\phi$
tight CMUP muon	36.53	0.48	0.40
loose muon	64.60	0.70	-2.13
b-tagged jet	97.12	0.63	1.00
jet	28.03	-0.81	3.59
jet	22.23	-0.60	3.08
jet	16.62	-0.11	4.89
$\cancel{E}_T$	8.51		4.95
$H_T$	271.91		
Z-boson, $M_{inv}(\ell\ell) = 93.27$	40.58	1.28	-1.58

Table F.12: Summary of event number 164352/57731. The event contains a  $Z$  boson and four jets.

Run/Event: 166779/3467414, $M_{top} = 109.58$ , $\chi^2 = 12.60$			
Identified Object	$p_T$	$\eta$	$\phi$
tight CMX muon	42.20	0.85	2.82
loose muon	39.47	0.06	0.63
jet	41.32	-1.93	4.68
b-tagged jet	30.17	-0.89	4.25
jet	23.69	-0.11	1.17
jet	21.49	1.23	0.65
$\cancel{E}_T$	3.42		2.81
$H_T$	200.77		
Z-boson, $M_{inv}(\ell\ell) = 79.79$	37.64	0.97	1.79

Table F.13: Summary of event number 166779/3467414. The event contains a  $Z$  boson and four jets.

Run/Event: 222271/20319806, $M_{top} = 91.65$ , $\chi^2 = 107.74$			
Identified Object	$p_T$	$\eta$	$\phi$
tight CMUP muon	60.14	0.23	-0.16
loose muon	51.08	0.00	1.92
b-tagged jet	37.39	0.61	4.00
jet	24.15	0.60	4.92
jet	18.08	0.60	5.37
jet	16.90	0.81	3.27
$\cancel{E}_T$	19.22		1.78
$H_T$	225.73		
Z-boson, $M_{inv}(\ell\ell) = 96.40$	56.89	0.25	0.74

Table F.14: Summary of event number 222271/20319806. The event contains a  $Z$  boson and four jets.

## REFERENCES

- [1] H. Fritzsch, t-Quarks May Decay into Z-Bosons and Charm, Phys. Lett. B **224**, 423 (1989).
- [2] J. Aguilar-Saavedra, Top Flavour-Changing Neutral Interactions: Theoretical Expectations and Experimental Detection, Acta Phys. Polon. **B35**, 2695 (2004), hep-ph/0409342.
- [3] F. Larios, R. Martinez, and M. A. Perez, Constraints on top-quark FCNC from electroweak precision measurements, Phys. Rev. D **72**, 057504 (2005), hep-ph/0412222.
- [4] P. Fox et al., Deciphering top flavor violation at the LHC with B factories p. 2 (2007), arXiv:0704.1482[hep-ex].
- [5] The CDF-II detector is described in more detail in many recent publications; see, for example, A. Abulencia et al., (CDF Collaboration), Phys. Rev. D **73**, 112006 (2006), and references therein.
- [6] N. Cabbibo, II Topical Conference on Proton-Antiproton Collider Physics, Rome, Jan. 1982; F. Halzen and M. Marsula, Phys. Rev. Lett. **51**, 857 (1983); K. Hikasa, Phys. Rev. D **29**, 1939 (1984); N.G. Deshpande et al., Phys. Rev. Lett. **54**, 1757 (1985); A.D. Martin, R.G. Roberts, and W. J. Stirling, Phys. Lett. **189B**, 220 (1987); E.L. Berger, F. Halzen, C.S. Kim, and S. Willenbrock, Phys. Rev. D **40**, 83 (1989).
- [7] W. M. Yao et al. (Particle Data Group), Review of particle physics, J. Phys. G **33**, 1 (2006).
- [8] F. Abe et al. (CDF Collaboration), Search for Flavor-Changing Neutral Current Decays of the Top Quark in  $p\bar{p}$  Collisions at  $\sqrt{s}=1.8$  TeV, Phys. Rev. Lett. **80**(12), 2525 (1998).
- [9] LEP Electroweak Working Group (EWWG), <http://lepewwg.web.cern.ch/LEPEWWG/>.
- [10] T. Aaltonen et al. (CDF Collaboration), Search for the Flavor Changing Neutral Current Decay  $t \rightarrow Zq$  in  $p\bar{p}$  Collisions at  $\sqrt{s}=1.96$  GeV (2008), arXiv:0805.2109[hep-ph].

- [11] Transverse momentum and energy are defined as  $p_T = p \sin \theta$  and  $E_T = E \sin \theta$ , respectively. We use the convention that “momentum” refers to  $pc$  and “mass” to  $mc^2$ .
- [12] A. Sill et al., Nucl. Instrum. Meth. A **447**, 1 (2000); A. Affolder et al., Nucl. Instrum. Meth. A **453**, 84 (2000); C.S. Hill, Nucl. Instrum. Meth. A **530**, 1 (2000).
- [13] The CDF coordinate system is right-handed with the  $x$  axis horizontal and out of the Tevatron ring, the  $y$  axis up, and the  $z$  axis along the proton beam;  $\phi$  is the azimuthal angle. The pseudorapidity  $\eta \equiv -\ln(\tan(\theta/2))$ , where  $\theta$  is the polar angle; the  $\eta$  regions for detector components are defined with respect to the center of the detector. The central region is defined as  $|\eta| < 1$ .
- [14] A. Affolder et al., Nucl. Instrum. Meth. A **526**, 249 (2004).
- [15] L. Balka et al., Nucl. Instrum. Meth. A **267**, 272 (1988).
- [16] S. Kuhlmann et al., Nucl. Instrum. Meth. A **518**, 39 (2004).
- [17] D. Acosta et al. (CDF Collaboration), Phys. Rev. D **71**, 032001 (2005).
- [18] M. G. Albrow et al. (CDF Collaboration), Nucl. Instrum. Meth. A **480**, 524 (2002).
- [19] F. Abe et al., Phys. Rev. Lett. **68**, 1104 (1992).
- [20] G. Ascoli et al. (CDF Collaboration), Nucl. Instrum. Meth. A **268**, 33 (1988).
- [21] T. Dorigo et al. (CDF Collaboration), Nucl. Instrum. Meth. A **461**, 560 (2001).
- [22] D. Acosta et al. (CDF Collaboration), Nucl. Instrum. Meth. A **494**, 57 (2002).
- [23] The checks agreed immediately for electrons, but turned up some problems with the complex run-dependent book-keeping for the muon system.
- [24] M. Coca and E. Halkiadakis, Central Electron Identification Efficiencies for the 200  $pb^{-1}$  Run 2 Dataset, CDF Note 6580, University of Rochester (Jan. 6, 2004).
- [25] S. Harper and G. Veramendi, Very High-Pt Electron Identification, CDF Note 7527, Fermilab (2005).
- [26] The fraction of electromagnetic energy allowed to leak into the hadron compartment  $E_{\text{had}}/E_{\text{em}}$  must be less than  $0.055 + 0.00045 \times E_{\text{em}}(\text{GeV})$  for central electrons, less than 0.05 for electrons in the end-plug calorimeters, less than  $\max[0.125, 0.055 + 0.00045 \times E_{\text{em}}(\text{GeV})]$  for photons.

- [27] M. Coca and E. Halkiadakis, Plug Electron Baseline Cuts Defined in Summer 2003 and Cut Efficiencies, CDF Note 6580, for the ETF group (Feb. 16, 2004).
- [28] D. Acosta et al. (CDF Collaboration), Phys. Rev. D **71**, 051104 (2005); hep-ex/0501023.
- [29] U. Grundler, L. Lovas, and A. Taffard, High-Pt muons recommended cuts and efficiencies for Winter 2007, CDF Note 8618, University of Illinois - Urbana-Champaign and Comenius University (Nov. 29, 2006).
- [30] The energy deposited in the calorimeter tower traversed by the muon must be less than  $2 + \max(0, 0.0115 \times (p - 100))$  GeV in the electromagnetic compartment and less than  $6 + \max(0, 0.028 \times (p - 100))$  GeV in the hadronic compartment.
- [31] A. V. Varganov, Ph.D. thesis, University of Michigan, 2004; AAT 3137951.
- [32] The muon “stub” in the muon systems must be within 7, 5, and 6 cm of the extrapolated COT track position, in the CMU, CMP, and CMX muon systems, respectively.
- [33] A. V. Kotwal, H. K. Gerberich, and C. Hays, Identification of cosmic rays using drift chamber hit timing, Nucl. Instrum. Meth. A **506**(1-2), 110 (2003), ISSN 0168-9002.
- [34] For tight muons and tight electrons at least 5 hits in each of 3 axial and 3 stereo layers of the COT are required; for loose muons with a matching muon stub this is relaxed to 3 axial and 2 stereo. Loose muons without a matching stub have an additional cut on the  $\chi^2$  for the fit to the track.
- [35] D. Hare, E. Halkiadakis, and T. Spreitzer, Electron ID Efficiencies and Scale Factors for Winter 2007 Analyses, CDF Note 8614, Rutgers University and University of Toronto (Dec. 7, 2006).
- [36] The maximum correction to the identification efficiency for central electrons is 1.7%, for “plug” electrons 6.3%, and for central muons is 7.4%.
- [37] B.-Y. Han and V. Boisvert, Trigger Efficiencies for the High  $E_T$  Central Electrons in the Gen6 data, CDF Note 8629, University of Rochester (2006).
- [38] A. Bhatti et al., Determination of the Jet Energy Scale at the Collider Detector at Fermilab, Nucl. Instrum. Meth. A **566**, 375 (2006), hep-ex/0510047.
- [39] See: Baseline Analysis Cuts for High Pt Photons V2.3, <http://www-cdf.fnal.gov/internal/physics/photon/docs/cuts.html>.

- [40] T. Stelzer and W. F. Long. *Comput. Phys. Commun.* **81**, 357 (1994); F. Maltoni and T. Stelzer, ILL-(TH)-02-9 For the code and instructions, see <http://madgraph.hep.uiuc.edu/>.
- [41] R. Field (for the CDF Collaboration), Jet physics and the underlying event at the Tevatron, *AIP Conf. Proc.* **828**, 163 (2006), we use Tune A.
- [42] PYTHIA v6.216 with a  $M(\gamma^*/Z) > 30$  GeV cut, Tune A, and the “Willis Sakumoto” corrections applied [60]. The Z + HF samples are produced with ALPGEN v2.10-prime (which has built-in MLM matching) and showered with PYTHIA v 6.326. The both generators used CTEQ5L parametrization of the parton distribution functions.
- [43] A. Abulencia et al. (CDF Collaboration), Measurements of Inclusive W and Z Cross Sections in p-pbar Collisions at  $\sqrt{s} = 1.96$  TeV, *J. Phys.* **G34**, 2457 (2007), [hep-ex/0508029](https://arxiv.org/abs/hep-ex/0508029).
- [44] F. A. Berends et al., Multijet production in W, Z events at  $p\bar{p}$  colliders, *Phys. Lett. B* **224**, 237 (1989).
- [45] A. A. Affolder et al. (CDF Collaboration), Measurement of the  $t\bar{t}$  production cross section in  $p\bar{p}$  collisions at  $\sqrt{s} = 1.8$  TeV, *Phys. Rev. D* **64**, 032002 (2001), [hep-ex/0101036](https://arxiv.org/abs/hep-ex/0101036).
- [46] The theoretical estimate of the top pair production cross-section is based on Ref. [59] using a top-quark mass of  $170.9 \pm 1.8$  GeV [55].
- [47] The scale factor for W+HF processes ( $W + b\bar{b}$ ,  $W + c\bar{c}$ , and  $W + c$ ) does not depend strongly on the number of  $t\bar{t}$  events since the  $t\bar{t} \rightarrow WbZc$  and  $t\bar{t} \rightarrow WbWb$  modes contribute mostly to a final state with a W and three or four jets in the final state.
- [48] The total transverse energy,  $H_T$ , is a scalar sum of  $E_T$  of all reconstructed objects (electrons, muons, photons, jets, missing transverse energy, and unclustered energy). The transverse energies of the objects are the same as those used for the calculation of the missing energy  $\cancel{E}_T$  in the event.
- [49] J. Alwall et al., MadGraph/MadEvent v4: The New Web Generation, *JHEP* **09**, 028 (2007), [arXiv:0706.2334\[hep-ph\]](https://arxiv.org/abs/0706.2334).
- [50] J.-F. Arguin, Measurement of the Top Quark Mass with In Situ Jet Energy Scale Calibration at CDF-II, CDF Note 7968 (2005).

- [51] S. Grinstein and D. Sherman, SecVtx Scale Factors and Mistag Matrices for the 2007 Summer Conferences, CDF Note 8910, Harvard, CDF Collaboration (2007).
- [52] M. Franklin et al., Measurement of the Top Pair Cross Section in Lepton+Jets in 1.12/fb, CDF Note 8767, Harvard, CDF Collaboration (April 26, 2007).
- [53] A. Abulencia et al. (CDF Collaboration), Top quark mass measurement using the template method in the lepton + jets channel at CDF II, Phys. Rev. D **73**, 032003 (2006), [hep-ex/0510048](#).
- [54] J. Alwall et al., Comparative study of various algorithms for the merging of parton showers and matrix elements in hadronic collisions, Eur. Phys. J. **C53**, 473 (2008), [arXiv:0706.2569\[hep-ph\]](#).
- [55] CDF and D0 Collaborations, A Combination of CDF and D0 results on the mass of the top quark (2007), fermilab-TM-2380-E, TEVEWWG/top 2007/01, [hep-ex/0703034](#).
- [56] M. L. Mangano et al., ALPGEN, a generator for hard multiparton processes in hadronic collisions, JHEP **07**, 001 (2003), [hep-ph/0206293](#).
- [57] T. Sjostrand, L. Lonnblad, and S. Mrenna, PYTHIA 6.2: Physics and manual (2001), [hep-ph/0108264](#).
- [58] A. Abulencia et al. (CDF Collaboration), Measurement of the  $t\bar{t}$  Production Cross Section in  $p\bar{p}$  collisions at  $\sqrt{s} = 1.96$ -TeV using Lepton + Jets Events with Jet Probability  $b^-$  tagging, Phys. Rev. D **74**, 072006 (2006), [hep-ex/0607035](#).
- [59] M. Cacciari et al., The  $t\bar{t}$  cross-section at 1.8 and 1.96 TeV: a study of the systematics due to parton densities and scale dependence, JHEP **04**, 068 (2004), [hep-ph/0303085](#).
- [60] D. Acosta et al. (CDF Collaboration), First measurements of inclusive W and Z cross sections from Run II of the Tevatron collider, Phys. Rev. Lett. **94**, 091803 (2005), [hep-ex/0406078](#).